Aus dem Bereich Molekularen Zellbiologie
Theoretische Medizin und Biowissenschaften
Der Medizinischen Fakultät
Der Universität des Saarlandes, Homburg/Saar

Splicing of human cardiac BIN1 isoforms and their effects on maintaining and regenerating transverse tubules and excitation-contraction coupling in cardiac myocytes

Dissertation zur Erlangung des Grades eins
MD/PhD
der Medizinnischen Fakultät
der UNIVERSITÄT DES SAARLANDES
2021

vorgelegt von: Jia Guo
geb. am: 22.11.1987 in Changde, Hunan, China

Content

1. Abbreviation 1

2. Abstract 3

3. Introduction 11

3.1 Cardiac physiology and EC-coupling 11

3.1.1 Physiological function of the heart 11

3.1.2 Cardiac conduction system 12

3.1.3 Electrophysiology of cardiomyocytes 15

3.1.4 EC-coupling of cardiomyocytes 17

3.1.5 L-type calcium channel 19

3.1.6 Ryanodine receptor 20

3.1.7 Nanoscopic structures of the calcium release unit 22

3. 2 Transverse tubules of cardiomyocytes 25

3.2.1 Characteristics of the T-tubule structure 26

3.2.2 Importance of T-tubules for cardiac EC-coupling 29

3.2.3 Mechanisms of T-tubule biogenesis 32

3.2.4 Regulation of T-tubule biogenesis 35

3.3 Amphiphysin 2/ BIN1 40

3.3.1 BIN1 gene and splice variants 40

3.3.2 Properties of BIN1 domains 42

3.3.3 The role of BIN1 in skeletal myocytes 44

3.3.4 The role of BIN1 in cardiomyocytes 45

3.4 hiPSC-derived cardiomyocytes 47

3.4.1 Reprogramming of human iPSC 47

3.4.2 Differentiation of hiPSC-derived cardiomyocytes 48

3.4.3 Strategies of promoting hiPSC-CMs maturation 49

3.4.4 Biogenesis of T-tubules in hiPSC-CMs 52

4. Materials and methods 53

4.1 Materials 53

4.1.1 Cell culture reagents 53

4.1.2 Consumables 54

4.1.3 Enzymes, nucleotides and markers 55

4.1.4 Kits 57

4.1.5 Laboratory apparatus 57
4.1.6 PCR primers for BNI1 transcription analysis 58
4.1.7 Primary and secondary antibodies 59
4.1.8 Buffers and solutions 61
4.2 Methods 63
4.2.1 Cell culture techniques 63
4.2.2 Plasmid transfection 64
4.2.3 Adenovirus packaging and transduction 65
4.2.4 Molecular biological methods 67
4.2.5 Vector construct preparation 73
4.2.6 Immunostaining and calcium signal labeling 76
4.2.7 Microscopic calcium imaging 78
4.2.8 Data processing and statistical analysis 80
5. Results 86
5.1 Identification of BIN1 isoforms in the human heart tissue ... 86
5.1.1 Screening of BIN1 splice variants in healthy human heart tissue .. 86
5.1.2 Analysis of the exon composition of the identified human cardiac BIN1 isoforms 88
5.2 Characterizing the properties of BIN1 isoforms in HEK cells 90
5.2.1 Effects of N-terminal fusion 90
5.2.2 Effects of C-terminal fusion 91
5.2.3 Application of the 2A cloning strategy for BIN1 isoforms 94
5.3 Effects of BIN1 isoforms on adult rat cardiomyocytes 95
5.3.1 Establishment of detubulation models in cultured adult rat ventricular myocytes 96
5.3.2 Maintenance of EC couplons by human cardiac BIN1 isoforms 98
5.3.3 Effects of BIN1 isoforms on maintaining cardiac EC-coupling 105
5.3.4 Effects of BIN1 isoforms on cardiac EC-coupling revealed by GCaMP6f-junctin 110
5.3.5 Effects of BIN1 isoforms on recovering cardiac T-tubules and EC-coupling 113
5.4 Role of BIN1 in de-novo generation of T-tubules in hiPSC-derived cardiac myocytes 115
5.4.1 T-Tubule biogenesis induced by expression of BIN1 isoforms in hiPSC-CMs 116
5.4.2 Tafficking of LTCCs to BIN1-induced tubules 117
5.4.3 Remodeling of the RyR2 distribution by BIN1-induced tubules.... 121

5.4.4 Effects of BIN1 expression on calcium handling in hiPSC-CMs analyzed by Fluo-4 123
5.4.5 Effects of BIN1 isoforms on EC-couplons in hiPSC-CMs analyzed by expression of GCaMP6f-junctin 126
5.5 Supplemental Figure 130
6. Discussions 131
6.1 Transcriptional splicing of BIN1 in human heart................ 131
6.2 Properties of human BIN1 isoforms................................. 135
6.3 Behaviour of BIN1 isoforms in adult rat cardiomyocytes... 140
6.4 Effects of BIN1 isoforms on EC-coupling in hiPSC-CMs... 148
6.5 Overall conclusion.. 156
7. Reference.. 158
8. Acknowledgement 177
9. Curriculum Vitae 181

1. Abbreviation

ECC	Excitation-Contraction Coupling
SAN	Sinoatrial node
AVN	Atrioventricular node
SCV	Superior vena cava
ICV	Inferior vena cava
LTCC	L-type calcium channel
RyR	Ryanodine receptor
CICR	Calcium-induced calcium release
PKA	Protein kinase A
FKBP	FK506 binding protein
CaMKII	Calmodulin-dependent protein kinase II
SR	Sarcoplasmic reticulum
ER	Endoplasmic reticulum
CRU	Calcium release unit
T-tubules	Transverse tubules
PIP2/PI (4,5) P2/ Ptdlns (4,5) P2	Phosphatidylinositol 4,5-bisphosphate
BAR	Bin-Amphiphysin-Rvs
JPH2	Junctophilin 2
BIN1	Bridge integrator-1
Cav-3	Caveolin-3
SH3	Src homology3
PI	Phosphoinositide
CLAP	Clathrin and AP2
MBD	Myc-binding domain

CNM	Centronuclear myopathy
iPSC	Induced pluripotent stem cell
ESC	Embryonic stem cell
iPSC-CM	iPSC-derived cardiomyocyte
CSQ	Calsequestrin
SERCA	SR Ca^{2+} ATPase
MYL2	Myosin regulatory light chain 2
TCAP	Telethonin/Titin-cap
MYOM2	Myomesin 2
ICM	Ischemic cardiomyopathy
DCM	Dilated cardiomyopathy
DMEM	Dulbecco’s modified eagle medium
FBS	Fetal Bovine Serum
EDTA	Ethylenediaminetetraacetic acid
EBSS	Earle's balanced salt solution
ITS	Insulin-Transferrin-Selenium
PBS	Phosphate buffered saline
PFA	Paraformaldehyde
HEKC	Human embryonic kidney cell
PEI	Polyethylenimine
CPE	Cytopathic effects
BSA	Bovine serum albumin
PCR	Polymerase chain reaction
NEXN	Nexilin F-Actin Binding Protein

2. Abstract

Cardiomyocytes are striated muscle cells in the heart that pumps blood to organs and tissues throughout the body. Their efficient contraction highly depends on a special property - Excitation-Contraction Coupling (EC-coupling), which translates electrical signals into mechanical contractions. EC-coupling is mainly mediated by the coupling of two ion channels: L-type calcium channels (LTCC) in the cell membrane and ryanodine receptors type II (RyR2) in the membrane of the sarcoplasmic reticulum (SR). These closely coupled proteins form the so-called calcium-releasing units (CRU), or EC couplons.

Structurally, efficient EC-coupling significantly depends on a type of highly specialized membrane invaginations: T-tubules. They coordinate activities of multiple ion channels in the plasma membrane and play indispensable roles in the regulation of membrane resting and action potential as well as EC-coupling. However, T-tubules can remodel or even disappear under certain pathological conditions such as heart failure. In addition, a lack of T-tubule can be also seen in human induced pluripotent stem cell-derived cardiomyocytes (hiPSC-CM), which significantly limits the efficiency of EC-coupling. Many proteins participate in the biogenesis of T-tubules. Amphiphysin2, alternatively known as BIN1, is considered to be a key protein responsible for T-tubule generation. Its mutations are associated with several types of skeletal myopathies. Although the occurrence of numerous human BIN1 isoforms is well established as a result of alternative splicing there is currently no detailed analysis of the BIN1 isoform pattern

in human heart tissue. The present thesis aims at identifying the potential splice variants of BIN1 in healthy human heart tissues and exploring their roles in cardiac myocytes.

A total of five BIN1 isoforms were identified from RNA samples of healthy human hearts. All isoforms were the result of distinct splicing events. Interestingly, two isoforms contain exon 11, which was previously regarded as skeletal muscle specific. When initially expressed in HEK cells, all isoforms without exon11 were located in the cytoplasm substantially and only induced short tubules. In contrast, exon11-containing isoforms were able to produce long tubules with very little cytosolic distribution.

In the following, I investigated all isoforms in cultured adult rat ventricular myocytes, a cellular system that served as a model for the loss of T-tubules occuring under pathological conditions such as heart failure. For this study I specifically designed two different approaches aiming on a detailed investigation of (i) T-tubule regeneration after loss and (ii) prevention of loss or maintenance of existing T-tubules. My data clearly indicated that all isoforms contributed positively to both processes. They prevented the loss of T-tubules (Instandhaltungsfunktion) function) and evoked their re-generation (rescue function) that was accompanied by a strong co-localization of key ion channels (LTCC and RyR2), as efficient, functional EC-coupling. Notably, the two BIN1 isoforms with exon11 depicted significant stronger effects than the others.

Moreover, the two exon11-containing isoforms, which displayed the most profound effects on both, T-tubulkes and EC-coupling, were further anaylsed in hiPSC-CMs. I found that their expression successfully evoked abundant T-tubules across the cytoplasm. These tubules were decorated with EC-couplon comprising both, LTCCs and RyR2s, and significantly improved the EC-coupling efficiency in hiPSC-CMs. Further analysis of electically evoked calcium transients with Fluo4 and the genetically encoded, diadic junction-specific calcium sensor junction-GCaMP6f revealed substantially improved and faster EC-coupling in the hiPS-CMs in close proximity to the newly formed T-tubules. These data demonstrated that BIN1 isoforms with exon 11 were effective in enhancing the properties of iPSC-CMs, both structurally and functionally.

In conclusion, in the present study I have identified a distinct set of BIN1 splice variants from human heart different from those previously reported in mouse hearts. These human BIN1 isoforms exhibited different abilities of generating tubules and contributed positively to the regeneration and maintenance of T-tubules in adult rat ventricular myocytes. I found that key ion channels and EC-coupling was vastly improvced in BIN1-expressing cultured adult rat cardiomyocytes. In particular, BIN1 isoforms with exon11 were substantially more efficient than the other isoforms, and showed strong effects on the *de-novo* generation of a T-tubule system in hiPSC-CMs, both structurally and functionally. Based on these findings, BIN1 could be a novel therapeutic target for improving the heart unfction in heart diseases and provide a potential strategy for driving the development of hiPSC-CMs.

Zusammenfassung

Das Herz ist ein gestreifter Muskel, der aus einzelnen Herzmuskelzellen den Kardiomyozyten aufgebaut ist und dessen Aufgabe es ist, Blut durch Organe und Gewebe des gesamten Körpers zu pumpen. Die Effizienz Ihrer Kontraktion hängt stark von einer ihrer speziellen Eigenschaften ab, dem Vorgang der Erregungs-Kontraktions Kopplung (EK-Kopplung). Dieser Prozess übersetzt eingehende elektrische Signale in mechanische Aktivität, die Kontraktion. Im Herzen erfolgt EK-Kopplung hauptsächlich aufgrund der Interaktion, d.h. Kopplung, von zwei Ionenkanälen: L-Typ Kalziumkanälen (LTCC) in der Plasmamembran und Ryanodinrezeptoren Typ II (RyR2) in der Membran des sarkoplasmatischen Retikulums (SR). Diese eng verbundenen Proteine bilden sogenannte Kalziumfreisetzungs-Einheiten (CRU) oder EC-Couplons.

Mit Hinblick auf die Struktur, hängt effiziente EK-Kopplung im Herzen von hochspezialisierten Membraneinstülpungen ab, den T-Tubuli. Dieses Membransystem koordiniert die Aktivitäten vieler Ionenkanäle in der Plasmamembran wie z.B. für die Regulation des Membranpotenzials oder EK-Kopplung. Allerdings wird dieses Membransystem in Herzkrankheiten, wie der Herzinsuffizienz, stark umgebaut oder verschwindet sogar teilweise ganz. Darüber hinaus fehlt ein ausgeprägtes T-tubuläres Membransystem in aus humanen induzierten pluripotenten Stammzell- abgeleiteten Herzmuskelzellen (hiPSC-CMs) völlig, was eine effiziente EK-Kopplung in diesen Zellen startk einschränkt und ihre Weiterdifferenzierung hin zu einem mehr adulten Pänotyp und

Genotyp behindert. An der Biogenese von T-Tubuli sind eine Vielzahl von Proteinen beteiligt. In diesem Zusammenhang wird Amphiphysin2, auch BIN1 genannt, als Schlüsselprotein angesehen. Genetische Mutationen im BIN1 Gen werden mit einer ganzen Reihe von Skelettmuskelerkrankungen in Zusammenhang gebracht. Obwohl die Existenz von BIN1 Isoformen als Ergebnis von alternativem Splicing etabliert ist, fehlt zurzeit eine detaillierte Analyse des Isoform Musters im humanen Herzgewebe. Die vorliegende Doktorarbeit hatte zum Ziel, das Expressionsmuster von BIN1 Isoformen im humanen Herzen zu identifizieren und deren Funktionen in lebenden Herzmuskelzellen zu etablieren.

Ich war erstmals in der Lage insgesamt 5 BIN1 Isoformen aus der Gesamt-RNS von Herzgewebeproben gesunder Probanden zu identifizieren, die alle das Ergebnis von alternativem Splicing waren. Interessanterweise konnte ich zwei BIN1-Isoformen finden, die das exon11 enthielten, das bisher ausschließlich als Skelettmuskel-spezifische Variante angesehen wurde. Ich habe diese 5 Isoformen initial in HEK293 Zellen exprimiert, um ihr prinzipielles Verhalten in lebenden Zellen zu verifizieren. Hierbei fand ich, dass diejenigen Isoformen ohne exon11 nur sehr kurze Membraneinstülpungen evozierten. Demgegenüber induzierten BIN1-Varianten mit exon11 zahlreiche und lange Membraneinstülpungen.

Im Folgenden habe ich alle humanen Isoformen in adulten Rettenventrikelzellen untersucht, einem etablierten Zellkulturmodell für den Verlust und den Umbau von T-Tubuli, wie er auch bei humanen Herzkrankheiten, wie der Herzinsuffizienz auftritt. Für diese Studien habe ich zwei spezifische experimentelle Ansätze benutzt, um sowohl die Regeneration von T-Tubuli nach Ihrem Verlust als auch die Verhinderung Ihres Verlustes zu untersuchen. Meine Ergebnisse haben klar gezeigt, dass die Expression einer der 5 gefunden humanen Isoformen alleine hinreichend war, um sowohl den Wiederaufbau von T-Tubuli nach Verlust zu evozieren (Regenerationsfunktion) wie auch die Unterdrückung des Umbaus und Verlusts von T-Tubuli (Instandhaltungsfunktion) zu bewirken. Beide Prozesse gingen mit einem hohen Ko-Lokalisationsquotienten zwischen LTCC und RyR2 und effizienter, funktioneller EK-Kopplung in den Kardiomyozyten einher.

In der vorherigen Studie zeigte es sich, dass die beiden BIN1 Isoformen mit exon11 die stärksten Regenerations- und Erhaltungsfunktionen zeigten. Ich daher diese beiden Isoformen in einer abschließenden Untersuchung an hiPS-CMs eingesetzt, um ihre Funktion in diese humanen Herzmuskelzellen zu analysieren. Virale Expression dieser beiden BIN-Isoformen führte in den hiPS-CMs zum Auftreten eines komplexen T-Tubulus Netzwerkes, das mit einer Vielzahl von EC-Couplons aus LTCCs und RyR2s dekoriert war. Die Analyse von elektrisch evozierten Kalziumtransienten zeigte eine substanzielle Verbesserung der EK-Kopplungseffizienz in diesen Zellen. Die Ausbildung von EC-Couplons wurde von mir auf zweierlei Weise quantifiziert. In Messungen mit dem Kalziumindikator Fluo4 benutzte ich den CACLEAN-Algorithmus aus meiner Arbeitsgruppe zur analytischen Identifizierung von funktionellen EK-Couplons. Die zusätzliche Expression des EC-Couplon spezifischen, genetisch kodierten

Kalziumsensors junctin-GCaMP6f erlaubte die exklusive Analyse von Kalziumtransienten in diadischen Kopplungen und die Ergebnisse untermauerte meine Schlussfolgerungen aus den vorherigen Fluo4 Messungen. Beide Methoden zeigten eine hohe Ko-Lokalisation zwischen *de-novo* T-Tubuli und funktionellen EC-Couplons. Mein Daten demonstrierten somit das hohe Potenzial einer Expression von BIN1-Isoformen mit exon11 für die Verbesserung sowohl der Struktur wie auch der EK-Kopplung in hiPSC-CMs.

In der vorliegenden Dissertation habe ich erstmals ein für gesunde menschliche Herzen einzigartiges Expressionsmuster für BIN1-Isoformen identifiziert. Diese BIN1-Varianten zeigen in adulten Ventrikelzellen aus der Ratte unterschiedliche Kapazitäten sowohl bei der Neubildung wie auch beim Erhalt von T-Tubuli. Sowohl die Ko-Lokalisation von Schlüsselproteinen für die EK-Kopplung als auch die EK-Kopplung selber waren in den BIN1-überexprimierenden adulten Herzmuskelzellen unter beiden Bedingungen signifikant verbessert. Dies gilt im Besonderen für solche BIN1-Varianten, die exon11 beinhalteten, da ihre Effizienz den drei anderen splice Varianten überlegen war. BIN1-Isoformen mit exon11 wurden dann ebenfalls in hiPS-CMs untersucht, die üblicherweise keine T-Tubuli zeigten. Ihre Expression induzierte die *de-novo* Ausbildung eines komplexen Netzwerks von T-Tubuli und substanziell verbessertes und schnellere EK-Kopplung. Die BIN1 Expression führte zu de-novo T-Tubuli, die mit EC-Couplon dekoriert waren. Dies erachte ich als mechanistische Grundlage der verbesserten EK-Kopplung. Als Fazit kann zusammengefasst werden, dass BIN1 als mögliche neue Zielstruktur für die Therapie von Herzinsuffizienz und der substanziellen Verbesserung der hiPSC-CMs Differenzierung hin zu einem mehr adulten Phänotyp angesehen werden kann.

3. Introduction

3.1 Cardiac physiology and EC-coupling

3.1.1 Physiological function of the heart

The circulation system, or cardiovascular system, is extremely important for the homeostasis of the human body. It provides all the tissues and organs with blood perfusion containing oxygen and various nutrients, which are necessary for all cellular activities. The cardiovascular system acts like an irrigating system, which is composed of a regulatory center in the brain, a power source in the heart, and a pipeline network involving various types of vessels spreading throughout the human body. The heart itself consists of four muscular chambers: two atria and two ventricles, the former is responsible for collecting blood via veins while the latter delivering blood to every single corner of the body via arteries. Due to its special structure and function, the heart, undoubtedly, sits in the center of the entire system.

The normal function of the heart relies on its unique electrophysiological as well as contractile properties. Particularly, cardiac muscle can contract autonomously and regularly in an orderly manner, producing a strong force that drives blood to the terminal microcirculation. To generate such rhythmical movements, it is essential for the cardiac muscle to transform electrical signals arising from certain types of heart cells, or pacemaker cells, to mechanical movements by working cardiomyocytes, the process of which is referred to as Excitation-Contraction Coupling (ECC). ECC is one of the most fundamental mechanisms regulating the function of cardiomyocytes, which will be dramatically affected if impaired.

3.1.2 Cardiac conduction system

To fulfill its normal systolic and diastolic function, the contraction and dilation of the cardiac chambers, the heart heavily depends on its unique electrophysiological property, which is regulated by a sophisticated electrical conduction system that is embedded in the cardiac tissue. The conduction system is composed of several types of highly specialized and autonomous cardiomyocytes that are intrinsically able to rhythmically depolarize and initiate action potentials, and work in a coordinated manner to govern surrounding working myocardium, giving rise to the sequential systolic and diastolic movements of the heart chambers (**Fig. 3.1**). Generally, cardiomyocytes can be categorized into two groups: pacemakers and non-pacemakers. The pacemakers can be further divided into a primary and secondary group. The primary pacemakers refer to those cells located in the sinoatrial node (SAN) while the secondary pacemakers comprise the atrioventricular node (AVN), bundles of His, and the Purkinje fibers. The SAN was discovered and confirmed as the site of origin of the cardiac electrical impulse by Arthur Keith and Martin Flack in 1906 (Keith & Flack 1907). Buried in the upper posterior area of the right atrium close to the entrance of the vena cava superior, the SAN serves as the primary pacemaker, which automatically produces electrical pulses that determine the rate and rhythm over other conductive cells and the cells of the working myocardium. The AVN was discovered as the origin of His Bundle by Sunao Tawara in 1906

(SUMA 2003). These cells, situated in the inferior/posterior region of the interatrial septum, act as the bridge of signal transmission from the atria to the ventricles. The Bundle of His was founded by Wilhelm His Jr in 1893 as a muscle bundle down the SAN and uniting the atrial and ventricular septal walls (Roguin 2006). Starting from the posterior wall of the right auricle near the atrial septum, the bundle extends along the atrioventricular groove and the upper margin of the ventricular septum until reaching near the aorta where it branches into the right and left limb. Purkinje fibers, however, are elements of the conduction system discovered the earliest by Jan Evangelista Purkinje in 1893 (Matousek & Posner 1969). As the terminal fibers of the Bundle of His, they form the distal part of the cardiac conducting system and are responsible for transducing electrical signals swiftly and uniformly to all ventricular myocytes. Non-pacemakers consist of atrial and ventricular cardiomyocytes, both of which are the working myocardial cells in the heart.

In a normal cardiac cycle, SAN pacemaker cells are the first cells that undergo spontaneous depolarization and produce action potentials of the highest rate (around 60-100 times per minute in humans), which rapidly spread down to the AVN by special conducting pathways in the atrial tissue. Myocytes of the AVN, whose intrinsic rate is around 40-60 times per minute, relays the cardiac impulses and intensifies them. Particularly, SA node holds the signals for around 0.09s and allows the ventricles to be filled with blood from the atria. Therefore, SA node sets the rhythm of the heartbeat while AV node sets the rhythm of cardiac contraction. After that the impulse passes on to the Purkinje network through the short bundle of His located at the inferior end of the interatrial septum. The Purkinje system, which can also produce spontaneous depolarization at the slowest rate (around 30-40 times per minute), spreads down the two sides of the interventricular septum and gives rise to multiple smaller fibers mediating the fast conduction of action potentials throughout the ventricular myocardium. Ventricular cardiomyocytes, therefore, undergo shortening in response to the stimulation from the Purkinje fibers, resulting in systolic contractions of the whole ventricular chambers.

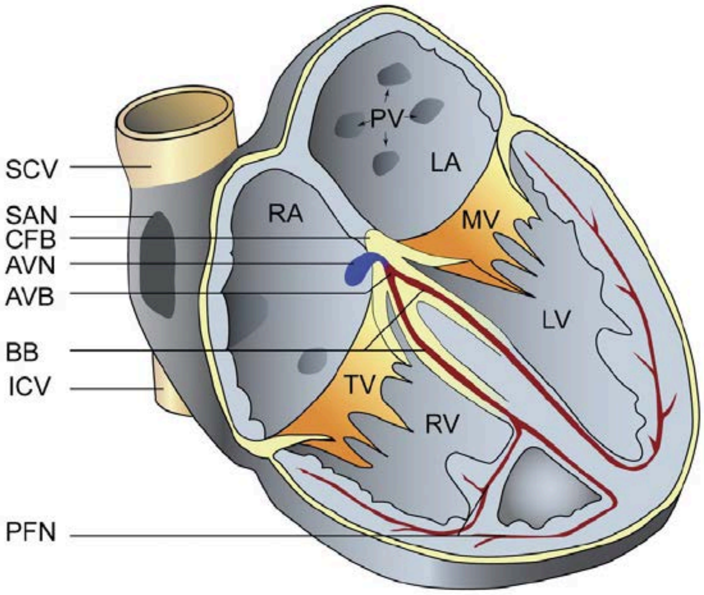

Figure 3.1 Conduction system of human heart. The sinoatrial node (SAN) is located at the entry of the superior vena cava (SCV) in the right atrium (RA). The atrioventricular node (AVN) is situated in an area defined by neighborhood structures: the inferior vena cava (ICV), the central fibrous body (CFB), and the tricuspid valve (TV). Continuing with the AVN, the atrioventricular bundle (AVB) divides into the bundle branches (BB), which originate the left and right Purkinje fiber networks (PFN). Other structures: LA, left atrium; PV, pulmonary veins; MV, mitral valve; RV, right ventricle; LV, left

ventricle. The figure was taken from Mangoni M E and Nargeot J. Physiological reviews, 2008, 88(3): 919-982.

3.1.3 Electrophysiology of cardiomyocytes

On the cellular level, the membrane action potential plays a critical role during the conducting process. There are a vast number of ion channels in the sarcolemma including sodium, potassium, and calcium channels, which act together to initiate action potentials. Generally, an action potential consists of several stages, which are mediated by the activity of different ion channels. For non-pacemaking or working cardiac myocytes, there are generally four phases (**Fig. 3.2**). The resting membrane potential is mainly produced by the outward K^+ currents (I_{K1}) due to K^+ leak through K_1 channels due to their high permeability for K^+, which is referred to as phase 4 of the action potential (Grant 2009). When the membrane is depolarized to a certain voltage level (around -70mV), the K^+ channels close and the fast Na^+ channels are activated and opens, rapidly increasing the membrane potential. The influx of Ca^{2+} through the slow L-type Ca^{2+} channels (LTCC) also contributes slightly to the depolarization effect. As a result, altered conductance depolarizes the membrane potential towards a positive equilibrium potential for Na^+ and Ca^{2+} while conversely away from K^+ equilibrium potential, which is termed as the phase 0 (Grant 2009; Nerbonne & Kass 2005). Followed by the closing of fast Na^+ channels and opening of another special K^+ channels (K_{to}), the membrane is slightly repolarized, which is referred to as phase 1 (Grant 2009; Nerbonne & Kass 2005; Schmitt et al. 2014). However, contrary to the transient Na+ inward, the entry of Ca^{2+} through LTCCs continues, causing another slow period of depolarization after phase1, or the phase 2 plateau. When the Ca^{2+} channels close, another type of K^+ channel (K_r) begins to work, yielding an outward K^+ current and thus repolarization, which is phase 3 (Grant 2009; Nerbonne & Kass 2005; Schmitt et al. 2014). The decrease of inward Ca^{2+} currents combined with the rise of outward K^+ currents finally brings about the complete repolarization of the cell membrane and restoration of the resting membrane potential which is then maintained by the opening of K_1 channels.

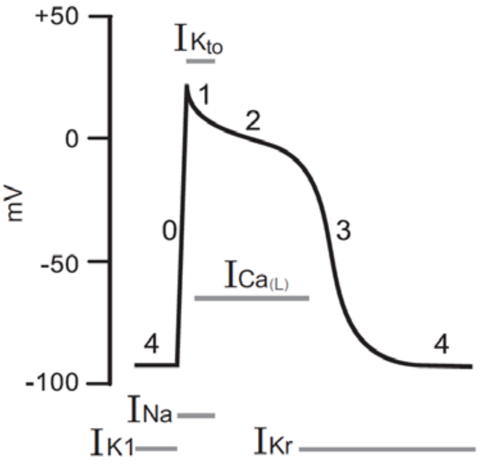

Figure 3.2 Action potential of non-pacemakers generated by different ion currents (*I*). 0-4: different phases of the action potential. Gray horizontal bars: time period of ion currents mediated by different channels (Na^+, Ca^{2+}, and K^+). Inward Na^+ and Ca^{2+} currents lead to depolarization while outward K+ currents repolarize the membrane. The figure was taken from Klabunde R E. Advances in physiology education, 2017, 41(1): 29-37.

Pacemaker cells, however, have different properties in terms of action potentials compared to working cardiomyocytes due to their unique activities of ion channels. Briefly, there are just three phases in an action potential. Instead of maintaining a stable resting membrane potential, they spontaneously undergo depolarization, which then triggers rapid depolarization followed by fast repolarization without the plateau phase found in ventricular myocytes (Klabunde RE 2012). Owing to these differences, only pacemaker cells are autonomous and regulate the rate and rhythm of the whole myocardium. In a word, action potentials, passing on from one cell to another, and from pacemakers to working cardiomyocytes, are the basis of all electrophysiological activities in cardiomyocytes. It is also responsible for initiating calcium activities across the sarcolemma, which mediates the so-called EC-coupling.

3.1.4 EC-coupling of cardiomyocytes

To convert the electric signal of the membrane into mechanical force by myofilaments within the cardiomyocytes, the unique mechanism of EC-coupling is central (Bers & Perez-Reyes 1999). By definition, EC-coupling is the process through which the electrical excitation mediated by action potentials is transduced into mechanical contractions of cardiomyocytes. This transformation is initially achieved by the co-operation of two ion channels, LTCC on the sarcolemma and RyR on the SR membrane (**Fig. 3.3**). In healthy cardiomyocytes, these two membrane networks are closely associated with each other, creating the structural basis for EC-coupling (Hayashi et al. 2009). Ca^{2+}, on the other hand, acts as the core messenger or link in EC-coupling. Generally, during each cardiac action potential, LTCCs are activated by membrane depolarization, leading to the inflow of Ca^{2+} (Cleemann & Morad 1991). This small amount of Ca^{2+}

entering then binds to the RyRs in the dyadic coupling between the sarcolemma and the SR, resulting in the opening of RyRs and hence large amount of Ca^{2+} released from the SR lumen into the cytoplasm (Bers & Perez-Reyes 1999). This coupling process between LTCCs and RyRs is referred to as calcium-induced calcium release (CICR) (Alexandre Fabiato 1983). With the combination of Ca^{2+} influx and release, the free intracellular Ca^{2+} ([Ca^{2+}]$_i$) within the dyadic cleft can rise to >100 μM rapidly while the global intracellular Ca^{2+} concentration only rises to about 500nM～1μM (Fearnley et al. 2011). Ca^{2+} then binds to the myofilament protein troponin C, thereby inducing the sliding of the two myofilaments (thick and thin), shortening of sarcomeres, and finally the contractile movement (Bers D 2001).

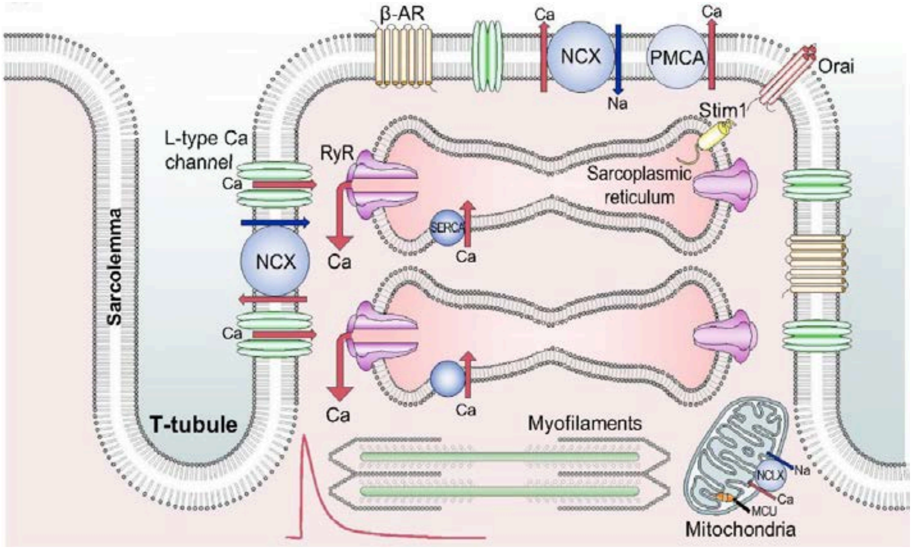
β-AR
Ca
NCX
Na
Ca
PMCA
Orai
Stim1
L-type Ca channel
Ca
RyR
Sarcoplasmic reticulum
SERCA
Ca
NCX
Ca
Sarcolemma
Ca
Ca
Ca
T-tubule
Myofilaments
NCLX
Na
Ca
MCU
Mitochondria

Figure 3.3 Schematic diagram of cardiac EC-coupling structure. It shows different components involved in EC-coupling: sarcolemma, transverse tubule, sarcoplasmic reticulum (SR), and mitochondria, as well as the multiple channels and transporters: L-type calcium channel (LTCC), ryanodine receptor (RyR), sodium-calcium exchanger (NCX), plasma membrane Ca-ATPase (PMCA), sarco/endoplasmic reticulum Ca-ATPase (SERCA). The

figure was taken from Eisner D A, Caldwell J L, Kistamás K, et al. Circulation research, 2017, 121(2): 181-195.

The relaxation of cardiomyocytes is initiated by Ca^{2+} recycling back into the SR or extrusion across the plasma, which is mainly brought about by four transporters, including the SR Ca^{2+}-ATPase, the sarcolemmal Na^{+}/Ca^{2+} exchanger, the sarcolemmal Ca^{2+}-ATPase, and the mitochondrial Ca^{2+} uniport (Periasamy & Huke 2001; Kang & Hilgemann 2004; Bassani et al. 1995; Drago et al. 2012). In the human heart at rest, the time period of each cycle from cardiac membrane depolarization, CICR from the SR, sarcomere shortening, and relaxation to final recovery is around 600 ms with an average heartbeat at approximately 70 times per minute.

3.1.5 L-type calcium channel

The L-type calcium channel or high-voltage-activated Ca^{2+} channel (LTCC or Cav) is one of the most important components of EC-coupling since it mediates the membrane depolarization-induced calcium entry which then triggers the opening of RyRs on the SR membrane. The LTCC channel is a heterotetrameric polypeptide ion protein complex consisting of multiple subunits, which includes a pore-forming α1 subunit, several auxiliary subunits (β, α_2/δ, and γ), and calmodulin (Gao et al. 1997; Bers & Perez-Reyes 1999). The LTCC α1 subunit contains four repeated transmembrane domains (I-IV) and each motif consists of six membrane-spanning α-helices (S1-S6) connected by loops (linkers) between the S5 and S6 areas in the cytoplasmic side. These motifs construct the main body of LTCC as well as the voltage sensor. So far, multiple α1 subunits of LTCC have been identified (Catterall et al. 2005). Generally, these α1 subunits can be categorized into four groups: Cav1.1 (α_{1S}), Cav1.2 (α_{1C}), Cav1.3 (α_{1D}), and Cav1.4 (α_{1F}) which are encoded by different genes and define the specific type of L-type Ca^{2+} channels (Bodi et al. 2005). Among them, Cav1.2$_{\mathbf{\alpha 1C}}$ (dihydropyridine-sensitive [DHP-sensitive]) is the dominant one highly expressed in cardiomyocytes while the others are expressed in other types of tissues such as skeletal muscle ($Cav_{1.1}$), neurons ($Cav_{1.3}$) and, retina ($Cav_{1.4}$). The large α1 subunits are the central building blocks and define most of the pharmacological and gating properties of LTCC. As for accessory subunits, they are bound to the α1 subunit to form the hetero-oligometric macroprotein, modulating its biophysical properties as well as targeting it to the cell membrane (Catterall et al. 2005; Catterall 2011; Dolphin 2012).

3.1.6 Ryanodine receptor

Another critical component of EC-coupling in both cardiac and skeletal myocytes are the ryanodine receptors located in the sarcoplasmic/endoplasmic reticulum membrane. They mediate Ca^{2+} release from the SR when activated by cytosolic increases in Ca^{2+}. The discovery of RyRs is associated with the plant alkaloid ryanodine, which has a high and specific affinity to RyRs and is being used to study the functional properties of the channel (Inui et al. 1987; Lai et al. 1988; Chu et al. 1990). Currently, there are three known mammalian types of RyR: RyR1, RyR2, and RyR3. Human RyR1 is encoded by a gene located on chromosome

19q13.2 with 104 exons, which is mostly expressed in skeletal muscle and localized in the junctional SR membrane (Takeshima et al. 1989; Zorzato et al. 1990; Franzini-Armstrong et al. 1999). There is also expressions of RyR1 in other types of tissue such as cardiac muscle, kidney, and cerebellum, but at low levels (Neylon et al. 1995; Nakai et al. 1990; Furuichi et al. 1994). RyR2 is encoded by a gene located on chromosome1q43 and contains 102 exons. RyR2 is the dominant isoform expressed in cardiac muscles (Nakai et al. 1990). Additional expression of RyR2 is found in Purkinje cells of the cerebellum and the cerebral cortex, and low levels of it are also reported in other tissues (Nakanishi et al. 1992; Sharp et al. 1993; Furuichi et al. 1994). As for RyR3, it is encoded by a gene on chromosome15q13.3-14 and spans 103 exons. It is widely expressed in a variety of tissues including the brain, striated muscles as well as multiple internal organs (Furuichi et al. 1994; Neylon et al. 1995; Giannini et al. 1992).

The activity of RyRs is regulated by a multitude of factors, including $Cav_{1.1}/_{1.2}$, PKA, FKBP12 and 12.6, calmodulin, CaMKII, triadin, junctin, and calsequestrin. All these proteins together with RyR form the core part of the macromolecular complex, which is responsible for Ca^{2+} release from the SR. All RyR isoforms possess similar properties with respect to their permeability with a high conductance for monovalent and divalent cations, and relatively low selectivity for Ca^{2+} (Fill & Copello 2002). RyR1 in skeletal muscles is activated by way of direct protein-protein interactions with the L-type calcium channel ($Cav_{1.1}$) to release Ca^{2+} from the SR evoking muscle contraction. Similarly, RyR2 is functionally triggered by the Ca^{2+} influx from $Cav_{\mathbf{1.2}}$ and predominantly mediates Ca^{2+} release in cardiomyocytes. RyR2 normally remains closed at low systolic [Ca^{2+}] (around 100-200nM) during cardiac diastole while its open probability increases at submicromolar systolic [Ca^{2+}] when Ca^{2+} binds to the high-affinity binding sites (Copello et al. 1997). The channel activity reaches its maximum when $[Ca^{2+}]_{cyto}$ comes to around at 10uM; however, when the Ca^{2+} concentration keeps rising, the open probability of RyR2 will subsequently decrease because of Ca^{2+} binding to low-affinity inhibitory sites in RyR2 (Copello et al. 1997; Laver et al. 1995; Ching et al. 2000). The membrane voltage-sensitive LTCC, which mediates Ca^{2+} influx during membrane depolarization, couples with RyR2, which tightly controls Ca^{2+} release from SR, Together they form the EC-coupling machinery, which is critical to cardiac function.

3.1.7 Nanoscopic structures of calcium release units

LTCCs and RyRs establish EC-coupling through very fine and exquisite interactions on the nanoscale in the dyadic space. LTCCs provide the trigger by mediating calcium influx for the coupled RyRs to initiate the much stronger calcium release from the SR. This process is the molecular basis of CICR. Previously, it was believed that the release sites were arranged in a 'common pool' without a special pattern (Stern 1992). A single LTCC activates a single RyR, which then activate adjacent RyRs through CICR, and eventually engulfing all RyRs. However, such a mechanism was not able to explain the fact that Ca^{2+} release can be graded instead of an all-or-none reaction (New & Trautwein 1972). Therefore, another model was consequently suggested:

LTCCs and RyRs were actually distributed in special patterns, or geometrically separated clusters, referred to as the ’cluster bomb model’ (Stern 1992). In this scenario, a LTCC only gates one or a limited number of RyRs, and clusters are sufficiently separated from each other by a distance that can avoid activating adjacent clusters. This model has been verified by studies reporting that clusters of LTCCs and RyRs couple with each other in a narrow junctional gap between SR and sarcolemmal membranes (around10-15nm) (Stern et al. 1997; Franzini-Armstrong et al. 1999; Cannell et al. 1995). This is also supported by the observation of spatially isolated Ca^{2+}sparks, providing the basis for the local Ca^{2+} control theory (Cheng et al. 1993).

With the application of super-resolution microscopy, more details of the organization of calcium release units have been revealed. It has been found that unlike RyR1s in skeletal muscles, RyR2s in cardiomyocytes are actually not regularly distributed in ’checkerboard’ patterns but arranged in an irregular way, including clusters of different sizes and patterns. For example, it was previously estimated that there were about 75-100 RyR2s in a single cluster (Yin & Lai 2000). However, recent studies found that clusters were irregularly packed and of different sizes with a much smaller average number of around 14-15 RyRs (Soeller & Baddeley 2013; Macquaide et al. 2015). Various studies have suggested that the properties of RyR2 clusters such as organization and size are able to impact the calcium release channels in multiple ways, including the sensitivity of activation (Sobie et al. 2006), termination of release (Soeller & Baddeley

2013), spark fidelity as well as spark durations (Walker et al. 2014; Sato et al. 2016).

One of the most significant features of the RyR channel is its clustering, which is believed to be due to allosteric coupling between channels enabling coupled gating (Marx et al. 2001; J. Gaburjakova & M. Gaburjakova 2014). Coupled RyR2 channels exhibit different properties distributed from single or orphaned channels with a longer period of opening and closing (Marx et al. 2001). Recent advances suggest that RyR2 channels cluster in two patterns of arrangement: **“**adjoining” and “oblique” (Cabra et al. 2016). The adjoining interaction is through side-by-side clustering while the oblique manner is to form the “checkerboard” pattern but with an angle of around 12° instead of being parallel. Because of this asymmetric interaction, it is therefore sterically difficult to establish a continuous checkerboard pattern resulting in an irregular and branched array. This is consistent with observations in cardiac tissue (Macquaide et al. 2015; Baddeley et al. 2009; Chen-Izu et al. 2006). Packing of RyR2 in such a manner has also been observed in rat ventricular cardiomyocytes. This study found that these two types of arrangement were labile or interchangeable under different conditions (Asghari et al. 2014). For example, high Mg^{2+} concentrantions favor the clustering in side-by-side way while low Mg^{2+} environment or phosphorylation promotes the oblique arrangement. However, it is still not fully clear about the detailed microarchitecture in nanoscale due to limitations such as the resolution of microscopy.

It has been suggested that alterations of the RyR organization are related to cardiac disease. For example, alterations of the cluster packing have been observed in cardiomyocytes from animals with atrial fibrillation (Macquaide et al. 2015; Sobie et al. 2006). Moreover, there is less allosteric regulation in smaller clusters or clusters with a lower regularity, which become more sensitive and fire more easily (Cheng & Lederer 2008). Similarly, orphaned or unclustered RyRs react differently to local Ca^{2+} changes when compared to clustered channels (Sobie et al. 2006). Changes of the RyR cluster organization may impact the properties of local calcium handling, and then influence the whole levels of calcium cycling in cardiomyocytes. However, it is still not completely clarified. The relationship between clustering patterns and functions of CRUs is far from a thorough understanding. Future investigations are needed to unveil issues such as the organizations of clustering, uniformity among CRUs as well as the effect of clustering pattern on RyR2 functions.

3. 2 Transverse tubules of cardiomyocytes

Since EC-coupling is critical to the function of cardiomyocytes, it is essential to establish effective coupling, LTCC in the sarcolemma and RyR2 in the SR membrane have to be physically close enough and coupled with each other within a nanometer-scale (around 10nm wide) space in a structure called dyad (Franzini-Armstrong et al. 1999). LTCCs couple with a cluster of RyR2 to form the calcium release unit (CRU) (Inoue & Bridge 2003). It is impossible, in normal cells, to build such a pairing microstructure because these two types of membrane structures are generally separated from each other. However, a highly specialized membrane structure, T-tubules, makes it possible to establish such coupling machinery, laying the structural foundation for efficient EC-coupling in cardiomyocytes.

3.2.1 Characteristics of the T-tubule structure

T-tubules are highly specialized, unique, and complex membrane invaginations present both in skeletal and cardiac myocytes (Severs et al. 1985; Sommer 1995) (**Fig. 3.4**). It is found that cardiomyocytes of almost all mammals investigated, such as mice, rats, guinea pigs, rabbits, dogs, and humans, possess T-tubules although there are certain differences across species (Heinzel et al. 2008; Soeller & Cannell 1999; Forbes & van Neil 1988; Haddock et al. 1999; He et al. 2001). T-tubules are predominantly present in ventricular cardiomyocytes whilst absent or severely underdeveloped in non-ventricular cells such as atrial, pacemaking, and conductive cells (Ayettey & Navaratnam 1978; Kirk et al. 2003). The majority of the T-tubule system consists of transverse tubules with a smaller portion of longitudinal extensions connecting the transverse elements (estimated 60% vs. 40%) in the cytoplasm (Forbes et al. 1984; Soeller & Cannell 1999). Most of the T-tubules occur at the Z-disc or the end of sarcomeres, with an interval of approximately 2μm, and only a small proportion of them stretch between the Z lines, resulting in a more complex transverse-axial tubular network in cardiomyocyte (Soeller & Cannell 1999).

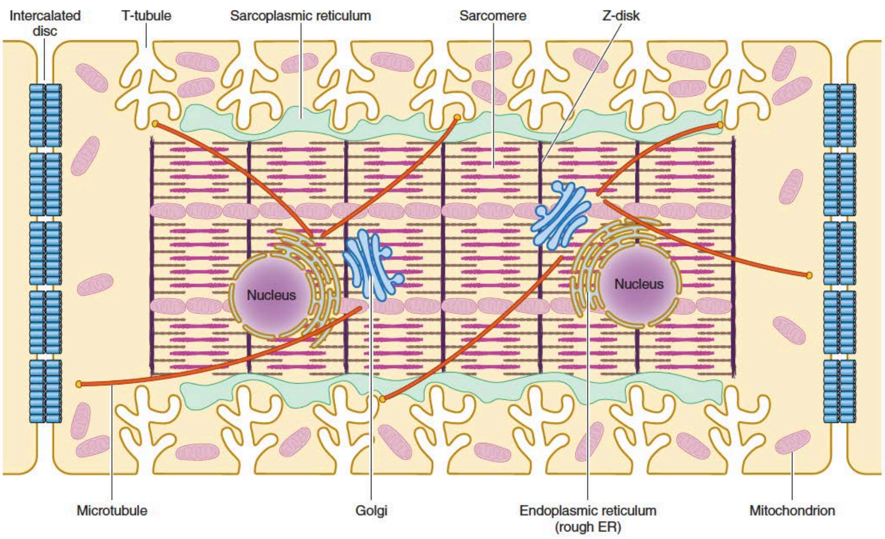
Intercalated disc
T-tubule
Sarcoplasmic reticulum
Sarcomere
Z-disk
Nucleus
Nucleus
Microtubule
Golgi
Endoplasmic reticulum (rough ER)
Mitochondrion

Figure 3.4 Schematic illustration of the T-tubule system and other internal structures of adult ventricular cardiomyocytes. T-tubules are invaginations of the plasma membrane, closely positioned near the sarcoplasmic reticulum. Sarcomeres are the units of cardiac contraction upon calcium binding. The Golgi apparatus and microtubules are responsible for the trafficking of ion channels to certain subdomains of the sarcolemma. Mitochondria are the cell power plant. Intercalated discs distribute at the longitudinal sides of the cell, which is necessary for intercellular propagation of action potentials. The figure was taken from Hong TT and Shaw R M. Physiological reviews, 2016, 97(1): 227-252.

Quantitative studies based on advanced microscopic and electrophysiological methods have revealed that the average luminal diameter of T-tubules is around 200 nm in murine and around 400nm in rabbit and human, apparently different from that in skeletal myocytes with the diameters range within a smaller scale（20 to 40 nm) (Wagner et al. 2012; Savio-Galimberti et al. 2008; Cannell et al. 2006; Franzini-Armstrong et al. 1975). It is estimated that the volume of T-tubules occupies only 1-3% of the total cell volume (Soeller & Cannell 1999). However, the percentage of plasma membrane located in T-tubules is much higher, making up a significant proportion of the whole sarcolemma, varying from 21% to 64% with an average of one-third of the entire plasma membrane (Severs et al. 1985; Soeller & Cannell 1999). The high proportion of the T-tubule membrane in sarcolemma is of great importance because the efficiency of EC-coupling would be dramatically decreased without sufficient membrane folding. Particularly, the membrane capacitance of T-tubules constitutes around 30% of the total membrane capacitance and more than 85% of LTCC current, reflecting their special and indispensable role in the electrophysiological properties of cardiomyocytes (Kawai et al. 1999).

It is believed that there are differences across species in terms of T-tubule density in cardiomyocytes. Early researches have showed that the density of tubules correlates with heart rates across species. For example, the density of T-tubules is greater in the rodents such as mice and rats than in large mammalian animals. Accordingly, the heart rate of rodents at rest (300-400bpm) is much higher than that of large mammalian animals such as rabbit, pig, and human (<100bpm) (Page & Surdyk-Droske 1979; Heinzel et al. 2008; Heinzel et al. 2002). It may be due to the fact that denser T-tubules are more efficient in Ca^{2+} cycling, which leads to more frequent and synchronous activations of the cells during EC-coupling. However, the situation for atrial cardiomyocytes is the opposite. Generally, atrial cells of rodents only have very scarce tubules while there is a heterogeneous distribution of tubules in mammalian atrial myocytes with more fractions of longitudinal components (Kirk et al. 2003; Tidball et al. 1991; Lenaerts et al. 2009; Richards et al. 2011).

3.2.2 Importance of T-tubules for cardiac EC-coupling

As previously mentioned, the outer cell membrane is physically separated from the inner ER membrane, which makes it almost impossible to form close connections between them in most cell types. However, T-tubules in cardiomyocytes bridge the gap. The very unique and most important role of T-tubules is to provide a structural basis for the coupling of the two membrane networks (**Fig. 3.5**). Depolarization of the cell membrane leads to Ca^{2+} influx via LTCCs that subsequently triggers the Ca^{2+} release from SR through RyR2s, a process referred to as calcium-induced calcium release (CICR). This process relies on the juxtaposition or coupling of sarcolemmal LTCCs and the SR-located RyR2s, which appose with each other and form a narrow space (10-15nm), or dyad. T-tubules, with their close proximity to SR, is exactly the key element in building such a dyadic microstructure (Brette et al. 2006; Franzini-Armstrong et al. 1999; GA & A 1996). Although only one-third of the membrane capacitance rises from T-tubules, the majority of Ca^{2+} influx that activates RyR2-mediated Ca^{2+} release from the SR occurs across T-tubules. As the major source of Ca^{2+} trigger, it is estimated that more than three-quarters of the LTCC current are mediated by T-tubules. This is largely because the distribution of LTCC in sarcolemma is not even, with a much higher fraction in the T-tubules than in the surface sarcolemma (Scriven et al. 2000).

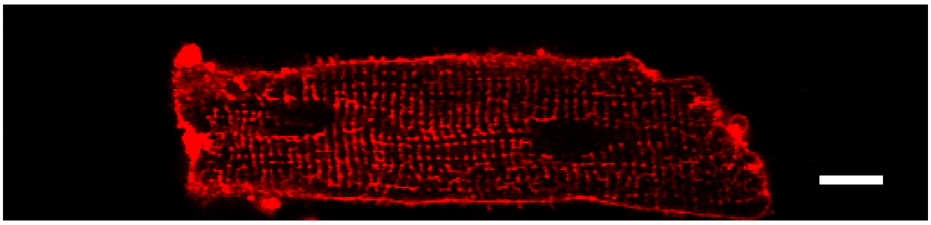

Figure 3.5 Membrane staining of T-tubules in rat cardiomyocytes. The cell membrane of freshly isolated cardiomyocytes was stained by CellMask DeepRed (red). Multiple transverse tubules can be seen inside the cell. Scale = 10 μm.

The myofilaments are the contractile complexes responsible for the contraction of cardiomyocytes. They are organized into sarcomeres and mostly located in the inner area of cell volume. When released from the SR into the sarcoplasm, Ca^{2+} binds to the troponin of myofilaments and initiates the movement of filaments that leads to the muscle contraction. T-tubules play a critical role in this process. When cells lose T-tubules, the Ca^{2+} influx from the sarcolemma spreads from the periphery of the cell into the centre mainly by simple diffusions, which initially activates the peripheral sarcomeres instead of those in deep areas. This temporally inconsistent activation of sarcomeres will result in unequal contractions between the outer area and inner area of the cardiomyocytes, leading to the production of sub-maximal forces (Hüser et al. 1996). Obviously, it is much less efficient than that in cells with T-tubules where Ca^{2+}, triggered by CICR from SR, can simultaneously and uniformly propagate to all myofilaments without significant delays between different areas.

In addition, T-tubules, with their narrow tubular structure, also create a barrier that restricts the diffusion of extracellular fluid in which the concentration of ions is relatively stable compared with the non-tubular extracellular space. It has been demonstrated that a structural “fuzzy space” or “slow diffusion zone” presents inside the T-tubules (Lederer et al. 1990; Swift et al. 2006; T. Hong et al. 2014). This is of great importance because it serves as a physical barrier restricting ion flow and deters the interference from the fluctuation of the extracellular environment and contributing to the homeostasis of cardiomyocytes (T. Hong et al. 2014).

Moreover, instead of being a pure membrane compartment, T-tubules are now increasingly considered as a nonuniform membrane network composed of various special microdomains that are essential to cardiomyocytes. For example, it was identified that the membranes on the sides of T-tubules are actually not simply straight and smooth, but instead with quite complex microfolds (T. Hong et al. 2014). These microfolds are sculpted by BIN1, a membrane folding protein participating in tubule biogenesis (discussed in a later section). Most LTCCs are enriched in T-tubules and localized to BIN1 through targeted trafficking by BIN1. They are responsible for around 80% of the membrane calcium current (T.-T. Hong et al. 2010). Moreover, it is suggested that BIN1-microfolds are not only enriched with LTCC but also attract RyRs from the junctional SR membrane (Y. Fu et al. 2016). Therefore, these special T-tubular microdomains play an important role in organizing cardiac dyads. The caveolae, another well-identified type of membrane subdomains, is found to be connected to both general sarcolemma and T-tubules in cardiomyocytes, expanding to the overall membrane area by 14-21% (Page 1978). It not only increases the complexity of T-tubules, but also acts as subdomains that concentrate different ion channels and signaling molecules for local regulation. For instance, many ion channels such as LTCC, Potassium Voltage-Gated Channel Subfamily A Member 5 (Kv1.5), Voltage-gated sodium channel Nav1.5 (Nav1.5), sodium-calcium exchanger (NCX) as well as signaling molecules like β-adrenergic receptors are enriched in caveoli (Wright et al. 2014; Balijepalli & Kamp 2008). In addition to BIN1-related microfolds and caveoli, another type of subdomains determined by ankyrin B, a membrane scaffolding protein, has been identified. It plays a vital role in the establishment of the macromolecular complex of NCX, sodium-potassium-ATPase (NKA), and inositol trisphosphate receptor (InsP3). This NCX/NKA/InsP3 complex is very important in transporting calcium out from the dyads between T-tubules and SR membrane, which facilitates muscle relaxation by reducing calcium concentration (Mohler et al. 2005). Therefore, under the cooperation of these different T-tubule-related microdomains, the calcium entry and removal in cardiomyocytes can be accurately regulated and balanced to maintain coordinated normal cardiac contraction.

3.2.3 Mechanisms of T-tubule biogenesis

T-tubule development in mammals starts relatively late. It is completed in the perinatal stage and is considered as a continuous process of membrane invagination. Generally, according to previous observations, T-tubules initiate at the peripheral area of the plasma membrane accompanied by the proliferation of caveolae that represent another type of small membrane invaginations lined by caveolin-3, the cardiac–specific splice variant of caveolin (Ezerman & Ishikawa 1967; Way & Parton 1995; Parton et al. 1997). Moreover, caveolin-3 is distributed together with T-tubules both in developing and adult cardiomyocytes. Therefore, caveolae formation may be an initial and esential step for the generation of T-tubules. In other words, caveolin acts as a trigger and location signal for the occurrence of deep membrane folding by establishing small and shallow membrane pits (Parton et al. 1997). Therefore, T-tubule biogenesis is considered as a process originating from peripheral invagination to extension and penetration of membrane folding towards the central part of the cell. This has been observed in both skeletal and cardiac myocytes (Forbes & Sperelakis 1976; Ferguson & Leeson 1983; Sedarat et al. 2000; Ishikawa 1968; Franzini-Armstrong 1991; Flucher et al. 1993; Takekura et al. 1993).

T-tubules are continuous with the sarcolemma and comprise both lipids and proteins. If caveolae provides the initiation signal, then another critical question about T-tubule biogenesis is how the membrane invaginations penetrate into the center of the cells and form long tubular structures. Moreover, exactly how key components of EC-couplons -LTCCs and RyR2- are assembled correctly into CRUs is to a great extent unknown. Two models have been proposed. One suggested that the lipids and proteins of the sarcolemma directly add to and flow inwardly into the elongating invaginations (from outside in) while the other believed that these building blocks were firstly synthesized and assembled in the cytoplasm and then added to the growing tubules (from inside out) (Di Maio et al. 2007). In the first scenario, LTCCs are trafficked via exocytosis into surface sarcolemma and developing

T-tubules initiated at caveolae in the peripheral sarcolemma. RyRs in SR dock and establish coupling with LTCCs, leading to peripheral coupling or dyadic pairing. Early studies have found in differentiating rabbit cardiomyocytes that, LTCCs are only distributed at the peripheral area of sarcolemma while RyRs can be observed both in the peripheral and interior areas (Sedarat et al. 2000). Only when T-tubules extend into the cell, LTCCs and CRUs can be found in the cell, which is consistent with the first scenario. However, other reports also found that in addition to T-tubules that connected with the surface sarcolemma, there were tubular components not continuous with the plasma membrane, indicating that a fraction of T-tubules is not derived from surface membrane but from internal synthesis, which proposed another possibility (Di Maio et al. 2007). In the second scenario, LTCCs-containing T-tubule building blocks and RyR-bearing vesicles are firstly produced and then establish an association with each other in the cytoplasm before fusing with nascent T-tubules and junctional SR network respectively. However, it is most likely that these two mechanisms coexist during the process of T-tubule development. While T-tubules are established from the cell periphery into the center and LTCCs are recruited to the tubular membrane through specific proteins such as BIN1 (discussed latter), RyR-bearing SR components are delivered close to T-tubules, form dyads as well as CRUs with the help of other proteins such as junctophilin-2 which helps to position RyR/LTCC couplings and bridge the dyadic space. This hybrid model is consistent with observations that the presence of RyRs are anterior to the appearance of LTCC clusters in differentiating cardiomyocytes; only when T-tubules start to develop, colocalizations of them can be found (Seki et al. 2003; Scriven et al. 2002). However, direct evidence for these models is still missing.

3.2.4 Regulation of T-tubule biogenesis

As the core structure for EC-coupling, T-tubules are not always present during the development. Instead, T-tubules are not present in embryonic cardiomyocytes until after birth according to previous reports (Flucher et al. 1993; Haddock et al. 1999; Seki et al. 2003; B. Chen et al. 2013; Reynolds et al. 2013). For example, studies in murine depicted that there is little evidence of T-tubules in ventricular cardiomyocytes of the neonatal heart even at postnatal Day8 and tubules did not appear until Day10 (B. Chen et al. 2013). Starting at postnatal Day10, T-tubules increased progressively until Day19 when the T-tubular system appeared completely mature, similar to that of adult mouse cardiomyocytes (B. Chen et al. 2013). In addition, the T-tubule system is not a static system that is unchangeable. In contrast, it is actually labile under different conditions. For example, when isolated and cultured *in vitro*, adult cardiomyocytes show a continuous reduction of T-tubule density, accompanied by a significant decrease in EC-coupling (Mitcheson et al. 1996). Moreover, T-tubule structure can be remodeled under many pathophysiological conditions such as increased cardiac ventricular stress, cardiac hypertrophy, cardiac ischemia, and heart failure, further suggesting that the T-tubule system is in a dynamic status (Frisk et al. 2016; Heinzel et al. 2008; Wei et al. 2010; Caldwell et al. 2014). Despite the fact that the development of T-tubules is spatially and temporally regulated along with embryogenesis, especially in the postnatal period, the underlying mechanisms are still not fully understood. So far as we know, several proteins have been demonstrated to participate in the generation and maintenance of the T-tubule system in cardiomyocytes (**Fig. 3.6**).

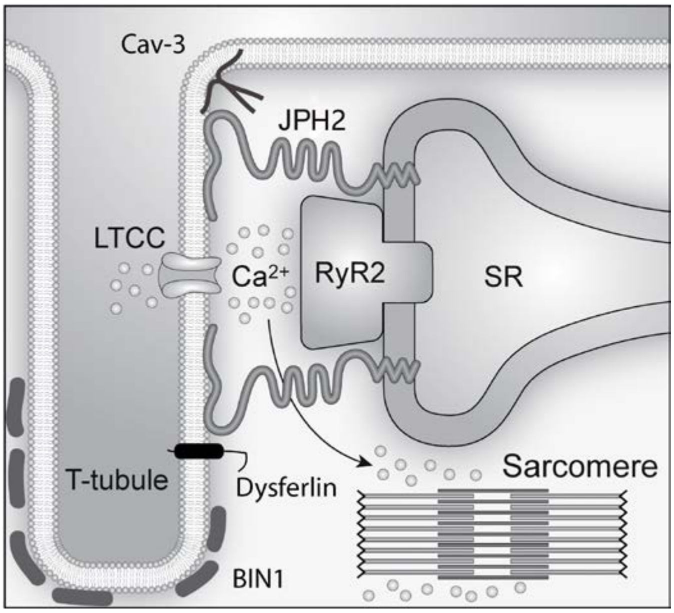

Figure 3.6 Schematic illustrations of proteins involved in T-tubule biogenesis. Several proteins are associated with T-tubule genesis in cardiomyocytes: Bridge integrator1 (BIN1), junctophilin2 (JPH2), caveolin-3 (Cav-3), and Dysferlin. The figure was taken with some modifications from Song, Long-Sheng, Ang Guo, and Richard Z. Lin. "MicroRNA: a toolkit fine-tuning the dyadic “fuzzy space”?" (2012): 816-818.

Amphiphysin2, also known as BIN1 belongs to the N-BAR domain family and is found to play a key role in T-tubule generation both in skeletal and cardiac myocytes. Early studies have found that BIN1 is expressed at high levels in skeletal muscle, located at T-tubules, and is necessary for their formation (Wechsler-Reya et al. 1998; Lee et al. 2002). Mutation or altered splicing of BIN1 in skeletal muscles can cause various kinds of centronuclear myopathy in human (Fugier et al. 2011; Böhm et al. 2010; Böhm et al. 2013; Böhm et al. 2014; L. L. Smith et al. 2014). In addition to skeletal muscle, BIN1 is also highly expressed in the heart. Particularly, studies in mice have revealed that several BIN1 isoforms are expressed in cardiomyocytes and are responsible for the formation of T-tubule-related membrane invaginations (Hong, T et al.2014). All these data suggest an indispensable role of BIN1 in T-tubule biogenesis. However, the expression and regulation of BIN1 in human cardiomyocytes are still elusive.

Another protein that has been reported to be important for T-tubule generation and maintenance is junctophilin-2 (JPH2), a structural protein localized at the calcium release units spanning the dyadic space (Takeshima et al. 2000). With its one end it binding to the cytoplasmic leaflet of the sarcolemma and the other inserted into the SR membrane, JPH2 acts as the bridge connecting the physical gap between the sarcolemma and the SR membrane, which plays a crucial role in the development and maintenance of EC-coupling microdomain. Previous research using a cardiac-specific short-hairpin-RNA-mediated JPH2 knockdown mouse model depicted that perinatal JPH2 knockdown can prevent T-tubule maturation and result in delayed, asynchronous subcellular Ca^{2+} activation (Reynolds et al. 2013). The perinatal deficiency of JPH2 can lead to congestive heart failure featured or even premature death, indicating its crucial role for cardiac function (Reynolds et al. 2013). Another study reported reflected similar results in that T-tubule maturation and Ca^{2+} handling are dramatically impaired when JPH2 is deficient in mice by cardiac-specific JPH2 knockdown, defining a key role for JPH2 in the maturation of the T-tubule network and the EC-coupling machinery during postnatal period (B. Chen et al. 2013). Human studies have also found that JPH2 mutations are strongly associated with cardiac diseases such as hypertrophic cardiomyopathies and atrial fibrillation (Landstrom et al. 2007; Quick et al. 2017; Beavers et al. 2013). When overexpressed, JPH2 can help attenuate or rescue cardiac function to some extent (Guo et al. 2014). Actually, instead of a pure structural protein, JPH2 might also regulate the function of RyR2 by contributing to its stabilization (Hill & Diwan 2013). However， JPH2 itself holds no capacity to fold plasma membranes, indicating a role distinct from that of BIN1.

Other proteins that are associated with the development of T-tubules include caveolin-3，dysferlin, and NEXN. The initiation of T-tubules is associated to caveolae, a specialized sarcolemma invagination which has a narrow neck with an approximately spherical shape (Gabella 1978). The biogenesis of the T-tubule network is a dynamic process and is believed to have a strong relationship to caveolae, which has been supported by the expression of caveolin-3 in T-tubules of skeletal and cardiac myocytes during development as well as adulthood (Way & Parton 1995; Parton et al. 1997; Voldstedlund et al. 2001). Generally, the formation of SR and peripheral membrane coupling occurs very early during embryogenesis, and becomes obvious prior to the appearance of T-tubules and dyads in mammal cardiomyocytes. The onset of T-tubule development at the cell periphery is in parallel to the emergence of caveolae with which T-tubules are connected (Ezerman & Ishikawa 1967). This indicates that the establishment of caveolae mediated by caveolin-3, enables the curving of cell membrane and is an essential step to membrane invagination (Parton et al. 1997). In other words, caveolin-3 may assist the development of T-tubule network by initiating the curving of the cell membrane and directing the membrane lipids for further invaginations that extend to the inner area of skeletal and cardiac myocytes. As for dysferlin, which belongs to the family of genes analogous to Caenorhabditis elegans ferlin, researches have implicated that it is involved in T-tubules formation in addition to its role in membrane repair in skeletal muscles (Bansal et al. 2003; Klinge et al. 2007; Klinge et al. 2010; Hofhuis et al. 2017). However, there is currently no evidence that dysferlin is involved in the T-tubule biogenesis of cardiomyocytes. In terms of NEXN, it was primarily isolated from rat brain and fibroblasts as a protein that can bind to actin filament (Ohtsuka et al. 1998). Particularly, it was identified to be a Z-disc protein enriched in cardiac myocytes. Reports have suggested that mutations of NEXN are associated with cardiomyopathies (Hassel et al. 2009; H. Wang et al. 2010). Global knockout of Nexn in mice can cause rapidly progressive cardiomyopathy, leading to lethality shortly after birth (Aherrahrou et al. 2015). These findings highlight its vital role in cardiac function2. Recently, several studies have found that NEXN may play an important role in T-tubule formation. Instead of being a Z-disk protein as previously considered, NEXN can interact with SR proteins and is required for T-tubule biogenesis. When Nexn was knocked out from cardiomyocytes, T-tubule development in the early stage and its maintenance in the adulthood were both impaired. Consequently, the association between the SR and sarcolemma was undermined, resulting in altered Ca^{2+} handling and cardiac function (C. Liu et al. 2019; Spinozzi et al. 2020). However, the precise mechanism of how NEXN regulates T-tubule architecture is not fully understood.

3.3 Amphiphysin 2/ BIN1

3.3.1 BIN1 gene and splice variants

Bridging integrator-1 (BIN1), also known as amphiphysin2, MYC box-dependent interacting protein-1 or SH3P9, is a commonly expressed nucleocytoplasmic protein that was initially identified as a factor able to bind to the MYC, a transcriptional factor, and also an interactor of the tyrosine kinase-Src SH3 ligand peptide (Butler et al. 1997; Sakamuro et al. 1996; Sparks et al. 1996). It has been described that BIN1 is involved in many cellular activities including cell endocytosis, membrane recycling, cytoskeleton regulation, cell cycle control, and apoptosis. When altered, BIN1 is associated with multiple pathophysiological conditions such as tumor progression, centromyopathy, heart dysfunction, and even Alzheimer’s disease (Kennah et al. 2009; Nicot et al. 2007; Muller et al. 2003; Tan et al. 2013).

Human BIN1/amphiphysin 2 and amphiphysin 1 both belong to the amphiphysin family, a type of protein that contains a highly conserved characteristic domain, known as the BAR (Bin-Amphiphysin-Rvs)-domain. This domain is required for their function, particularly the ability to tubulate membranes (Frost et al. 2009; Takei et al. 1999). However, they share only 49% homology of amino acid sequence and possess different properties in terms of expression and function (Leprince et al. 1997; Owen et al. 1998). While amphiphysin 1 was first identified as a brain protein associated with synaptic vesicle endocytosis, BIN1 is found to express more universally with diverse roles in multiple cellular programs (Bauerfeind et al. 1997).

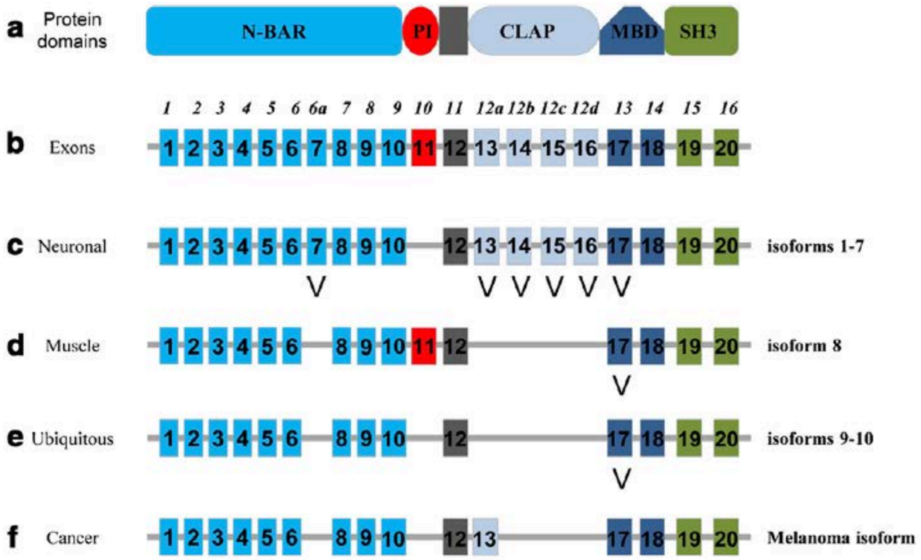
a Protein domains
N-BAR
PI
CLAP
MBD
SH3
1 2 3 4 5 6 6a 7 8 9 10 11 12a 12b 12c 12d 13 14 15 16
b Exons
1 2 3 4 5 6 7 8 9 10 11 12 13 14 15 16 17 18 19 20
c Neuronal
isoforms 1-7
d Muscle
isoform 8
e Ubiquitous
isoforms 9-10
f Cancer
Melanoma isoform
V

Figure 3.7 Schematic illustration of BIN1 functional domains and tissue-specific isoforms. a. BIN1 protein domains: N-BAR domain is involved in membrane invagination; PI domain is involved in phosphoinositides binding; CLAP domain is involved in clathrin and AP2 binding, only present in neuronal isoforms; MBD domain binds to c-Myc and is involved in its regulation; SH3 domain is involved in protein-protein interaction such as dynamin. The domain encoded by exon12 is a linking area. b. Gene organization of BIN1. The main nomenclature used is from NCBI while the italic one is the nomenclature by Weschler-Reya et al. 1997. c-d. Tissue-specific BIN1 isoforms identified in brain (c), skeletal muscle (d), most of other tissues (e), and tumor (f). V shape arrows indicate alternative exons. The figure was taken from Prokic I et al. Journal of molecular medicine, 2014, 92(5): 453-463.

Previous studies have found that BIN1 is ubiquitously and expressed in many tissues, such as brain, retina, striated muscles, lung, liver, and kidney (Tsutsui et al. 1997). BIN1 gene contains 20 exons in total, and different exons encode distinct protein domains. The exons 1-10 are responsible for the N-BAR domain, and exons 19-20 encode the C-terminal SH3 domain, both of which are present in all isoforms. However, due to the splicing of some of the exons, the BIN1 gene can also be transcripted into different isoforms (**Fig. 3.7**). Particularly, some of these isoforms are tissue-specific. For example, isoforms with exon 7,13,14,15, and 16 (isoform 1-7) are mostly brain-specific (Butler et al. 1997; Tsutsui et al. 1997; Ellis et al. 2012). In contrast, exon 11-containing isoforms such as isoform 8 and isoform13, are considered exclusively in skeletal muscles (Mao et al. 1999; Wechsler-Reya et al. 1997; Toussaint et al. 2011). However, isoform 9 and 10 are thought to be ubiquitously expressed across many tissues without particular preference.

3.3.2 Properties of BIN1 domains

The function of BIN1 is highly associated with its structural properties. With multiple exons, the BIN1 protein has several distinct functional domains encoded by different groups of exons. Particularly, the conserved N-terminal BAR domain is encoded by exon1-10 and is shared by all BIN1 isoforms. When in dimerized configuration, it is able to bind to lipid membranes, generating and sensing membrane invaginations (Peter et al. 2004; Frost et al. 2009). This is mediated by the N-terminal amphipathic helix since the surface of the N-BAR domain is positively charged and can interact with the negatively charged phospholipids in the inner leaflet of the plasma membrane (Peter et al. 2004). Exon11 encodes the phosphoinositide (PI) binding motif, a short polybasic sequence that shows an high affinity towards the negatively charged lipids PtdIns (4,5) P_2 and/or PtdIns3P and PtdIns5P and can significantly increase the membrane curvature (Lee et al. 2002; Fugier et al. 2011). Compared to other isoforms, BIN1 isoforms with this motif display distinct properties and play vital roles in striated muscle cells, such as forming T-tubules (Kojima et al. 2004). Another domain is the clathrin and AP2 (CLAP) binding domain, which is encoded by exon13-16 and located between the N-BAR and the SH3 domain (Butler et al. 1997; Tsutsui et al. 1997). Isoforms with this domain are mostly expressed in brain tissue, can bind to the endocytic proteins clathrin and AP2 and this plays an important role in synaptic vesicle endocytosis (Wigge et al. 1997; McMahon et al. 1997). The Myc-binding domain (MBD), next to the SH3 domain, is encoded by exons 17 and 18, which can be found in several BIN1 isoforms and is considered to be related to tumor suppression (Sakamuro et al. 1996). The Src homology3 (SH3) domain, a conserved domain shared by all BIN1 isoforms, is encoded by the last two exons (exon 19 and 20). This domain is crucial for the function of BIN1 because it permits interactions with other proteins such as dynamin2 and myotubularin to regulate cell functions in skeletal muscles (Nicot et al. 2007; Royer et al. 2013; Cowling et al. 2017). Due to these various domains, the function of BIN1 isoforms can be regulated via transcriptional splicing of specific exons.

3.3.3 The role of BIN1 in skeletal myocytes

It is established that BIN1 plays a crucial role in skeletal muscle cells. Early studies found that BIN1 was highly expressed in several types of tissue including skeletal muscles, suggesting its importance for this tissue (Sparks et al. 1996; Sakamuro et al. 1996; Butler et al. 1997). Moreover, BIN1 is upregulated in myotomes or progenitors of skeletal muscle during embryogenesis, and necessary for its differentiation (Wechsler-Reya et al. 1998; Mao et al. 1999). BIN1 can negatively regulate dynamin2 in muscle development and organization (Cowling et al. 2017). More importantly, BIN1 is indispensable for the development of T-tubules and the EC- coupling machinery in skeletal muscles. For example, it has been described in Drosophila found that BIN1, instead of binding clathrin, was located to T-tubules and tubulated lipids *in vitro* (Razzaq et al. 2001). When BIN1 was mutated, it can lead to severe disorganization of T-tubules and the EC-coupling system, hence the flightless of flies (Razzaq et al. 2001). Further studies confirmed that BIN1 was able to fold the plasma membrane in both muscle and non-muscle cells and the effect of tubulation requires the PI motif (Lee et al. 2002). In addition to results from animal experiments, numerous findings in human patients have also demonstrated that mutations or mis-splicings of BIN1 can result in various centronuclear myopathies (CNM), confirming the fundamental role of BIN1 for the function of skeletal muscles (Nicot et al. 2007; Fugier et al. 2011; Böhm et al. 2013; Böhm et al. 2014).

3.3.4 The role of BIN1 in cardiomyocytes

Even though BIN1 has been studied widely and in-depth in skeletal muscles, its role in cardiomyocytes is not fully clarified. Similar to skeletal muscles, heart tissue also has high levels of BIN1 expression located in T-tubules. BIN1 disruption in mice had no obvious impact on endocytosis or cytoskeleton organization; however, its loss leads to perinatal death (Muller et al. 2003). Although no striking abnormalities were found in skeletal muscles of BIN1 knock-out embryos, severe ventricular cardiomyopathy was identified, along with pronounced disorganization of myofibrils in these embryos (Muller et al. 2003). In addition to tubule biogenesis, another important function of BIN1 is that it can specifically localize the LTCC to cardiac T-tubules through a microtubule and BIN1-dependent mechanism, further demonstrating its crucial role in cardiomyocytes (T.-T. Hong et al. 2010). A systematic study in mouse, for the first time, revealed the transcriptional profile of BIN1 isoform in mouse cardiomyocytes, finding that several BIN1 splice variants were expressed, among which the BIN1 variant with both exon13 and exon17 was able to recruit actin for folding T-tubules, creating a ’fuzzy space’ which can buffer ion flux in this restricted compartment (T. Hong et al. 2014). When the level of this isoform is downregulated as seen in cardiomyopathy or heart failure, it brings about T-tubule remodeling and even arrhythmia (T. Hong et al. 2014). Furthermore, it is also found that disruption of BIN1 in the heart precipitates stress- and age-associated dilated cardiomyopathy in mice (Laury-Kleintop et al. 2015). Recently, another study profiled the expression of BIN1 splice variants in rat cardiomyocytes and identified 6 BIN1 isoforms, including those with PI motif encoded by the exon11, which was not found in mouse cardiac myocytes (Lin-Lin Li 2020). It suggested that the PI-containing BIN1 (pBIN1) variant can form robust membrane tubules but cannot anchor to Z-lines. In contrast, the ubiquitous BIN1 isoform (uBIN1) exhibited no affinity to membranes but was able to accummulate along Z-lines. Working together, pBIN1 recruits uBIN1 to membrane invaginations while uBIN1 attaches pBIN1 tubules to Z-lines, providing a novel mechanism of T-tubule formation by BIN1 in cardiomyocytes (Lin-Lin Li 2020). All these substantiate the conclusion that BIN1 plays a cardinal role in T-tubule organization and EC-coupling of cardiomyocytes.

However, there are still some questions unsolved. For example, current information about BIN1 splicing in cardiomyocytes is only from murine (mouse and rat) study, and there is still no detailed analysis in human heart given possible differences across species, which has been seen between mouse and rat. In addition, the study in mice showed that there was no isoform containing exon11 found in cardiomyocytes and BIN1+13+17 was the one responsible for T-tubules biogenesis. In contrast, PI-containing BIN1 isoforms were identified in rat cardiomyocytes. As mentioned previously, the membrane tubulating ability of BIN1 was largely attributed to the PI motif encoded by exon11, which possesses a high affinity to specific membrane lipids. The membrane-curving ability of BIN1 isoforms without the PI motif is much weaker than those with this domain. The inconsistent findings between mouse and rat cardiomyocytes suggest that the situation in the human heart may be different. Therefore, the properties and effects of

BIN1 isoforms need further investigation in the future, especially in human cardiomyocytes.

3.4 hiPSC-derived cardiomyocytes

3.4.1 Reprogramming of human iPSC

Induced pluripotent stem cells (also known as iPSC) are a type of pluripotent stem cells that are able to maintain self-renewal and differentiate into multiple cell types. Different from embryonic stem cells (ESC), these cells are generated directly from somatic cells by reprogramming them with four genetic factors (OCT_4, SOX_2, KLF_4, and c–MYC), which was established by Shinya Yamanaka and Kazutoshi Takahashi (Takahashi & Yamanaka 2006; Okita et al. 2007). These cells have normal karyotypes and telomerase activity and feature human ESCs by expressing certain cell surface markers and maintain the ability to differentiate into various types of cells. Similar studies from other laboratories were carried out and confirmed these results, suggesting the advent of a new era and shedding new light on future biomedical research (Wernig et al. 2007; Yu et al. 2007; Maherali et al. 2007; Park et al. 2008).

Nowadays it is widely available to cultivate iPSCs in long term and induce differentiation into multiple cell types with specific protocols using growth factors, small molecules, co-culturing of cells, and specific matrices, which makes it possible to apply iPSCs in diverse fields of biomedical researches, including regulation of human development, mechanisms of human disease, drug screening and regenerative therapy for tissue injury or lost (Saha &

Jaenisch 2009; Egawa et al. 2012; Liang et al. 2013). There have been multiple reports of differentiating human iPSCs (hiPSC) into various types of cells, including neurons (Chambers et al. 2009), retinal pigment epitheliums (Kanemura et al. 2013), skin cells (Shalom-Feuerstein et al. 2013), melanocytes (Nissan et al. 2011), cardiomyocytes (Moretti et al. 2010), skeletal muscle cells (Chal et al. 2015), lymphocytes (M. J. Smith et al. 2015), cartilage cells (Umeda et al. 2015), kidney cells (Takasato et al. 2015), liver cells (Hannan N R F et al. 2013) and so on. Due to their convenient availability and similar though immature properties to adult cells, these iPSC-induced cells have been widely applied in biomedical research and have largely facilitated researches in related fields.

3.4.2 Differentiation of hiPSC-derived cardiomyocytes

Among all the application arenas of hiPSCs, heart research is definitely one of the hottest and most advanced fields. Since the discovery of iPSCs, many scientists have turned their attention to differentiate iPSCs effectively and efficiently into cardiac-like myocytes. As heart diseases can cause injury and even loss of cardiac tissue and there is little evidence that cardiomyocytes can regenerate on their own, iPSC-derived cardiomyocytes (iPS-CMs) provide a possibility for future research and applications. Compared to ESC-derived cardiomyocytes, iPS-CMs have more advantages such as easier access to primary cells (various sources of somatic cells), no immune rejection of allogeneic cell grafts (because of autologous source), and patient-specific modification of genetics (such as repairing mutated genes). Human iPSCs (hiPSC) were firstly reported to successfully differentiate into cardiomyocytes using the embryoid body differentiation system in 2009 (Zwi et al. 2009). These cells are similar to adult cardiomyocytes in molecular, structural, and functional properties. For example, they can initiate spontaneous contractions. Whereas, the efficiency was quite low, ranging from 5% to 10%. Since then, continuous studies have been carried out and developed numerous methods to improve the productivity. One study reported that by adding chemical compounds to inhibit the Wnt signaling, the differentiation rate was greatly enhanced (Ren et al. 2011). Another study improved this differentiation process by a 3-step system, which only used chemically defined factors for culturing instead of serum (Burridge et al. 2014). Progresses in methods for inducing and culturing hiPS-CMs pave the way for implementations in the future.

3.4.3 Strategies of promoting hiPSC-CMs maturation

Although it is well established now to differentiate cardiomyocytes from hiPS cells, they are still on the road of development and much less mature than adult cells. In other words, compared to the end-differentiated adult cardiomyocytes, hiPSC-CMs can be regarded as still being in this infant stage (**Fig. 3.8**). For example, hiPSC-derived cardiac myocytes are a heterogeneous mixture of different cardiomyocytes including ventricular-, atrial-, and nodal-like subtypes. Currently, it is still very difficult to achieve single subtype differentiation and separation. Considering that each subtype possesses distinct electrophysiological properties, unpurified cells may cause unknown risks, which may hinder their applications in the future. Moreover, these cells are mostly structurally in round or polygonal shape and chaotically organized in contrast to the rod-shaped and highly organized adult cardiomyocytes (Zwi et al. 2009). Besides, they normally express lower levels of important SR genes (CSQ, RyR2, SERCA) and sarcomeric genes (MYL2, MTH7, TCAP, MYOM2) when compared to adult cardiomyocytes (Synnergren et al. 2012; Funakoshi et al. 2016). Particularly, one of the most pronounced differences is that hiPS-CMs are not able to develop T-tubules, the key structural basis for efficient EC-coupling in adult cardiomyocytes (Lieu et al. 2009). Accordingly, the capacity of calcium handling in hiPSC-CMs is also weaker and less synchronous than that of their mature counterparts (Lieu et al. 2009; Itzhaki et al. 2011; S. Li et al. 2013). This is of crucial importance because the central factor regulating the contractile property of cardiomyocytes is the ability of calcium handling, which is immature in hiPSC-CMs. If such cells were applied for repairing injured myocardium, probable risks of side effects such as arrhythmia may arise from uncoordinated electrophysiological activities or calcium handling. Therefore, it is cardinal to drive the maturation of human hiPSC-CMs so that they can develop better structures and functions.

In order to promote hiPSC-CMs maturation, a variety of methods have been tested in the past few years. These strategies include longer time in culture (Lundy et al. 2013; Ivashchenko et al. 2013; Kamakura et al. 2013; Otsuji et al. 2010), electrical stimulation (Lieu et al. 2013; Chan et al. 2013; Radisic et al. 2004; Nunes et al. 2013), mechanical strain (Kensah et al. 2013; Mihic et al. 2014; Tulloch et al. 2011), chemical stimulation (Cao et al. 2012; Yang et al. 2014), co-culture with non-cardiomyocytes(Kim et al. 2010;

Thavandiran et al. 2013), 3D culture (Nunes et al. 2013; Zhang et al. 2013), addition of extracellular substrates (Rao et al. 2013; Hazeltine et al. 2012; Salick et al. 2014), and ectopic expression or direct regulation of related genes (Lieu et al. 2013; J. Liu et al. 2009; J.-D. Fu et al. 2011). Even though these strategies can somehow promote the maturation of hiPSC-CMs such as upregulation of gene expression, improvement of cell morphology as well as enhancement of electrophysiological and calcium handling properties, there is so far very few reports about successful induction of T-tubules in hiPSC-CMs, which has been a major stumbling block in this area. Progresses in this aspect will definitely enhance the capabilities of hiPSC-CMs and their applications like disease modeling or tissue regeneration, through which we may move a big step forward and eventually, harness the weapon against heart diseases.

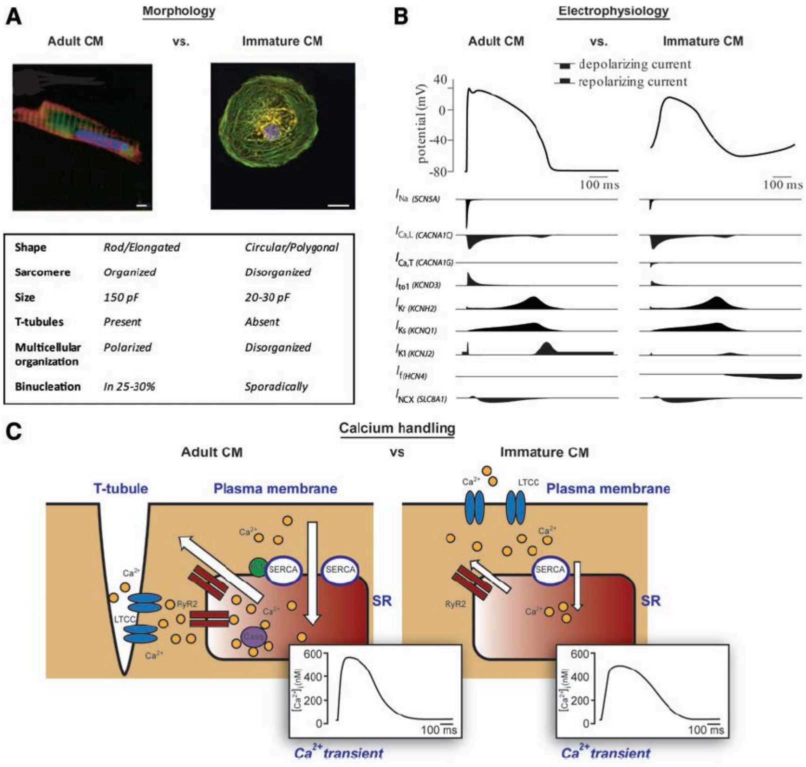
A
Morphology
Adult CM
vs.
Immature CM
B
Electrophysiology
Adult CM
vs.
Immature CM
depolarizing current
repolarizing current
potential (mV)
40
0
-40
-80
100 ms
100 ms
I_{Na} (SCN5A)
$I_{Ca,L}$ (CACNA1C)
$I_{Ca,T}$ (CACNA1G)
I_{to1} (KCND3)
I_{Kr} (KCNH2)
I_{Ks} (KCNQ1)
I_{K1} (KCNJ2)
I_{f} (HCN4)
I_{NCX} (SLC8A1)
C
Calcium handling
Adult CM
vs
Immature CM
T-tubule
Plasma membrane
Ca^{2+}
LTCC
RyR2
SERCA
SR
Casq
Ca^{2+} transient
600
400
200
0
$[Ca^{2+}]_i$ (nM)
100 ms

Shape	*Rod/Elongated*	*Circular/Polygonal*
Sarcomere	*Organized*	*Disorganized*
Size	*150 pF*	*20-30 pF*
T-tubules	*Present*	*Absent*
Multicellular organization	*Polarized*	*Disorganized*
Binucleation	*In 25-30%*	*Sporadically*

Figure 3.8 Comparison between adult cardiomyocytes and iPSC-CMs. A) Summary of the typical morphological features of these two cell types. B) Comparison of electrophysiological features (action potentials and related ion currents) between them. C) Differences in calcium handling features between them. Notice that T-tubules are deficient in immature CM and the transient is also different. The figure was taken from Veerman C C et al. Stem cells and development, 2015, 24(9): 1035-1052.

3.4.4 Biogenesis of T-tubules in hiPSC-CMs

As mentioned above, one of the major blockages in the hiPSC-CMs maturation is T-tubule deficiency. So far as we know, there is only one latest study showing that it is possible to induce T-tubule development by applying thyroid and glucocorticoid hormones during the differentiation process, combined with specially modified culture matrix-Matrigel mattress, which enhanced the EC-coupling of these hiPSC-CMs (Parikh et al. 2017). However, even if T-tubules were successfully formed with this method, they were still much less organized and effective than those of adult cardiomyocytes. Moreover, it did not provide clear and direct evidence whether the changes were due to newly built T-tubules or other improvements such as up-regulation of EC-coupling related genes. Particularly, it is unknown whether or not there are EC couplons formed at and calcium released from these tubules, which is the most important evidence of EC-coupling. Therefore, it is necessary to develop effective strategies to drive the progress of T-tubule development and EC-coupling maturation of hiPSC-CMs in the journey of cardiac differentiation.

4. Materials and methods

4.1 Materials

4.1.1 Cell culture reagents

Name	Manufacturer	Catalogue Number
Dulbecco’s modified eagle medium (DMEM)	Gibco	41965039
Fetal Bovine Serum heat inactivated (FBS)	Gibco	10270122
Penicillin/Streptomycin (100X)	Gibco	15140122
Trypsin/EDTA (1X), 0.05%	Gibco	25300054
Collagenase, Type II, powder	Gibco	17101015
Medium199/EBSS +Earle’s Balanced Salt +L-Glutamine	Hyclone	SH30253.01
Kanamycin (100X)	Gibco	15160054
Insulin-Transferrin-Selenium (100X)	Gibco	41400045
Dulbecco's Modified Eagle Medium/Nutrient Mixture F-12 (DMEM/F-12)	Invitrogen	21331020
GlutaMax (100X)	Invitrogen	35050061
MEM Non-Essential Amino Acids Solution (100X)	Gibco	11140035
β -Mercaptoethanol	Gibco	31350010
Fibronectin Bovine plasma F1141-	Sigma	2891492

5MG	Aldrich	
HEPES dry powder	Sigma Aldrich	7365459
Phosphate buffered saline (PBS) tablet (100X)	VWR LifeScience	E4040200TABS

4.1.2 Consumables

Material	Specification	Manufacturer	Catalogue Number
Cell Culture Plate, flate, sterile	12 well	CELLSTAR	665180
Cell Culture Plate, flate, sterile	6 well	CELLSTAR	657160
Cell Culture Flasks, PS, Sterile	50ml, 25cm^2	CELLSTAR	690160
Cell Culture Flasks, PS, Sterile	250ml, 75cm2	CELLSTAR	658170
Falcon tubes, sterile	15 and 50 ml	CELLSTAR	188271 227261
Tissue Culture Dishes, sterile	4 well	NUNC	179830
Serological Pipettes, sterile	5 and 10ml	CELLSTAR	606180 607107
Microcentrifuge tube, PP	0.5, 1.5, and 2.0ml	SARSTEDT	72.695.500 72.690.001 72.699
Pipette tips, filter,	1250 µl	SurPhob	VT0270

Sterile		Biozyme	
Pipette tips, filter, Sterile	10µl and 200 µl	STARLAB	S11213810 S11208810
PCR tubes, thin-wall, sterile	0.2ml	Biozyme	710970
Bacteriological dishes	10cm	Corning	351007
Microscope coverslips, sterile	20mm	Thermo Scientific Menzel	11961988

4.1.3 Enzymes, nucleotides and markers

Name	**Supplier**	**Catalogue Number**
Phusion Hot StartII DNA Polymerase, 500U	Thermo Scientific	F-549S
Dream Taq DNA Polymerase, 500U	Thermo Scientific	EP0702
5X Phusion GC Buffer	Thermo Scientific	F-519
10X DreamTaq Green Buffer	Thermo Scientific	LT-02241
100% Dimethylsulfoxide (DMSO)	Finnzymes	F-515
dNTPMiX, 10mM	Thermo Scientific	R0192
iScript reverse transcriptase, 25 µl	BIO-RAD	170-8896

5XiScript select reaction mix, 400 µl	BIO-RAD	170-8896
Oligo (dT) $_{20}$ primer mix	BIO-RAD	170-8896
Random primer mix	BIO-RAD	170-8896
T4 DNA Ligase, 500U	Fermentas	EL0016
10X T4 DNA Ligase Buffer	Fermentas	B69
EcoRI, 10U/ µL	Fermentas	ER0271
KpnI, 10U/ µL	Fermentas	ER0521
NotI, 10U/ µL	Fermentas	ER0591
XbaI, 10U/ µL	Fermentas	ER0681
XhoI, 10U/ µL	Fermentas	ER0691
HindIII, 10U/ µL	Fermentas	ER0501
PacI, 10U/ µL	Thermo Scientific	ER2201
10 X Buffer EcI136II, PacI, SacI	Fermentas	B26
10 X Tango Buffer	Fermentas	BY5
GeneRuler 1kb DNA Ladder	Thermo Scientific	SM0311
GeneRuler Low Range DNA Ladder	Thermo Scientific	SM1193
Fluo-4, AM	Invitrogen	F14201
Cell Mask Deep Red Plasma Membrane Stain	Invitrogen	C10046
Bovine Serum Albumin	Sigma-Aldrich	A7906-50G
LE Agarose, 500g	Biozyme	840004
Tween 20, 100mL	VWR	437082Q
Triton X-100, 50mL	VWR	437002A

4.1.4 Kits

Kit	**Supplier**	**Catalogue Number**
QIAquick Gel Extraction Kit (250)	QIAGEN	28706
QIAprep Spin Miniprep Kit (250)	QIAGEN	27106
Plasmid Maxi Kit	QIAGEN	12163
ISOLATE II RNA Micro Kit 50 Preps	BIOLINE	BIO-52075
CloneJET PCR Cloning Kit, 40rnxs	Thermo Scientific	K1232
RAPAd CMV Adenoviral Expression System	CELL BIOLABS	VPK-252

4.1.5 Laboratory apparatus

Apparatus	**Specifications**	**Manufacturer**
Cell culture hood	Holtern LaminAir 1.8	Thermo Scientific
Cell incubator	Direct Heat CO_2	Thermo Scientific
Electrophoresis chamber	Fusion FX VILBER Chemiluminescence	PEQLAB
pH meter	Laboratory pH meter/ bench-top inoLab 7110	WTW

Osmometer	VAPRO Pressure Osmometer	ELITechGroup
Thermocell mixing block	MB-102	Alpha laboratories
PCR machine	ProFlex PCR System	Applied biosystems
PCR machine	LabCycler	SensoQuest
Microcentrifuge	Biofuge Pico	Heraeus
Refrigerated Microcentrifuge	2019R	NAPCO
Microwaver	KOR6M5R	DAEWOO
Pipette controller	Accu-jet pro	Brand tech
Electronic scale	Portable series	Fisher Scientific
Spectrophotometer	Lambda Bio+	Perkin Elmer
Magnetic stirrer	MR3001K	Heidolph
Shaker	RS-DS5-Analog 3D	Phoenix
Electrophoresis System	E865	Consort
Water purification system	Direct-Q3 UV	Merck Millipore

4.1.6 PCR primers for BNI1 transcription analysis

Name	**NCBI reference**	**Primer**	**Annealing Temp*, °C**
hBIN1-sp1-F	NM_004305.3	GCCCAGCCCAGAAAGAAAAG	50
hBIN1-	NM_004305.3	GGGCCTGTACCTTGAA	50

sp1-R		CATGA	
hBin1-sp2-F	NM_139343.2	GCCCAGCCCAGTGACAAC	50
hBin1-sp2-R	NM_139343.2	GGGCCTGTACCTTGAACATGA	49
hBin1-sp3-F	NM_139348.2	AGTCCCCATCTCAGCTCCG	50
hBin1-sp3-R	NM_139348.2	CTGGGCCTGTACCTTGAACAT	49
hBin1-sp4-F	NM_139343.2	AAGCCTGTCTCGCTGCTTG	50
hBin1-sp4-R	NM_139343.2	GAGGTTCTGGTTGAGCTTGC	49
hBIN1-Spl-F	NM_004305.3	AGCAAGCTCAACCAGAACCT	47
hBIN1-Spl-R	NM_004305.3	CCAGCCTTCATCCTGCTCTT	49
hBin1-nest-F	NM_004305.3	CTCATCAAAGCCCAGAAGGTG	49
hBin1-nest-R	NM_004305.3	ACCACACATTTTTCGGGAGGA	47

*Temp: temperature

4.1.7 Primary and secondary antibodies

Antibody	**Supplier & Catalogue No.**	**Final concentration**	**Usage**
Rabbit	Novus	1:200	IF

Anti-BIN1	Biologicals NBP2-15587		
Mouse anti-BIN1 Clone99D	Sigma Aldrich B-9428	1:150	IF
Rabbit Anti-Cav1.2	Prof.Flockerzi Ab790	1:100	IF
Mouse Anti-RyR2	Sigma Aldrich C3-33	1:150	IF
Mouse Anti-α-actinin Clone EA-53	Sigma Aldrich 029K4844	1:200	IF
Goat anti-Junctopilin-2 (Y-15)	Santa Cruz Sc-51313	1:150	IF
Rabbit Anti-Scn5a	Sigma Aldrich AV35542	1:200	IF
Donkey anti-Rabbit IgG(H+L),Secondary antibody,DyLight488	Invitrogen SA5-10038	1:300	IF
Donkey anti-Mouse IgG(H+L),Secondary Antibody,DyLight488	Invitrogen SA5-10166	1:300	IF
Donkey anti-Rabbit IgG(H+L),Secondary Antibody,DyLight650	Invitrogen SA5-10041	1:300	IF
Donkey anti-Mouse IgG(H+L),Secondary Antibody,DyLight650	Invitrogen SA5-10169	1:300	IF

*IF, Immunofluorescence

4.1.8 Buffers and solutions

Tyrode solution, pH7.4

3.95g (136mM/L) Sodium chloride (NaCl, VWR), 0.2g (5.4mM/L) Potassium chloride (KCl, Merck), 0.9g (10mM/L) D-(+)-Glucose (Roth), 1.19g (10mM/L) Herpes (Sigma), 900ml 1.0mM (1.8mM/L) Calcium chloride ($CaCl_2$, Merck) stock and 500ml 1.0mM (1.0mM/L) Magnesium chloride ($MgCl_2$, Merck) stock were dissolved with ultrapure water to 500ml in total. pH was adjusted with Sodium hydroxide (NaOH)/Hydrogen chloride (HCl) solutions to 7.4. The osmolarity was adjusted to around 300 mOsmol before used in live cell imaging.

10X Tris-borate-EDTA (TBE) buffer, pH8.0

Weigh out 3.72g EDTA disodium salt (Merck) and dissolve it in deionized water to 500ml stock solution (0.5M). Adjust the pH with NaOH to about 8.0. Weigh out 108g boric base (Sigma) and dissolve it in 500ml deionized water. Carefully add 55g glacial acid (VWR) and 40ml of 0.5M EDTA (pH 8.0). After that, adjust the volume to 1 liter. The stock solution can be stored at room temperature. For a working TBE solution, dilute the stock with deionized water to 0.5x TBE buffer before used in agarose gel electrophoresis.

4% Paraformaldehyde (PFA) solution

Weigh 4mg Paraformaldehyde (Riedel-de Haen) and dissolve it in100ml 1X PBS solution. Add a small amount of NaOH to help dissolve PFA. After that adjust the pH with 5% HCl solution to 7.35

before applied to cell or tissue fixation. The solution should be covered from light and stored at room temperature.

Luria-Bertani (LB) medium

10g Tryptone (Sigma), 10g NaCl, 5g yeast extract (Sigma) were dissolved in 950ml deionized water until totally mixed well. Adjust the pH to 7.0 with 5N NaOH. Then adjust the final volume of the solution to 1L with deionized water. The LB medium was sterilized by autoclaving for 15 minutes at 121 ˚C. Store the LB medium at room temperature.

1% Agarose plate

Weigh out 4mg agarose (Biozym Scientific) and add it to 100ml 0.5x TBE buffer. Heat the solution in a microwave oven until it is totally dissolved. Add 10 ml Ethidium Bromide (Sigma) to the solution and mix well. Store the solution in a constant temperature oven (60°C). Agarose plates can be made by adding around 20ml agarose solution to an electrophoresis chamber and keep it at room temperature till it is cooled down and become consolidated.

1% Triton X-100 PBS solution

Add 1ml Triton X-100 (VWR) into 100ml 1X PBS buffer and mix well before further applications.

0.25% Tween-20 PBS solution

Add 250µl Tween-20 (VWR) into 100ml 1X PBS buffer and mix well prior to further experiments.

Sterilization of solutions

Heat insensitive solutions and plastic ware was sterilized at 121°C, 105Pa for 60 min via autoclaving. Heat sensitive solutions were sterile-filtered through a disposable sterile filter (0.2µm pore size). Glasswares were sterilized overnight at 220°C by autoclaving.

4.2 Methods

4.2.1 Cell culture techniques

Culture of HEK cells

Human embryonic kidney (HEK) cell line 293A was cultured in Dulbecco’s modified minimal essential medium (DMEM) medium supplemented with 10% fetal bovine serum (FBS), 1% Penicillin/Streptomycin, and 1% L-glutamine. Cells were passaged around every 3 days by trypsin digestion.

Culture of hiPSC-CMs

Human iPSC-CMs were induced, isolated and cultured as previously described (Z. Chen et al. 2017). Briefly, at day15-25 of iPSCs differentiation, contracting islets were manually microdissected and maintained on fibronectin-coated plates with EB2 medium (DMEM-F12, 2% FCS, 1% L-glutamine, 1% MEM-NEAA, 1% penicillin/streptomycin, 0.1mM β-mercaptoethanol). For isolation and culture, explants were dissociated into single cells by collagenase II (1.5mg/ml) at 37°C for around 2 hours and seeded on 12-well plates with glass coverslips coated with fibronectin as a single layer. Cells can be maintained for 3-5 days for certain experiments.

Isolation and culturing of rat cardiomyocytes

Ventricular cardiomyocytes were isolated from rat hearts according to previous report(Tian et al. 2012).Isolated fresh rat cardiomyocytes were cultured with specialized medium (Medium199/EBSS, 1% Penicillin/Streptomycin, 0.1% kanamycin, 0.1% ITS) on fibronectin-coated glass coverslips for 3-5 days. Cell medium was changed every two days.

4.2.2 Plasmid transfection

For normal plasmid transfection, the NanoJuice transfection kit (Novagen, 71902-3) was used according to the manufacturer's protocol. Briefly, cells were cultured in a 12-well plate before transfection. The cells should be 50-80% confluent at the time of transfection. For each well, a mixture of transfection reagents was prepared. Firstly, 0.5µl NanoJuice Core Transfection Reagent and 1µl NanoJuice Booster Reagent were added to 50µl DMEM medium and mixed well. Then the Nanojuice reagents and medium mixture were incubated at room temperature for 5 min. After that, 0.5-1µg plasmid DNA was added to the master mixture and mixed well. The total transfection mixture was incubated at room temperature for 20 min. Finally, the transfection mixture was transferred to one of the wells in the 12-well plate in a drop-wise fashion. The transfection mixture was evenly distributed by rocking the plate. Finally, the cells were incubated for 24-72h at 37°C (5% CO2) before further characterization.

For viral vector transfection, a PEI (Polyethylenimine) transfection method was used which was considered to be more suitable for virus packaging (Baker et al. 1997). Briefly, 293A cells were cultured in a 6-well plate to 50-80% confluence before transfection. Transfection mixtures for each well were prepared. Firstly, around 3μg plasmids (1μg linearized shuttle vector: 2μg linearized backbone vector) were diluted in 150μl NaCl (150mM) solution. 45 μl PEI (15μl per 1μg plasmid) was diluted in 150μl NaCl (150mM) solution. Both mixtures were vortexed gently and spun down briefly. Then the 150μl PEI mixture was added to the 150μl plasmid mixture and mixed immediately. The transfection mixture was incubated for 20 minutes at room temperature. Generally, the total volume of the PEI/DNA mixture equals one-tenth of the total volume of the culture medium (for 6-well plates, around 300μl for each well). Finally, the transfection mixture was added to the well in a drop-wise manner. The plate was gently swirled by a slow hand rotation. The cells were incubated at 37°C (5% CO_2) in a moist chamber.

4.2.3 Adenovirus packaging and transduction

To generate adenovirus that contains genes of interest, a CMV Adenoviral Expression System kit (RAPAd Adenoviral Expression System, VPK-252, Cell Biolabs) was utilized. Experiments were carried out according to the manufacturer’s protocol. Briefly, genes of interest (BIN1 isoforms and GCaMP6f-junctin) were firstly cloned into the pacAd5 CMVK-NpA shuttle vector (Part No. 325201) by restriction enzyme digestion and DNA ligation. 4μg of shuttle vector containing genes of interest and 1μg backbone vector pacAd5 9.2-100 were then linearized by PacI restriction enzyme digestion at 37°C overnight to completely digest the constructs. Run a small amount of each digested DNA and undigested DNA on a 0.8% agarose gel to confirm the completion of PacI digestion (For pacAd5 9.2-100, one band of ~33 kb and the second band of 2.0 kb were expected). To obtain the linearized plasmid, the digestion mixture was firstly analyzed by electrophoresis. The recycled gel was then purified with QIAquick Gel Extraction Kit. The linearized DNA was resuspended in sterile dH_2O. For transfection, 293A cells were cultured in a 6-well plate to 50-80% confluence before transfection. Cells were then transfected with the linearized shuttle and backbone vectors following the PEI transfection protocol as previously described. Incubate cells at 37°C (5% CO_2) in a moist chamber. The medium containing transfection reagent was removed the next day and replaced by 3 ml fresh culture medium. After around 7 days, the presence of plaques was checked. If the cells were ready for harvest (>50% of cells lifted), the crude viral lysate was collected. If not, the cells will be fed with 1ml of fresh medium and continue to culture. The culture plate was kept checking until the presence of plaques. The plate should not be maintained for more than 15 days. The adenovirus-containing cells were then harvested with a 5 or 10ml sterile serological pipette. The cells and medium were transferred to a sterile 15ml tube. A cell lifter may be used to scrape the cells into the medium if necessary. To release the viruses, the cells were processed by freeze/thaw cycles (10 min each in 37°C water bath and dry ice-methanol bath). After that, the cell lysate was centrifuged in a tabletop centrifuge at 3000 rpm for 15 minutes at room temperature to pellet the cell debris. The crude viral lysate (initial viral stock) was then aliquoted and stored at -80°C.

To amplify the virus, 293A cells were seeded in a 250ml, 75cm^2 cell culture flask to 50-80% confluence. Afterwards 50% of the crude viral lysate was added to the culture. During 24-48 hours after infection, the monolayer was checked twice a day under the microscope for cytopathic effects (CPE). When CPE was nearly complete (i.e. most cells rounded but not yet detached from the bottom of the flask), cells were harvested by pipetting culture medium up and down to wash the infected cells from the flask into the medium. Infected cells and medium were pooled and centrifuged. The supernatant was then removed and the cell pellet was suspended in PBS. To release the adenoviruses from the cell suspension, freeze/thaw cycles were performed three times. Cell debris was pelleted by centrifugation and discarded while the supernatant was saved as viral stock. The viral supernatant was then stored at -80°C or immediately purified or titered.

For transduction of the cardiac cells cultured in the 12-well plate, 10-20µl of viral supernatant (viral titer ≈1x10^7 IFU/mL) was added to the 12-well plate. After 24 hours, the virus-containing medium was removed and replaced by the fresh complete medium. The cells were then incubated at 37°C (5% CO_2) for 2-3 days before further treatment.

4.2.4 Molecular biological methods

RNA isolation

RNA samples of healthy human heart tissue were purchased from the biotrend company (Cat Nr. R1234122-50-D02) and stored at -80°C for further use. Samples of human heart tissue were also collected from patients with heart diseases during surgical operations from the cardiology department of the university hospital at the Saarland Medical School. Tissues were stored at -80°C before further process. Total RNA was isolated using Bioline ISOLATE II RNA Micro kit (BIO-52075) according to the manufacturer’s protocol. Briefly, frozen heart tissue was placed in a dounce and powdered by grinding the frozen tissue fragments in a pre-chilled mortar and occasionally adding liquid nitrogen into the mortar to prevent thawing. Once the tissue was grounded to fine powders, the denaturing solution was added to the mortar, and the semi-frozen mixture was stirred. The sample mixture was transferred to a sterile 1.5ml microcentrifuge tube and 100µl Lysis Buffer RLY as well as 2µl TCEP were added. The mixture was then vortexed vigorously to obtain cell lysis and homogenization. 5µl Carrier RNA working solution was put into the lysate and mixed well by vortexing. An ISOLATE II Filter was placed in a 2ml Collection Tube and loaded with the lysate, which was followed by centrifuging 30s at 11,000xg. 100µl ethanol (70%) was mixed well with the homogenized lysate by pipetting up and down 5 times. The lysate was loaded into an ISOLATE II RNA Micro Column placed in a 2 ml Collection Tube and centrifuged for 30s at 11,000xg to bind RNA. After that, the column was placed in a new 2ml Collection Tube followed by adding 100µl Membrane Desalting Buffer and the centrifuge to desalt the silica membrane. 25µl DNase I reaction mixture was put directly onto the center of the silica membrane and incubated at room temperature to digest DNA. After three rounds of washing and drying the silica membrane, 10µl RNase-free water was directly added onto the center of silica membrane and RNA was eluted by centrifuging at

11,000xg 30s. RNA was stored at -20°C before further applications.

cDNA synthesis by RT-PCR

For cDNA synthesis, 1µg of RNA combined with oligo-dT-primers was reversely transcripted by iScript Reverse Transcriptase (BIO-RAD 1708890) according to the manufacturer's instruction. Briefly, the reaction mixture was prepared as follows.

Component	Volume per reaction
5x iScript Reaction Mix	4µl
iScript Reverse Transcriptase	1µl
Nuclease-free water	5µl
RNA template (100fg to1µg total RNA)*	10µl
Total Volume	20µl

*When using larger amounts of input RNA (>1µg) the reaction was scaled up e.g. 40µl reaction for 2µg, 100µl reaction for 5µg to ensure optimum synthesis efficiency.

The complete reaction mix was incubated as follows:

5 minutes at 25°C
30 minutes at 42°C
5 minutes at 85°C
Hold at 4°C (optional)

The cDNA was stored at -20°C or directly used for further analysis.

Normal/high fidelity/colony PCR

PCR was carried out to amplify the double-stranded plasmid DNA or single-stranded cDNA. Generally, the cDNA was amplified with

DreamTaq DNA Polymerase in DreamTaq reaction buffer. In high fidelity PCR, the cDNA was amplified with Phusion Hot StartII DNA Polymerase in GC/HF reaction buffer to avoid possible mutation during the reaction. In colony PCR, bacterial DNA was amplified with DreamTaq DNA Polymerase in DreamTaq butter. The reaction mixture was then analyzed to check PCR bands. In this way, positive colonies were picked out. All amplifications were performed according to the manufacturer’s protocol and modified to optimal conditions for each specific sequence of interest (different primers require different melting temperatures during PCR). PCR reactions were performed in sterile 0.2 ml thin-wall PCR tubes described as below.

Normal PCR

PCR component	Volume	Final Concentration
10x DreamTaq Buffer	2 µl	1x
10mM NTP Mix	2 µl	0.2 mM
10µM Forward primer	0.5 µl	0.2 µM (0.05-1 µM)
10µM Reverse primer	0.5 µl	0.2 µM (0.05-1 µM)
Template DNA	1 µl (variable)	<1,000 ng
DreamTaq polymerase	0.1 µl	
Nuclease-free water	13.9 µl	
Total	20 µl	

High fidelity PCR

PCR component	Volume	Final Concentration

5x Phusion HF or GC Buffer	4 µl	1x
10 mM dNTPs	0.4 µl	0.2 mM
10 µM Forward primer	1 µl	0.5 µM
10 µM Reverse primer	1 µl	0.5 µM
Template DNA	1 µl (variable)	<1,000 ng
DMSO	0.6 µl	3%
Phusion DNA Phusion Polymerase	0.2 µl	
Nuclease-free water	11.8 µl	
Total	20 µl	

Colony PCR

PCR component	**Volume**	**Final Concentration**
10x DreamTaq Green Buffer	2 µl	1x
10mM NTP Mix	2 µl	0.2 mM
10µM Forward primer	0.5 µl	0.2 µM (0.05-1 µM)
10µM Reverse primer	0.5 µl	0.2 µM (0.05-1 µM)
Bacteria colony sample	1 µl	
DreamTaq polymerase	0.1 µl	
Nuclease-free water	13.9 µl	
Total	20 µl	

PCR cloning of BIN1 splice variants

To screen possible BIN1 splice variants in human heart cDNA, primer pairs were designed: Forward primer 5’-AAGAAGGATGAAGCCAAAATTGCCAAG-3’, Reverse primer 5’-GAAGGTCTCCACCACGACAGC-3’. The first pair of primers starts from exon6 and ends at exon18, both of which belong to the conservative parts of BIN1 sequence. Therefore, this primer pair should be able to detect all potential BIN1 splice variants. The PCR reaction was performed with Phusion High-Fidelity DNA Polymerase according to the manufacturer's protocol. PCR products were separated by agarose gel electrophoresis and assessed by UV light. To obtain the whole-length sequence of the BIN1 isoforms, the appropriate PCR product was used for PCR cloning applying the CloneJET PCR Cloning Kit according to the protocol of the manufacturer. Briefly, the reaction was set up on the ice as below.

Component	**Volume**
2x Reaction Buffer	10 µl
Non-purified PCR product	1 µl
Water, nuclease-free	6 µl
DNA Blunting Enzyme	1 µl
Total volume	18 µl

The reaction mixture was vortexed briefly and centrifuged for 3-5s. The mixture was incubated at 70 °C for 5 min and then chilled on ice. Then ligation reaction was set up on the ice and the blunting reaction mixture was prepared as below.

Component	**Volume**
pJET1.2/blunt Cloning Vector (50ng/ µl)	1 µl
T4 DNA ligase	1 µl
Total volume	20 µl

The reaction mixture was vortexed briefly and centrifuged for 3-5 s to collect drops. The ligation mixture was incubated at room temperature for 5 min. The ligation mixture was directly used for transformation or kept at -20°C if transformation is postponed. Positive colonies selected by PCR were purified for further sequencing. Results were blasted in the NCBI database for verification of possible isoform sequences.

4.2.5 Vector construct preparation

Bacterial transformation

For bacterial transformation, the DH5a competent cells (Invitrogen, 18265017) were used. Briefly, competent DH5a cells were thawed on ice. The cells were gently mixed with the pipette tip and 50 μl was used for each transformation in a 1.5 ml tube that has been pre-chilled on ice. 1-5 μl DNA or ligation mixture (1-100ng) was then added to the cells and mixed gently. The tube was incubated on the ice for 30 minutes before heat shock at 42°C for exactly 60 seconds without shaking. After that, the tube was placed on ice for 2 minutes. 250μl of pre-warmed (37°C) LB (without antibiotics) was added in the tube which was then shaken at 37°C for another 1 hour. The transformation mixture was spread onto LB plates (with appropriate antibiotics). The plate was inverted and put at 37 °C overnight. Checking of positive colonies was carried out the next day.

Restriction enzyme digestion

For plasmid cloning, vectors and gene sequences were firstly digested by the appropriate restriction enzymes or restriction endonucleases. Different restriction enzymes require different reaction buffers or different concentrations. Reactions were set in 0.2ml tubes as described below (double restriction enzyme digestion by XhoI/XbaI was taken as an example as follows).

Component	**Volume**
10x Tango buffer*	2 μl
XhoI, 10U/ μl	1 μl
XbaI, 10U/ μL	1 μl
Vector or DNA fragment	Variable (0.5-1 μg)
Nuclease-free water	Up to 20 μl
Total	20 μl

The reaction master was gently mixed by pipetting and centrifuging. The tube was placed at 37 °C for 2 hours. Digested fragments were then purified by gel electrophoresis before used in ligation.

DNA ligation

For all DNA ligations, reactions were done with the T4 DNA ligase. Generally, vectors and inserts (target gene or DNA) were digested with certain restriction enzymes. When vectors and inserts were purified, ligation reactions were set up in a microcentrifuge tube on the ice as described below.

Component	**Volume**
10X T4 DNA ligase buffer	2 μl
Vector DNA*	2 μl
Insert DNA*	8 μl

T4 DNA ligase	1 µl
Nuclease-free water	7 µl
Total volume	20 µl

* The molar ratio between the insert and the vector was in a wide range from 0.5:1 to 15:1 with the optimal ratio of 3:1.

The reaction was gently mixed by pipetting up and down and centrifuged briefly. For cohesive (sticky) ends, the mixture was incubated at room temperature for 10 minutes. For blunt ends or single base overhangs, the mixture was incubated at room temperature for 2 hours. Then the reaction mixture was heat-inactivated at 65°C for 10 minutes and immediatedly chilled on ice. Normally, for each 50µl competent cell, 1-5 µl of reaction mixture was used for the transformation.

DNA construct preparation

Several different constructs containing BIN1 isoforms were made. All constructs were based on the *pacAd5 CMVK-NpA* plasmid (the shuttle vector of the RAPAd® CMV Adenoviral Expression system (Cell Biolabs, Part No.325201)). *PacAd5-CMVK-NpA-BIN1-TagRFPT* was generated through cloning BIN1 sequences into the KpnI and XhoI sites while the TagRFPT sequence was cloned into the BamHI and XbaI sites to form a fusion protein sequence. *PacAd5-CMVK-NpA-TagRFPT-BIN1* was constructed with the BIN1 sequences cloned between the EcoRI and XbaI site while the TagRFPT sequence was placed between the KpnI and XhoI sites. *PacAd5-CMVK-NpA pm-TagRFPT-2A-BIN1* was constructed by inserting the TagRFPT sequence between the XhoI and HindIII sites, a short 2A sequence between the HindIII and EcoRI sites, and the BIN1 sequence between the EcoRI and XbaI sites. In addition, a plasma membrane localization sequence was cloned between the KpnI and XhoI sites just in front of the TagRFPT sequence. Thus the sequences of TagRFPT and BIN1 were linked by the 2A sequence. All BIN1 constructs were verified via DNA sequencing before further cloning or viral packaging and no missense mutation was found.

4.2.6 Immunostaining and calcium signal labeling

For immunofluorescent labeling, cells cultured on coverslips were firstly fixed by 4% PFA for 20 minutes at room temperature and washed with PBS buffer for three times. Cells were then permeabilized by 1% Triton X-100 PBS solution for 20 minutes at room temperature and washed with PBS buffer for three times. After that, cells on coverslips were blocked with 5% BSA PBS solution for 60 minutes at room temperature. After incubation with the primary antibodies at 4°C overnight, coverslips were then washed with 0.1% Tween-20 PBS solution (PBST) for three times, for 10 minutes each. The cells were incubated with Dylight conjugated secondary diluted in blocking buffer for 1 hour at room temperature. After washing with 0.1% PBST for three times (each with 10min), the coverslips were mounted on glass slides with ProLong Gold anti-fade reagent (P36930, Invitrogen) and stored at 4°C before further imaging. Slides were then put in a box to prevent light exposure.

Cell membrane staining

To stain the plasma membrane of living cells, CellMask Deep Red Plasma membrane Stain (Invitrogen, C10046) was used. Briefly, a fresh working solution of the CellMask plasma membrane stain was prepared in a physiologically relevant buffer (Tyrode solution) from the provided 1000X concentrated stain solution. Normally, 0.25ul stock solution was diluted and mixed in 1mL tyrode solution for each coverslip. Cells (HEK cells, rat cardiomyocytes, or hiPSC-CMs) were grown on coverslips with culture medium before staining. When cells have reached appropriate confluence, the coverslip was removed from the culture medium, washed with tyrode solutions, and incubated with the staining solution for 15 minutes at room temperature. After that, the staining solution was removed and the cells were rinsed with tyrode buffer for three times before imaging. As for the isolated rat cardiomyocytes, when the cells were grown onto the coverslips, similar staining procedures as described above were performed to stain the plasma membrane of adult cardiomyocytes.

Labeling of calcium in cardiomyocytes

To measure the intracellular calcium changes in living cells, the chemical small molecule Ca^{2+} indicator Fluo-4 (as Cell-permeant AM ester, Invitrogen, F14201) was used. Generally, to prepare a stock solution, the aliquot of AM ester stock powder was mixed with 20% (w/v) Pluronic in DMSO to obtain a stock solution of 1 mM. Then an aliquot of stock solution was diluted to a final concentration of 1-5 μM in Tyrode solution. Cardiomyocytes were incubated with the AM ester for 30 minutes at room temperature before being washed with indicator-free Tyrode solution to remove extracellular. Finally, the cells were incubated in indicator-free tyrode solution for a further 15-30 minutes to allow complete de-esterification of intracellular AM esters before fluorescence measurements.

4.2.7 Microscopic calcium imaging

To measure the intracellular calcium alterations in cardiomyocytes, two kinds of calcium labeling techniques were used. On one hand, the chemical small molecule Ca^{2+} indicator Fluo-4 was applied as previously described. On the other hand, a genetically encoded calcium indicator, GCaMP6f-junctin, was implemented. Briefly, the adenovirus that expresses GCaMP6f-junctin was generated as described above. The adenoviral supernatant was added to transduce cardiomyocytes for 24 hours and the cells were cultured for another 48 hours after the culture medium was changed. To simultaneously stain the cell plasma membrane, CellMask DeepRed plasma membrane dye (C10046, Thermo Scientific) was used (0.25μl in 1ml Tyrode) for 15 minutes incubation at room temperature. Finally, the coverslip was fixed in a small chamber and placed under the microscope for further imaging.

For calcium imaging by the microscope, rat cardiomyocytes and hiPSC-CMs were imaged with a confocal microscope (Leica SP5II with a resonant scanner, software Leica LAS AF, Germany) through a HCX PL Apo x63/1.40 oil immersion objective. An Argon gas laser (488nm), a solid-state laser (561nm), and a HeNe laser (633nm, a self-contained laser module with AOTF) were combined for excitation while emision from the cells was captured by Hybrid

GaAsp detectors or photomultiplier tubes. The emission wavelength is 498-550nm (excitation 488nm), 570-620nm (excitation 561nm), and 650-800nm (excitation 633nm) respectively. The scanning speed of the confocal module was set to bidirectional 8000 Hz with resonant scanning, which enables a recording speed of 100 frames per second. The frame size of the scanning is 512 x 120 pixel. All experiments were conducted at ambient room temperature (22-25°C).

To measure Ca^{2+} in hiPSC-CMs by Fluo-4, a high-speed 2D-array confocal scanning, VT-Infinity (Visitech International, Sunderland, United Kingdom), was coupled to a Nikon EclipseTi microscope. Solid-state laser lines at 488 nm and 633 nm (Cobolt AB, Solna, Sweden) were combined and guided into the confocal module via a light guide. A Hamamatsu ORCA-Flash 4.0 sCMOS camera (Hamamatsu Photonics, Hamamatsu City, Japan) was coupled to the confocal module and the images were transferred to a computer via camera link adaptors. The scanning speed of the confocal module was set to 600 Hz, 60% of the chip area of the camera was used at its highest readout speed resulting in a recording speed of 147 images/second (1024x614 pixels). The camera operated in its 2x2 binning mode yielding a pixel size of 215 nm. The cells were imaged through a Nikon Plan Fluor 60X oil DIC objective (NA = 1.40, NIKON, Tokyo, Japan). Imaging of GCaMP6f-junctin expressing iPSC-CMs was performed at 37°C by the heating system of the microscope.

All the cells, including rat cardiomyocytes and hiPSC-CMs were electrically field stimulated with a MyoPacer (Ion Optics, Westwood, MA, USA) with a voltage of 7 Volt at 1Hz during microscopic imaging of the calcium signals. Cells loaded with Fluo4 were measured at ambient room temperature (22-25°C) while cells expressing GCaMP6f-Juntin were measured at 37°C.

4.2.8 Data processing and statistical analysis

All microscopic images were deconvoluted by AutoQuant X3 software (Media Cybernetics, USA). Before further processing, all images were denoised through the ImageJ software through its build-in plugin PureDenosie(Luisier et al. 2010). Imaging processing and calculation were based on customized Matlab (R2014_a) algorithms. When thresholding, all images were processed by the Matlab build-in function graythresh which is based on the Otsu method (Otsu & Nobuyuki 1979.)

Calculation of the tubule density and length in HEK cells

To calculate the tubule density generated by BIN1 in HEK cells, a Matlab based method was used. Briefly, HEK cells cultured on coverslips were stained with DeepRed membrane staining dye. Microscopic imaging was done using the Leica confocal microscope as previously described. To obtain a stack of the images of the cell volume, a Z-stack scanning (Z-resolution at 0.1 µm) was carried out. When the stacks were thresholded by the Matlab function ’graythresh’, seven image slices were sampled from the stacks of each cell. The tubule density of each section was calculated as the ratio of positive pixels above the threshold level against the whole pixels of the cell area. The tubule density of the cell was then defined and calculated as the weighted average density of all sections according to the fraction of each section area in the total cell area.

$$\frac{\mathrm{Density1} \times \mathrm{S1} + \mathrm{Density2} \times \mathrm{S2} + \cdots \mathrm{Density7} \times \mathrm{S7}}{\mathrm{S1} + \mathrm{S2} + \cdots \mathrm{S7}}$$

Calculation of tubule length in HEK cells was performed by Imaris 8.2.0 (BITPLANE, 2015). Briefly, the z-stacks of each cell were reconstructed into a 3D volume in the software using the '3D volume rendering' modes. The cell membrane and connected tubules (stained by CellMask DeepRed) were thresholded with manual threshold adjustments to remove the background. Tubules in the software were demonstrated as spines. 15 spines in each cell (120 spines from 8 cells in total) were selected and the lengths were measured through its 'measurement point' feature. The average length of tubules was then calculated and compared.

Calculation of correlation coefficients

Pearson correlation coefficients were calculated in Matlab with a custom-designed program based on the build-in function corr2 (2-D correlation coefficient). Briefly, images or stacks were pre-processed as described above. All images were thresholded by the Matlab function graythresh. Then paired images or stacks of two channels were processed through the corr2-based method for the correlation coefficients. To compare the coefficients between multiple groups, data were statistically processed by the analysis of variance (ANOVA) (one-way or two-way), followed by post-hoc multiple comparisons by Tukey's multiple comparison tests in GraphPad Prism.

Calculation of t-tubule regularity in rat cardiomyocytes

To evaluate the regularity of t-tubules in rat cardiomyocytes, a custom program in Matlab was applied to calculate the FFT power of the sarcomeric spatial frequency of 0.58 μm-1 (the distance between adjacent t-tubules in rat cardiomyocyte is approximately 1.72μm) as the indicator of tubule regularity. Briefly, rat cardiomyocytes were labeled by the plasma membrane dye CellMask DeepRed and imaged in the middle section of the cell through a confocal microscope. All images were noise-removed before further steps. All images were processed by a Matlab based algorithm as previously described (Tian et al. 2012). The data was further statistically processed by the analysis of variance (ANOVA) (one-way), followed by post-hoc Tukey's multiple comparison tests in GraphPad Prism.

Analysis of the calcium release in rat cardiomyocytes and hiPSC-CMs

To analyze calcium release in rat cardiomyocytes and hiPSC-CMs, image series of Fluo4-loaded cells were processed by the CaCLEAN algorithm as previously described (Tian et al. 2017). Briefly, imaging data was loaded into Matlab through custom code based on the LOCI bio-format tools (Linkert et al. 2010). The appropriate short image series in the upstroke stage of each Ca^{2+} transient was extracted with custom Matlab codes. The stacks were then processed to remove noise with custom Matlab functions based on the 'CANDLE' de-noising algorithm (Coupé et al. 2012). A reference image involving the camera offset and the fluorescence baseline was calculated by an average of two or three frames captured prior to electrical stimulation. The image was subtracted from all subsequent frames. Then the preprocessed data were passed to the CaCLEAN algorithm. After that, the results containing data such as properties of EC coupling including the amplitude (FF0), the upstroke time of calcium transient, as well as EC couplons were generated and automatically saved in the “mat” file format. The data were exported and further processed by an analysis of variance (ANOVA), followed by post-hoc Tukey’s multiple comparison tests in GraphPad Prism.

Investigation of the distance between EC couplons and membrane invaginations in iPSC-CMs

To calculate the shortest distance between calcium release sites or EC couplons and membrane invaginations, a custom-built Matlab based program was used. Briefly, calcium release sites of each image were calculated and generated by the CaCLEAN algorithm. The pixels with regional maximal intensity were calculated through the Matlab build-in function imregionalmax, and these pixels were defined as the centers of the calcium release units. An image of the labeled cell membrane at the same Z-position was thresholded to identify positive ‘membrane’ pixels. The distances between each calcium release site and all positive tubule pixels were calculated. Usually, calcium release units within 0μm, 0.5μm and 1.0μm distance to the nearest membrane were considered as functional EC couplons instead of orphaned RyRs. The fraction of calcium release sites within each of these distances over the total number of calcium release sites was generated and pooled together in the respective group. The data were exported and further analyzed by an analysis of variance (ANOVA), followed by post-hoc Tukey's multiple comparison tests in GraphPad Prism.

Analysis of EC couplons in Fluo4-loaded hiPSC-CM

To evaluate the properties (density and amplitude) of calcium release units in Fluo-4 loaded hiPSC-CM, a custom-built Matlab based program was used. Briefly, calcium release units were identified in each image by the CaCLEAN algorithm. With this algorithm, the total number of EC couplons was identified and the amplitude (dF/F0) of each EC couplon was computed. The cell size was defined as the total pixels within the circumvent of the cell drawn by hand. The density and amplitude of EC couplons were assessed as following:

$$Couplon\ density = Couplon\ number / Cell\ size$$

$$Couplon\ amplitude = Sum\ of\ couplon\ amplitude\ / Couplon\ number$$

Analysis of EC couplons in electrically paced rat cardiomyocytes and hiPSC-CM expressing GCaMP6f-junctin

To analyze EC couplons in rat cardiomyocytes as well as hiPSC-CMs expressing GCaMP6f-junctin, a Matlab based custom-build program was used. Briefly, all images were denoised in ImageJ with the plugin-PureDenosie before further processing. To identify EC couplons, the first 10 images from any calcium transient were selected and thresholded by the Matlab function graythresh (Otsu's method). EC couplons were identified using the Matlab function imregionalmax. After the locations of EC couplon were identified, the amplitudes of all couplons (*F*) were extracted. The baseline of the calcium signal of a given image (*F0*) was defined by the mean value of 10 resting images right before the start of calcium transient. The size of the cell area was defined as the total number of pixels within the circumvent of the cell drawn by hand. After that, the density as well as the amplitude of the EC couplon (dF/F0), were calculated as following:

$$Couplon\ density = Couplon\ number/Cell\ size$$

$$Couplon\ amplitude = Sum\ of\ couplon\ amplitude/Couplon\ number$$

$$single\ couplon\ amplitude(dF/F0) = (F - F0)/F0$$

Statistics and plotting

Quantitative data were analyzed in GraphPad Prism 6.0b (GraphPad, La Jolla, CA, USA). All data were expressed as mean ± SEM. All data were initially tested for their normal distribution using a D’Agostino-Pearson omnibus normality test. When the data were normally distributed, data between two groups were compared using an unpaired t-test; otherwise, a Mann-Whitney test was employed. For more than two groups, data comparisons were done by one-way or two-way ANOVA followed by post-hoc Tukey’s multiple comparison tests. Statistically differences were determined by p-values and categorized as follows: $p < 0.05$ (*), $p < 0.01$ (**), $p < 0.001$ (***).

All data were plotted in GraphPad Prism 5.0b. In bar plots, error bars in the figures represent the standard error of the mean. In line plots, different groups were represented by different symbols and colors. The box and whisker plot was applied to display the scale and variation of the data (e.g. tubule lengths in HEK cells).

5. Results

5.1 Identification of BIN1 isoforms in the human heart tissue

Although several BIN1 isoforms have been identified in the mouse heart, there is currently no detailed analysis of its transcription and splicing in the human heart. To address this issue, methods such as PCR and cloning were used to study this issue in human cardiac samples.

5.1.1 Screening of BIN1 splice variants in healthy human heart tissue

RNA samples of healthy human heart tissue were purchased as previously mentioned in the methods and materials section. To assess the transcription and splicing of BIN1, a primer pair spanning from the conservative N-terminus BAR domain (exon6) to the conservative C-terminus SH3 domain (exon18) was designed, which is able to detect all possible BIN1 isoforms. The result showed that there were five bands of different sizes in the gel analysis of PCR product (**Fig. 5.1A, a-e**), implying that there were several BIN1 splice variants in human heart tissue. These bands were confirmed later to be different BIN1 isoforms by DNA sequencing. Similarly, in order to see if there are any exons spliced in the N-BAR domain area, a pair of primers were designed to detect the N-BAR domain(exon1-10). The PCR results demonstrated a single band, indicating a consistent presence of exons 1-10 in all BIN1 variants (**Fig. 5.1B**). The sequence of the

N-BAR domain was found to include exons from 1 to 10 except exon7 by DNA sequencing.

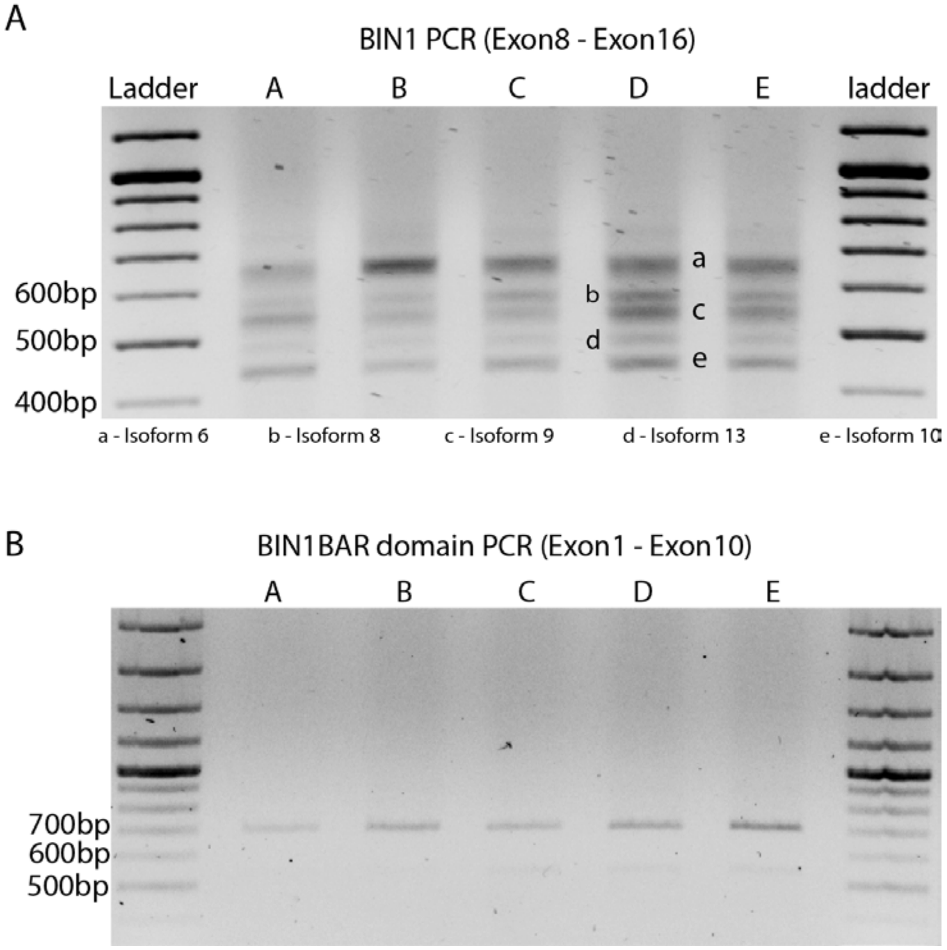
A
BIN1 PCR (Exon8 - Exon16)
Ladder
A
B
C
D
E
ladder
600bp
500bp
400bp
a
b
c
d
e
a - Isoform 6
b - Isoform 8
c - Isoform 9
d - Isoform 13
e - Isoform 10
B
BIN1BAR domain PCR (Exon1 - Exon10)
A
B
C
D
E
700bp
600bp
500bp

Figure 5.1 Analysis of BIN1 transcription and splicing in healthy human heart samples. A) PCR results of healthy human heart samples. Five bands (a-e) were identified in gel analysis: a. BIN1+E13+E17 b. BIN1+E11+E17 c. BIN1+E17 d. BIN1+E11 e. BIN1. The exact composition of each isoform was later determined by DNA sequencing. B) PCR results of the N-BAR domain. Only one type of BIN1 BAR domain was identified.

5.1.2 Analysis of the exon composition of the identified human cardiac BIN1 isoforms

In order to analyze the exon composition of these BIN1 isoforms, PCR cloning and DNA sequencing were further carried out. Generally, PCR fragments from the primer pair (exon6-18) detecting all BIN1 isoforms were ligated with T vectors. After that, the ligation mixture underwent bacterial transformation. Positive clones were then selected based on the results of colony PCR. Results of one healthy human heart sample was analyzed. The colony PCR results showed that there were bands of different sizes (**Fig. 5.2A**). Positive clones were then purified for DNA sequencing, which demonstrated that these five BIN1 splice variants included isoform6, isoform8, isoform9, isoform10, and isoform13 according to blast results in the NCBI database (**Fig. 5.2B**). These isoforms share a conserved N-terminus BAR domain encoded by exon1-10 except exon7, a conserved linking domain by exon12, and a conserved C-terminus SH3 domain by exon19-20. Interestingly, a very small band was found in the gel analysis (**Fig. 5.2A, red arrow**). However, by DNA sequencing, we found that it did not refer to any gene sequence in the database. Therefore, it might possibly be a non-specific band. Moreover, the sequence contained several stop codons so that it appeared unlikely to be translated into any protein or peptide. Therefore, this band was excluded in the following research.

It is important to note that some exons are differentially spliced among these isoforms in addition to those conservative exons. Particularly, isoform6 contains exon13 and17, isoform9 contains exon17 while isoform10 contains neither of them (the smallest BIN1 isoform). In contrast, there are two exon11-containing isoforms (isoform8 and isoform13), which were previously considered to be exclusively expressed in skeletal muscle cells(T. Hong et al. 2014). Overall, these results revealed that there were five different BIN1 isoforms expressed in human heart tissues.

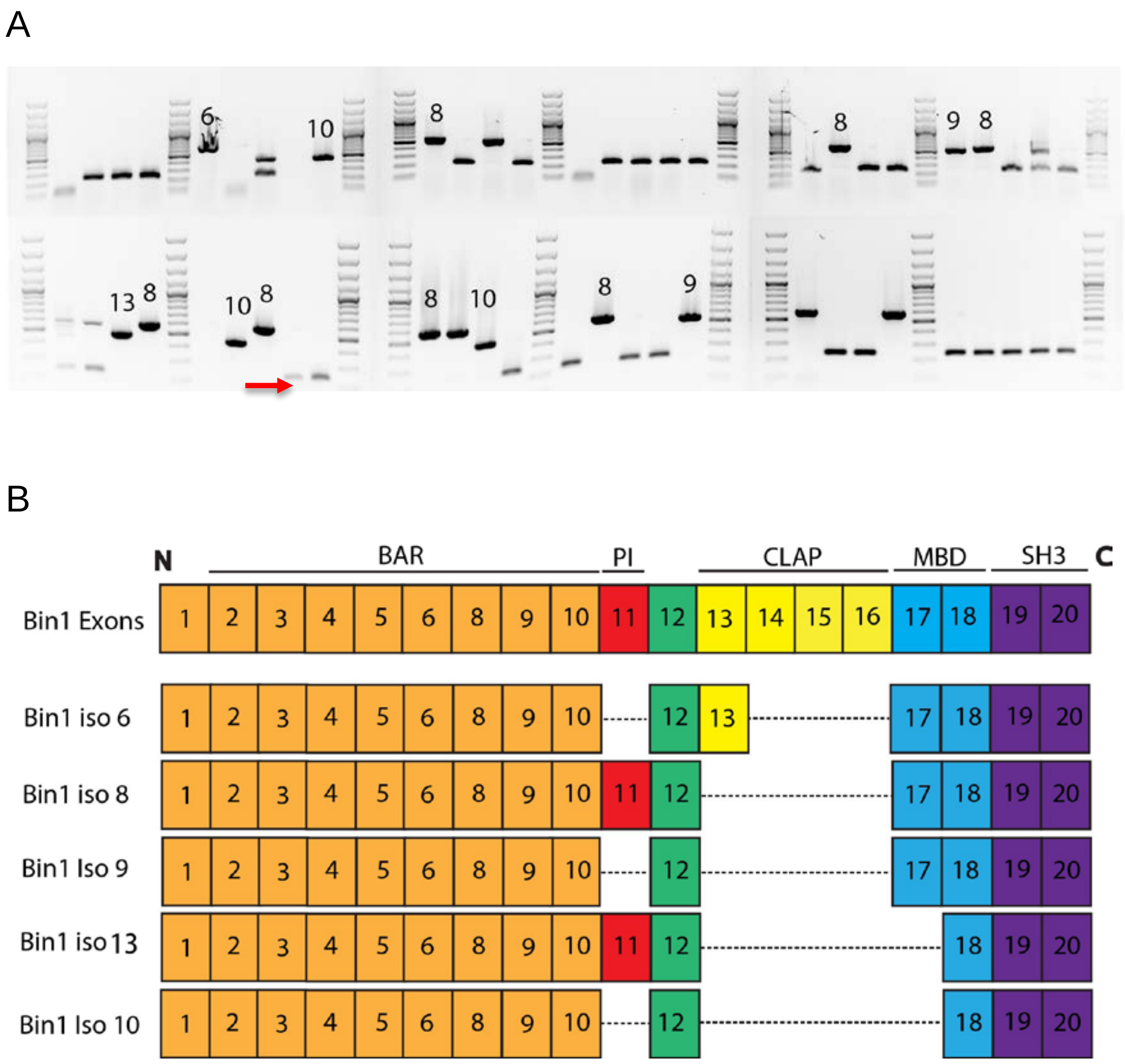
A
6
10
8
8
9
8
13
8
10
8
8
10
8
9
B
N
BAR
PI
CLAP
MBD
SH3
C
Bin1 Exons: 1 2 3 4 5 6 8 9 10 11 12 13 14 15 16 17 18 19 20
Bin1 iso 6: 1 2 3 4 5 6 8 9 10 12 13 17 18 19 20
Bin1 iso 8: 1 2 3 4 5 6 8 9 10 11 12 17 18 19 20
Bin1 Iso 9: 1 2 3 4 5 6 8 9 10 12 17 18 19 20
Bin1 iso13: 1 2 3 4 5 6 8 9 10 11 12 18 19 20
Bin1 Iso 10: 1 2 3 4 5 6 8 9 10 12 18 19 20

Figure 5.2 Analysis of exon composition of BIN1 isoforms by PCR cloning and DNA sequencing. A) Colony PCR results of healthy human heart samples. Different positive BIN1 colonies were purified and sent for DNA sequencing. B) Exon compositions of different isoforms based on sequencing and blasting results.

5.2 Characterizing the properties of BIN1 isoforms in HEK cells

BIN1 proteins are structurally compact and their functions are domain-dependent: the N-terminal conservative BAR domain (exon1-10) is responsible for membrane invagination(or tubulation), and the C-terminal SH3 domain for protein-protein interaction. As for domains encoded by exons differentially spliced among isoforms, their roles vary and are not fully elucidated. In order to study the effects of these BIN1 isoforms on cardiac myocytes, fluorescent proteins were fused to these proteins in different manners, and the properties of these isoforms were individually characterized in HEK cells.

5.2.1 Effects of N-terminal fusion

Firstly, the red fluorescent protein TagRFPT was fused to the N-terminus of BIN1 and cloned into the pacAd5 CMVK-NpA vector. Plasmids of these fusion proteins were then transfected into HEK cells and expressed for two days before confocal imaging. The results showed that almost all fusion proteins were expressed in the cytoplasm (**Fig. 5.3**). No specific tubular structures were labeled, suggesting that N-terminal fusion severely impaired the tubulating ability of the BIN1 proteins conferred by the N-terminus BAR domain. In another word, N-terminal fusion resulted in a loss of this function. Therefore, this fusion strategy was inappropriate to study the functional properties of BIN1.

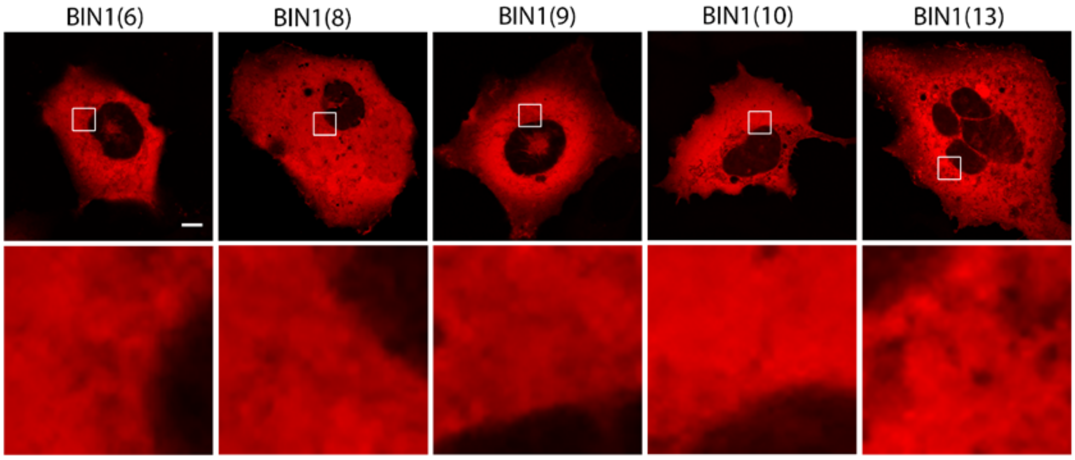

Figure 5.3 Expression of pacAd5-TagRFPT-BIN1 in HEK cells. Fluorescent protein TagRFPT was tagged to the N-terminus of BIN1 and plasmids were transfected in HEK cells. Images were taken with confocal microscopy. Scale = 10μm.

5.2.2 Effects of C-terminal fusion

Since N-terminal fusion abrogated BIN1's ability to induce tubule formation, C-terminal fusion was then assessed. Briefly, TagRFPT was fused to the C-terminus or SH3 domain of BIN1 and then cloned into the pacAd5 CMVK-NpA vector. HEK cells were transfected with the modified plasmids, the plasma membrane labeled with CellMask DeepRed, and imaged by confocal microscopy. In contrast to the cytoplasmic distribution of N-terminal fusion proteins, results here showed different results. All BIN1 isoforms were capable of generating membrane tubules to different degrees (**Fig. 5.4**).

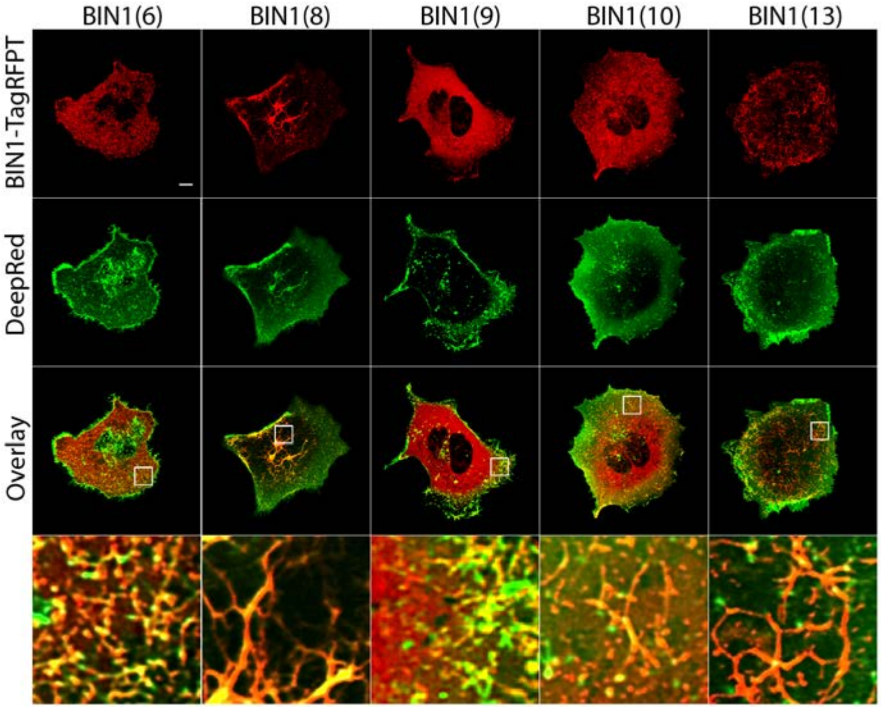

Figure 5.4 Tubule generation induced by pacAd5-BIN1-TagRFPT expressed in HEK cells. Fluorescent protein TagRFPT was fused to the C-terminus of BIN1 isoforms and transfected into HEK cells (red). The cell membrane was labeled by CellMask DeepRed (green, false color). Significantly abundant and longer tubules were mostly seen in the group of isoform13 and isoform8. Scale = 10μm.

Because the Cellmask DeepRed dye can only stain the membrane from the extracellular space, therefore the positive staining of these membrane tubules indicated that they were connected with the plasma membrane and their tubular space were continuous with the extracellular environment, which was similar to T-tubules in cardiomyocytes. However, isoform6, isoform9, and isoform10 were still partially present in the cytoplasm and mostly produced tubules of simple and small lengths (**Fig. 5.4**). In contrast, isoform8 and isoform13 were capable of generating extensive, abundant, and much longer tubules across the whole cell area, suggesting a stronger ability for tubule biogenesis than the other isoforms (**Fig. 5.4**).

A

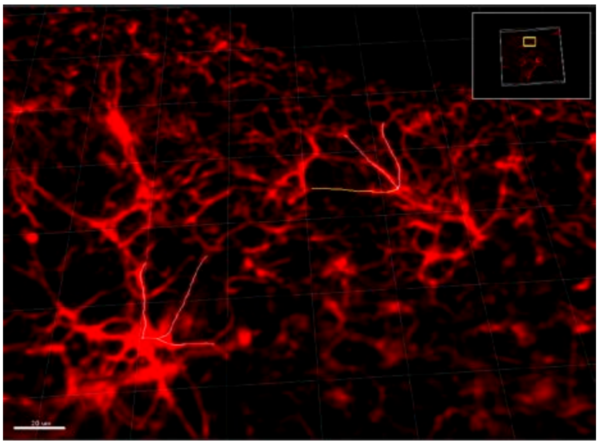

B

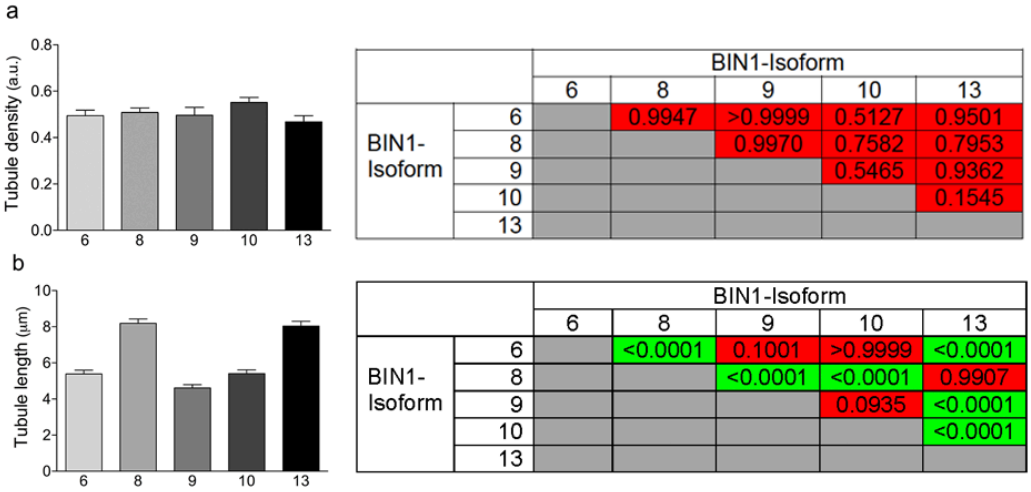

		BIN1-Isoform				
		6	8	9	10	13
BIN1-Isoform	6		0.9947	>0.9999	0.5127	0.9501
	8			0.9970	0.7582	0.7953
	9				0.5465	0.9362
	10					0.1545
	13					

		BIN1-Isoform				
		6	8	9	10	13
BIN1-Isoform	6		<0.0001	0.1001	>0.9999	<0.0001
	8			<0.0001	<0.0001	0.9907
	9				0.0935	<0.0001
	10					<0.0001
	13					

Figure 5.5 Analysis of the properties of tubules generated by pacAd5-BIN1-TagRFPT expressed in HEK cells. A) Tubule length was measured by IMARIS software. B) Tubule density (a, n = 15 cells) and length (b, n = 120 tubules from 15 cells) were analyzed among BIN1 isoforms. Comparisons between groups were analyzed by one-way ANOVA the P values were displayed in tables either as significant difference (green) or no significant difference (red). Scale = 20μm.

In order to analyze tubulation in detail, densities and lengths of tubules produced by BIN1 in HEK cells were quantified with IMARIS software (see methods and materials section) (**Fig. 5.5A**). Eight tubules were randomly selected from 15 cells in each group. The lengths were measured by IMARIS and then averaged. Density was defined as the value of tubule amount dividing the cell volume. The results showed that the tubule densities were similar across all isoforms, showing no significant difference (**Fig. 5.5B,a**). Nevertheless, tubules produced by isoform8 and isofom13 were significantly longer than those formed by other isoforms, suggesting isoforms containing exon11 were more potent in inducing tubules (**Fig. 5.5B,b**).

5.2.3 Application of the 2A cloning strategy for BIN1 isoforms

The previous study has demonstrated that the C-terminal SH3 domain of BIN1 is necessary for the function of protein-protein interaction such as trafficking of certain ion channels and sarcomere assembly(Takei et al. 1999). If the C-terminus was fused to other protein tags such as TagRFPT, it may hinder the normal functions of BIN1. Therefore, to study the functions of BIN1 isoforms properly and maintain their full function at the same time, it was necessary to avoid fusion events at any terminus. Therefore, a new strategy was implemented for cloning. A small sequence of 2A peptide was inserted between the TagRFPT and the BIN1. After plasmid transfection and protein translation, the resulting protein is believed to be split into two independent entities, which are thought to function independently and therefore minimize the adverse effects resulted from N-or C- terminal fusion. As expected, the results showed that this type of approach could induce abundant tubules similar to those by the C-terminus fusion constructs without significant cytosol retention, suggesting that BIN1's ability to induce tubule formation was preserved (**Fig. 5.6**).

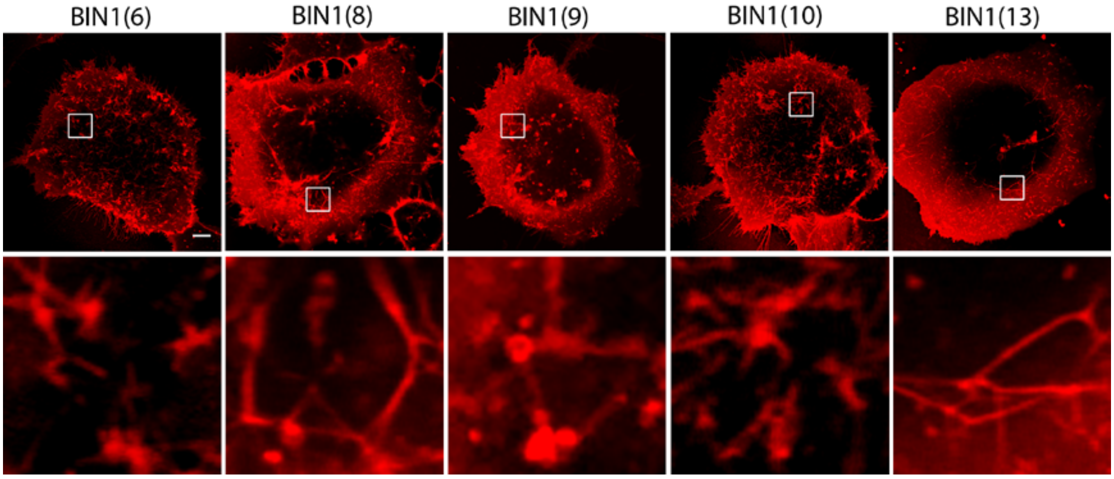

Figure 5.6 Tubule formation induced by pacAd5-TagRFPT-2A-BIN1 expressed in HEK cells. Fluorescent protein TagRFPT was fused to the N-terminus of BIN1 isoforms via a short 2A sequence. Vectors were transfected in HEK cells. The cell membrane was labeled by CellMask DeepRed. Images were taken with confocal microscopy. Scale = 10μm.

5.3 Effects of BIN1 isoforms on adult rat cardiomyocytes

It is known that BIN1 plays an important role in both skeletal and cardiac myocytes. However, the roles of BIN1 isoforms are not fully understood. Because I have identified five different BIN1 isoforms in the human heart, it is necessary to study their roles in cardiomyocytes.

5.3.1 Establishment of detubulation models in cultured adult rat ventricular myocytes

The model of cultured adult rat ventricular myocytes was established by isolating adult rat cardiomyocytes and culturing them *in vitro*. Cells were supported with medium M199 supplemented with antibiotics and ITS (Insulin-Transferrin-Selenium). Under such a condition cells were able to last up to around one week. The most iconic change during culture is that rat cardiomyocytes dramatically lose their T-tubules (a process called detubulation) (FOWLER 2004), which was verified in a three-day culture and imaging. It is apparent that the density of T-tubules is significantly declined compared to freshly isolated cardiomyocytes (**Fig. 5.7A, a-c; B)**. When cells were supplemented with Cytochalasin D (Tian et al. 2012), a compound reported to be able to maintain the cytoskeleton of cultured cardiomyocytes, the density of T-tubules was maintained (**Fig. 5.7A, d-e; B**). Interestingly, it was reported in several studies that the density and regularity of T-tubules was largely decreased in various cardiac pathological conditions, especially in failing hearts (Lyon et al. 2009; Wei et al. 2010; Guo et al. 2013). Therefore, this *in vitro* culture is a useful model to test the effects of candidate proteins or reagents on cardiomyocytes, especially with respect to their effects on the T-tubule system and EC-coupling.

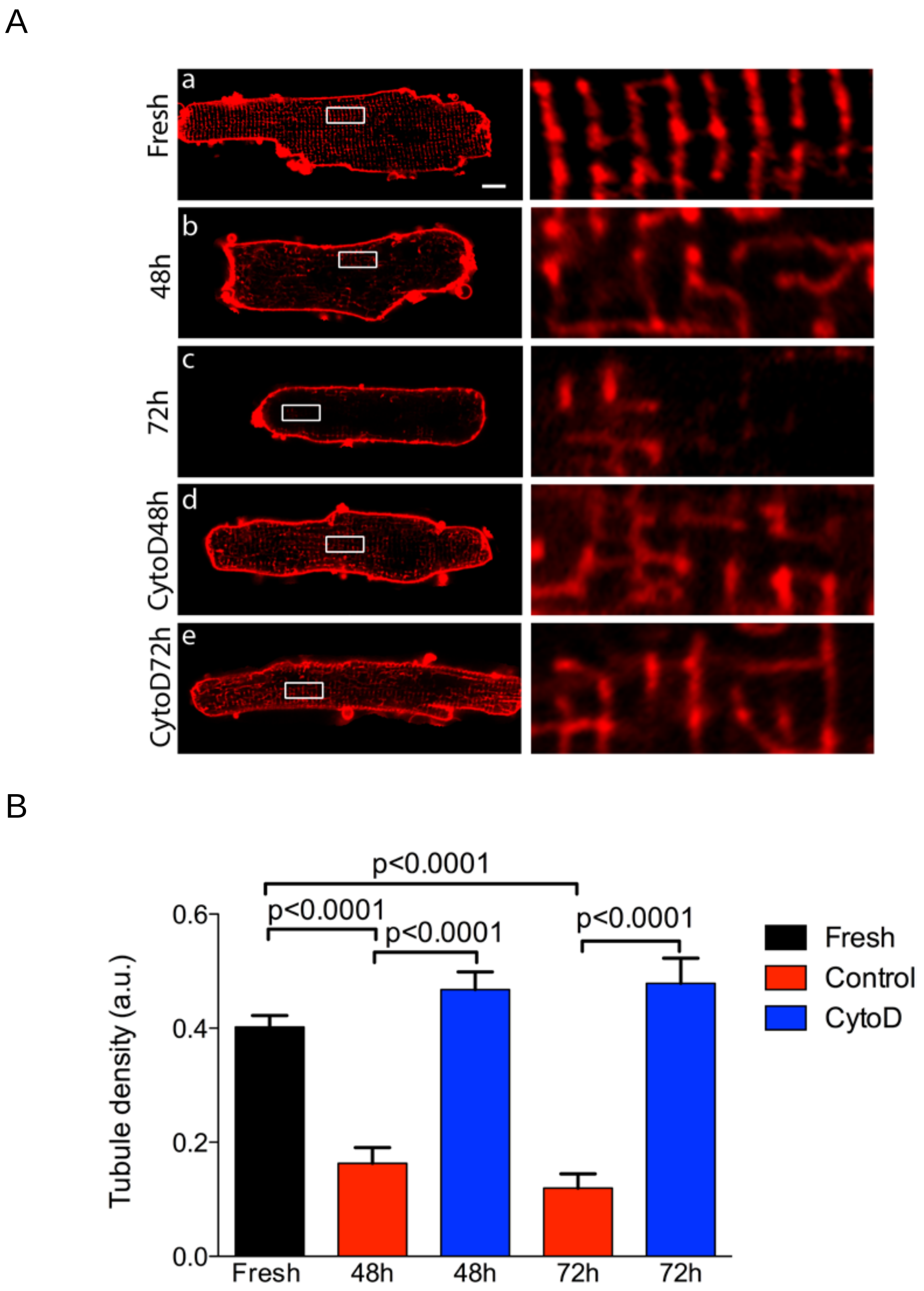
A
a
Fresh
b
48h
c
72h
d
CytoD48h
e
CytoD72h
B
p<0.0001
p<0.0001
p<0.0001
p<0.0001
0.6
0.4
0.2
0.0
Tubule density (a.u.)
Fresh
48h
48h
72h
72h
Fresh
Control
CytoD

Figure 5.7 Detubulation of adult rat ventricular myocytes during culture *in vitro*. A) Isolated or cultured rat cardiomyocytes. a) freshly isolated rat cardiomyocytes. b-c) isolated rat cardiomyocyts cultured for 48hrs and 72hrs respectively. d-e) cultured rat cardiomyocytes supplemented with Cytochalasin D for 48hrs and 72hrs. Cells were stained by CellMask DeepRed membrane dye. B) Statistics of T-tubule densities of cultured rat

cardiomyocytes. Comparisons between groups were analyzed by one-way ANOVA and the P values were displayed. n = 30 cells. Scale = 10 μm.

5.3.2 Maintenance of EC couplons by human cardiac BIN1 isoforms

To study the effects of BIN1 isoforms on adult cardiomyocytes, a series of experiments was carried out to investigate whether BIN1 is effective in upholding EC couplons formed by LTCCs and RyR2s. Particularly, two different approaches were applied. On one hand, their effects on maintaining EC coupling during culture were assessed; on the other, their effects on recovering the decline of EC coupling during culture were also evaluated. Similarly, two types of calcium labeling techniques were used, Fluo-4 and GCaMP6f-junctin.

Briefly, isolated adult rat ventricular myocytes were transduced with adenovirus of the BIN1 isoforms and cultured for 72 hours thereafter before confocal microscopic imaging. It is established that LTCCs and RyR2s are key components of EC couplons. Moreover, BIN1 expression has been associated with the trafficking of LTCCs while junctophilin-2 is considered crucial to bridge the dyads to form EC couplons. Therefore, it appears necessary to study the expression and correlation of these proteins, which I analyzed using immunofluorescent staining.

First of all, the results showed that while BIN1 expression was significantly reduced in control cells after a period of 3 days in culture, transduction with BIN1 adenoviruses restored the expression of the protein (**Fig. 5.8A**). Interestingly, cells expressing the isoform8 and isoform13 displayed immunolabeling with some resemblance of a tubular network while the other isoforms were stained without certain patterns. As for the RyR2, while its arrangement and density were maintained in BIN1-expressing cells, its density was decreased in control (**Fig. 5.8B; C, b**). Similarly, the expression of LTCC demonstrated better immunolabeling in BIN1 expressing myocytes compared to the control group, in which LTCCs were sparsely distributed with reduced density (**Fig. 5.8B; C-a**). In addition, the colocalization between LTCC and RyR2, which is a hallmark of efficient EC-coupling, was also analyzed. Colocalization in BIN1-expressing myocytes was significantly higher than that in the control, similar to that of freshly isolated cardiomyocytes (**Fig. 5.8C, c**).

A

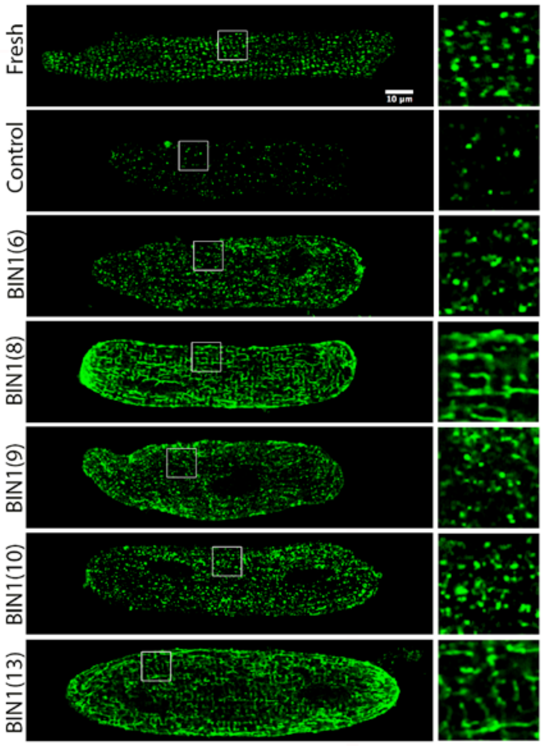

B

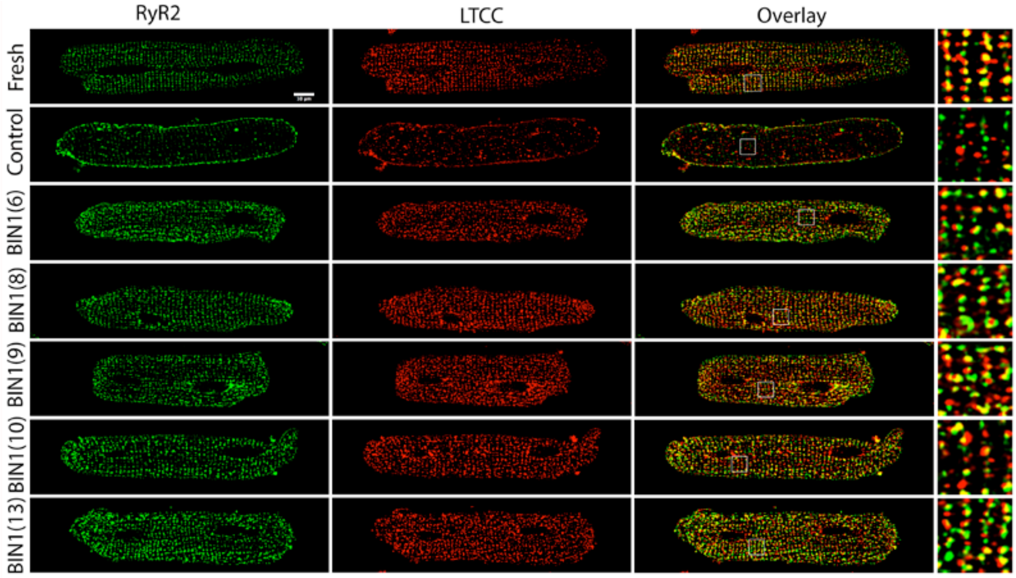

C

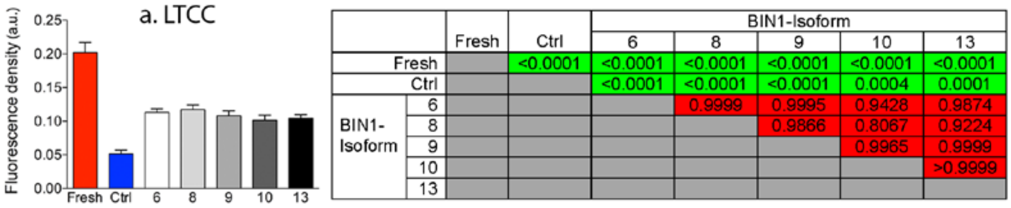

		Fresh	Ctrl	BIN1-Isoform				
				6	8	9	10	13
Fresh			<0.0001	<0.0001	<0.0001	<0.0001	<0.0001	<0.0001
Ctrl				<0.0001	<0.0001	<0.0001	0.0004	0.0001
BIN1-Isoform	6				0.9999	0.9995	0.9428	0.9874
	8					0.9866	0.8067	0.9224
	9						0.9965	0.9999
	10							>0.9999
	13							

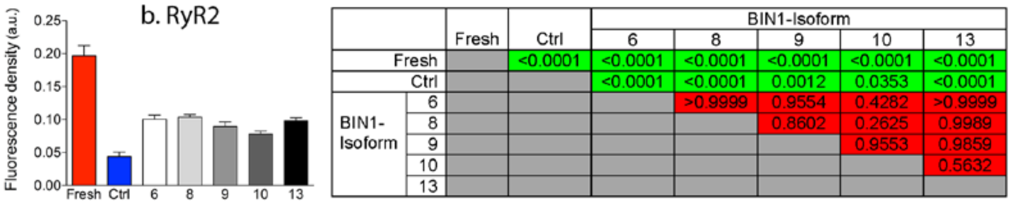

		Fresh	Ctrl	BIN1-Isoform				
				6	8	9	10	13
Fresh			<0.0001	<0.0001	<0.0001	<0.0001	<0.0001	<0.0001
Ctrl				<0.0001	<0.0001	0.0012	0.0353	<0.0001
BIN1-Isoform	6				>0.9999	0.9554	0.4282	>0.9999
	8					0.8602	0.2625	0.9989
	9						0.9553	0.9859
	10							0.5632
	13							

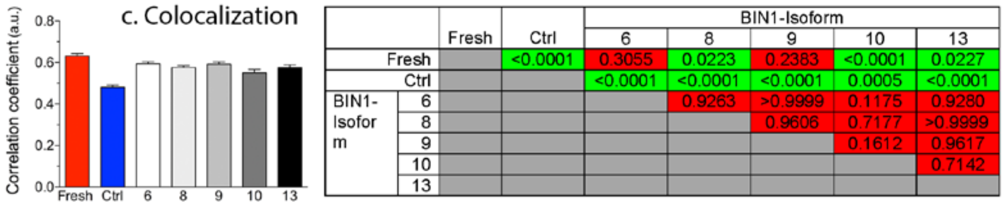

		Fresh	Ctrl	BIN1-Isoform				
				6	8	9	10	13
Fresh			<0.0001	0.3055	0.0223	0.2383	<0.0001	0.0227
Ctrl				<0.0001	<0.0001	<0.0001	0.0005	<0.0001
BIN1-Isofor m	6				0.9263	>0.9999	0.1175	0.9280
	8					0.9606	0.7177	>0.9999
	9						0.1612	0.9617
	10							0.7142
	13							

Figure 5.8 Analysis of immunofluorescent labeling of LTCC and RyR2 in cultured rat cardiomyocytes. A) Representative images of BIN1 isoforms immunostaining in cultured rat cardiomyocytes (rabbit anti-BIN1, green). B) Representative images of double immunostaining of LTCC (red) and RyR2 (green) in rat cardiomyocytes. C) Fluorescence density of LTCC (a) and RyR2 (b). Pearson correlation coefficients between LTCC and RyR2 in rat cardiomyocytes(c). Comparisons between groups were analyzed by one-way

ANOVA and the P values were displayed in tables either as significant difference (green) or no significant difference (red). n = 26-30 cells from three independent experiments. Scale = 10µm.

In addition, along with the decrease of T-tubules, another key protein for efficient EC-coupling, junctophilin-2, was also significantly downregulated and disorganized after cardiomyocytes were cultured for 3 days *in vitro* (**Fig. 5.9**). Interestingly, when BIN1 isoforms were overexpressed in rat cardiomyocytes, the density and distribution of junctophilin-2 were maintained compared to that of control cells (**Fig. 5.9B**). Further analysis showed that cells expressing BIN1 isoforms, particularly isoform8 and isoform13, demonstrated significantly higher colocalization than control cells(**Fig. 5.9C**).

A

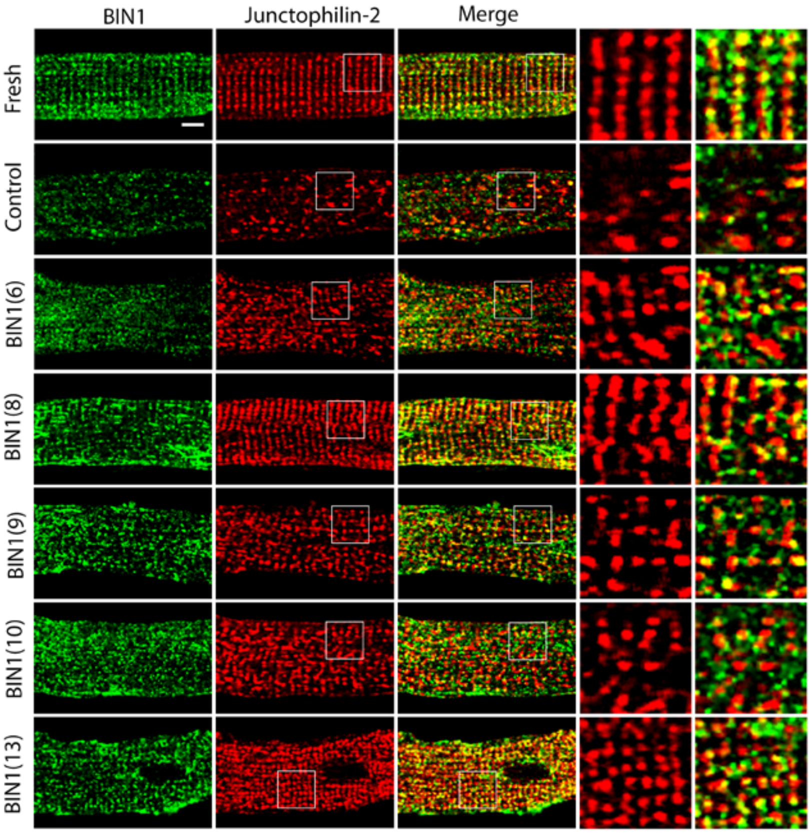

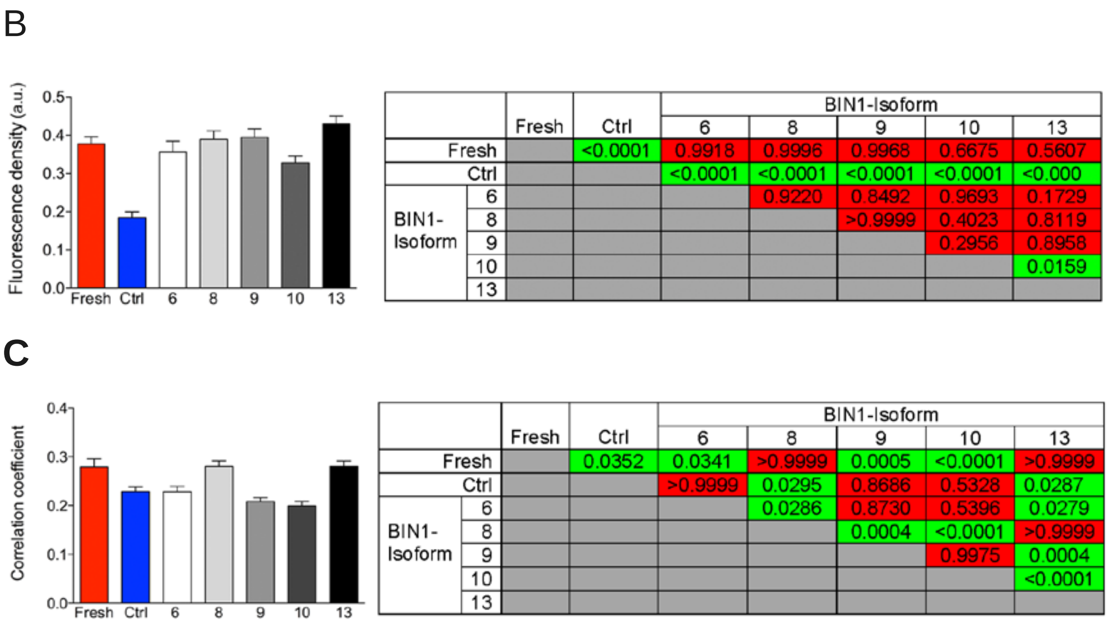

B

		Fresh	Ctrl	BIN1-Isoform				
				6	8	9	10	13
Fresh			<0.0001	0.9918	0.9996	0.9968	0.6675	0.5607
Ctrl				<0.0001	<0.0001	<0.0001	<0.0001	<0.000
BIN1-Isoform	6				0.9220	0.8492	0.9693	0.1729
	8					>0.9999	0.4023	0.8119
	9						0.2956	0.8958
	10							0.0159
	13							

C

		Fresh	Ctrl	BIN1-Isoform				
				6	8	9	10	13
Fresh			0.0352	0.0341	>0.9999	0.0005	<0.0001	>0.9999
Ctrl				>0.9999	0.0295	0.8686	0.5328	0.0287
BIN1-Isoform	6				0.0286	0.8730	0.5396	0.0279
	8					0.0004	<0.0001	>0.9999
	9						0.9975	0.0004
	10							<0.0001
	13							

Figure 5.9 Analysis of immunofluorescent staining of BIN1 and junctophilin-2 in cultured rat cardiomyocytes. A) Representative images of BIN1 (green) and junctophilin-2 (red) immunostaining in rat cardiomyocytes. B) Analysis of fluorescence density of junctophilin-2 in rat cardiomyocytes. C) Colocalization analysis of BIN1 and junctophilin-2 in rat cardiomyocytes. Comparisons between groups were analyzed by one-way ANOVA and the P values were displayed in tables either as significant difference (green) or no significant difference (red). n = 15 cells. Scale = 10μm.

Moreover, it revealed that along with the culture and reduction of junctophilin-2, the colocalization between RyR2 and junctophilin-2, which is also very important for EC-coupling, similarly decreased in control (**Fig. 5.10A-B**). However, when BIN1 was overexpressed, their colocalizations were obviously well maintained when compared to the control (**Fig. 5.10A-B**). Noteworthily, BIN1 isoform13 appeared to be particularly efficient in this aspect.

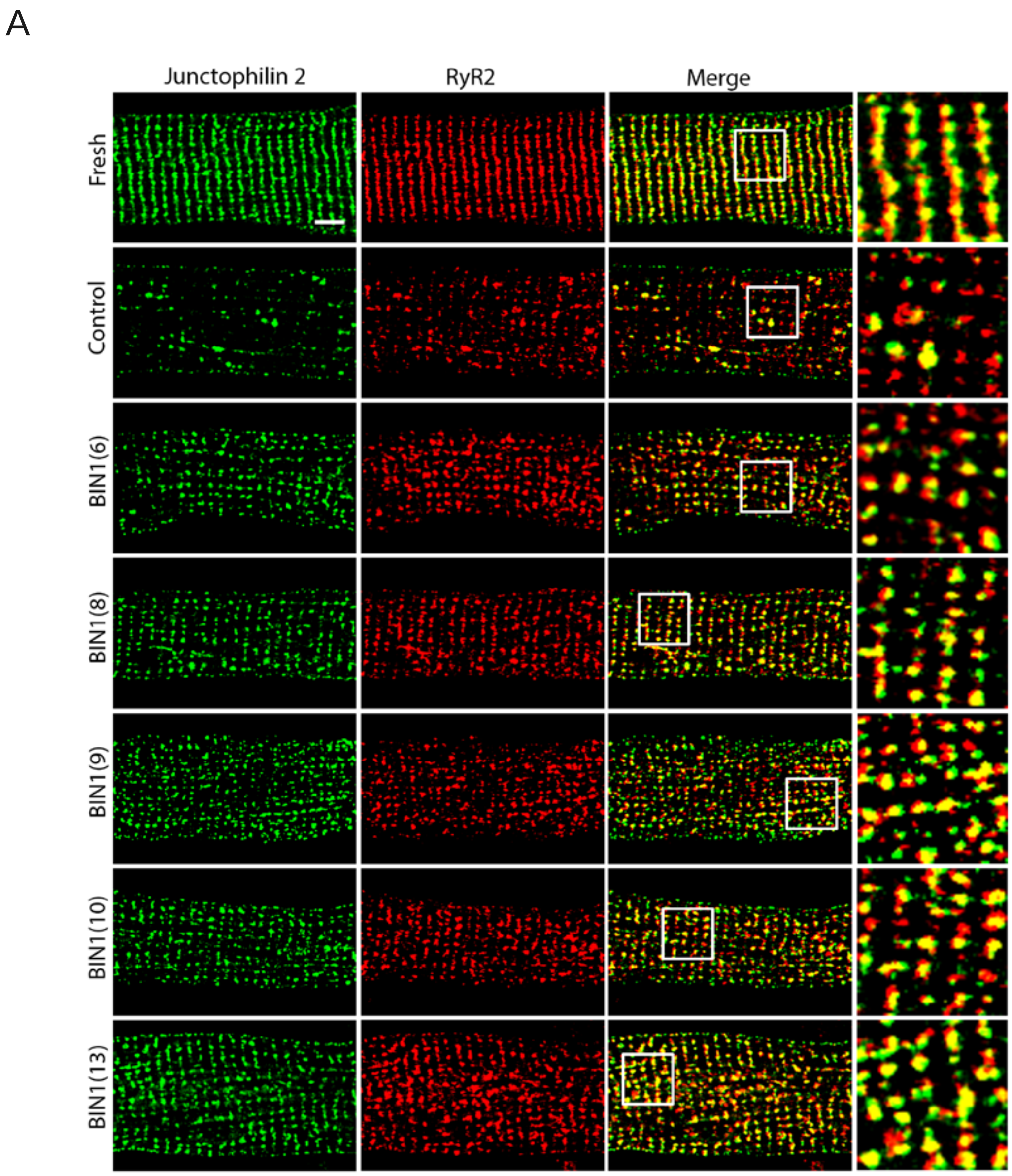
A
Junctophilin 2
RyR2
Merge
Fresh
Control
BIN1(6)
BIN1(8)
BIN1(9)
BIN1(10)
BIN1(13)

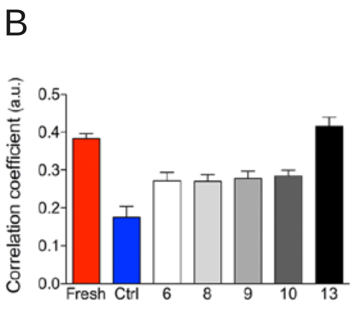

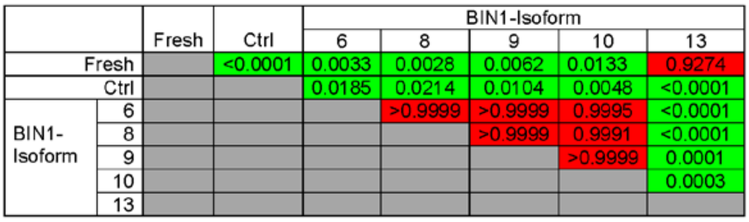

		Fresh	Ctrl	BIN1-Isoform				
				6	8	9	10	13
Fresh			<0.0001	0.0033	0.0028	0.0062	0.0133	0.9274
Ctrl				0.0185	0.0214	0.0104	0.0048	<0.0001
BIN1-Isoform	6				>0.9999	>0.9999	0.9995	<0.0001
	8					>0.9999	0.9991	<0.0001
	9						>0.9999	0.0001
	10							0.0003
	13							

Figure 5.10 Analysis of immunofluorescent labeling of junctophilin-2 and RyR2 in cultured rat cardiomyocytes. A) Representative images of junctophilin-2 (green) and RyR2 (red) immunostaining in rat cardiomyocytes. B) Pearson correlation coefficients between junctophilin-2 and RyR2.

Comparisons between groups were analyzed by one-way ANOVA and the P values were displayed in tables either as significant difference (green) or no significant difference (red). n = 15 cells. Scale = 10μm.

Other ion channels such as sodium channels (Scn5a) are also important to EC-coupling. Here, the expression of the cardiac sodium channel was also evaluated by immunofluorescent labeling. My experimental results showed that expression of Scn5a was significantly downregulated in control cells compared to myocytes expressing the BIN1 isoform6, 8,13(**Fig. 5.11**). In particular, the expression of Scan5a was decreased in central areas, but not in the periphery. This trend appeared consistent with the change of T-tubules as previously(**Fig. 5.7**). On the contrary, Scn5a-expression maintained in cardiomyocytes transduced with BIN1 adenovirus (**Fig. 5.11**). This may be attributed to the maintenance of T-tubules by BIN1 expression since a significant fraction of sodium channels are distributed in these structures of the sarcolemma(Domínguez et al. 2008).

A

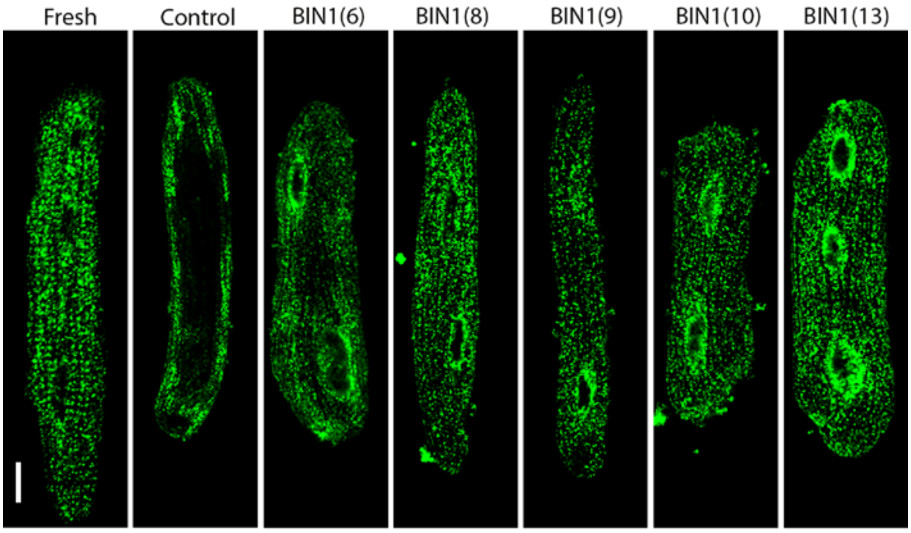

B

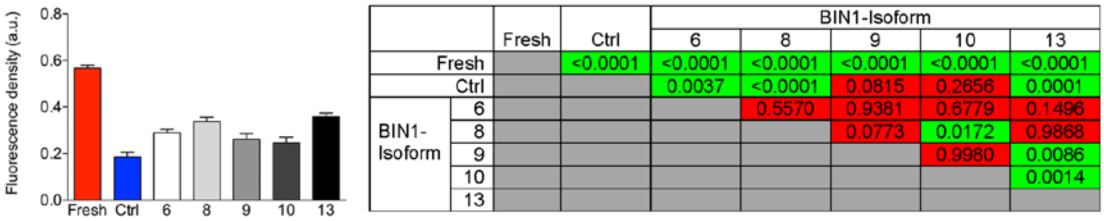

		Fresh	Ctrl	BIN1-Isoform				
				6	8	9	10	13
Fresh			<0.0001	<0.0001	<0.0001	<0.0001	<0.0001	<0.0001
Ctrl				0.0037	<0.0001	0.0815	0.2656	0.0001
BIN1-Isoform	6				0.5570	0.9381	0.6779	0.1496
	8					0.0773	0.0172	0.9868
	9						0.9980	0.0086
	10							0.0014
	13							

Figure 5.11 Immunofluorescent staining of Scn5a in cultured rat cardiomyocytes. A) Representative images of Scn5a (green) immunostaining in rat cardiomyocytes. B) Analysis of fluorescence density of Scn5a in rat cardiomyocytes. Comparisons between groups were analyzed by one-way ANOVA and the P values were displayed in tables either as significant difference (green) or no significant difference (red). n = 13 cells. Scale = 10µm.

5.3.3 Effects of BIN1 isoforms on maintaining cardiac EC-coupling

In order to analyze the role of BIN1 isoforms in living cells, experiments of live imaging were carried out to analyze calcium handling in rat cardiomyocytes. As previously described, isolated rat cardiomyocytes were transduced with adenovirus encoding for various BIN1 isoforms and cultured for 72 hours before undergoing confocal microscopic imaging to investigate the effects of BIN1 isoforms (**Fig. 5.12A**). Cells were co-stained by CellMask DeepRed dye to label membrane invaginations and loaded with Fluo-4 to measure calcium. For the quantitative analysis of calcium release, the CaCLEAN algorithm developed by our lab was implemented to characterize the properties of EC couplons (Tian et al. 2017). Calcium release points were calculated out through the algorithm and indicate the location of functional EC-couplons formed by RyRs/LTCCs, which allows the evaluation of the status of EC-coupling in these cells.

My data indicated that cells transduced with either empty vectors or expressing TagRFPT lost most of the T-tubules except those in the periphery (**Fig. 5.12B, upper panel**). Along with that, the density of calcium release sites was significantly reduced compared to that of freshly isolated cells as well as BIN1 overexpressing cardiomyocytes. Where there were no tubules, EC-coupling was weak or absent. In contrast, after over-expression of BIN1 isoforms, the T-tubules, as well as functional calcium release sites, were largely maintained when compared to the control group (**Fig. 5.12B, lower panel**). A significant fraction of T-tubules were preserved in the central area of the cells, which is important for efficient EC-coupling because it favors the establishment of EC couplons in the inner area of cardiomyocytes, and promotes the calcium release as well as myofilament contractions in the inner cellular space.

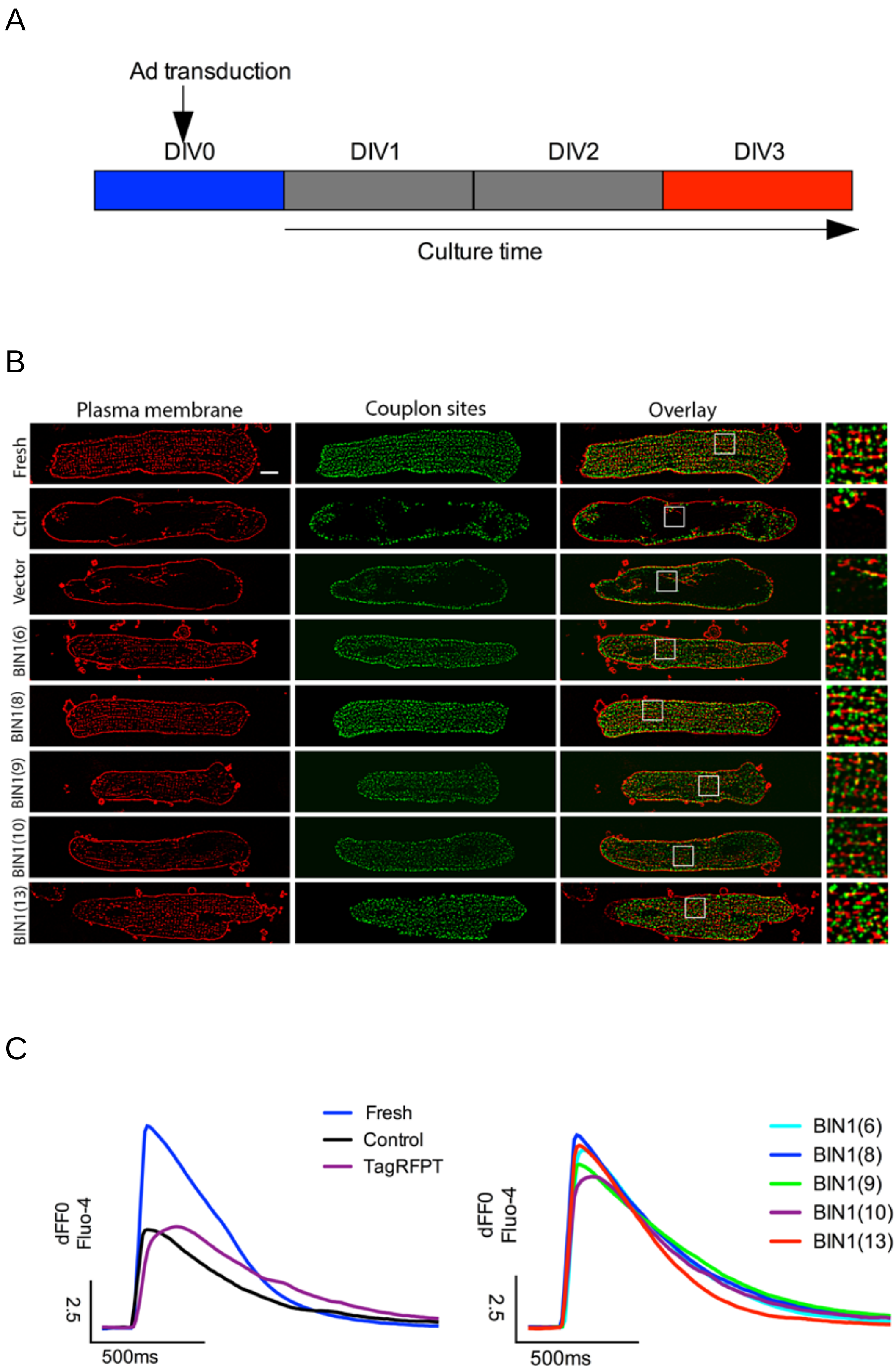
A
Ad transduction
DIV0
DIV1
DIV2
DIV3
Culture time
B
Plasma membrane
Couplon sites
Overlay
Fresh
Ctrl
Vector
BIN1(6)
BIN1(8)
BIN1(9)
BIN1(10)
BIN1(13)
C
Fresh
Control
TagRFPT
dFF0
Fluo-4
2.5
500ms
BIN1(6)
BIN1(8)
BIN1(9)
BIN1(10)
BIN1(13)
dFF0
Fluo-4
2.5
500ms

D

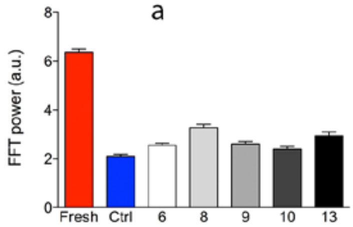

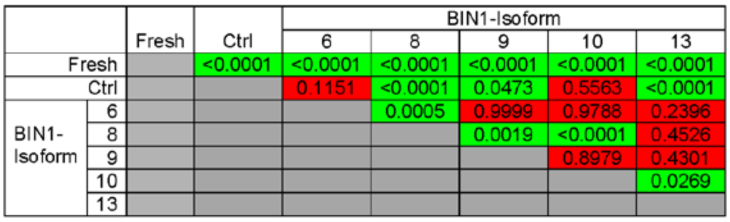

		Fresh	Ctrl	BIN1-Isoform				
				6	8	9	10	13
Fresh			<0.0001	<0.0001	<0.0001	<0.0001	<0.0001	<0.0001
Ctrl				0.1151	<0.0001	0.0473	0.5563	<0.0001
BIN1-Isoform	6				0.0005	0.9999	0.9788	0.2396
	8					0.0019	<0.0001	0.4526
	9						0.8979	0.4301
	10							0.0269
	13							

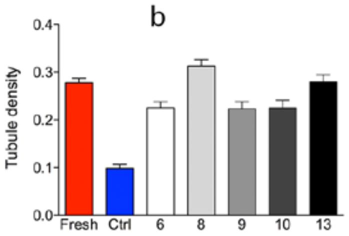

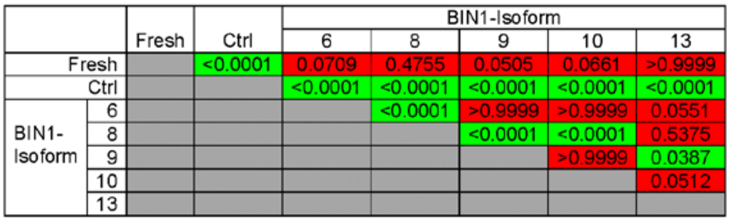

		Fresh	Ctrl	BIN1-Isoform				
				6	8	9	10	13
Fresh			<0.0001	0.0709	0.4755	0.0505	0.0661	>0.9999
Ctrl				<0.0001	<0.0001	<0.0001	<0.0001	<0.0001
BIN1-Isoform	6				<0.0001	>0.9999	>0.9999	0.0551
	8					<0.0001	<0.0001	0.5375
	9						>0.9999	0.0387
	10							0.0512
	13							

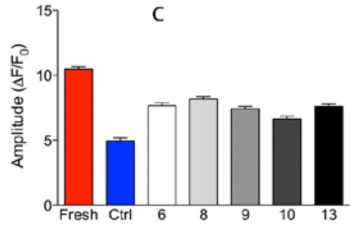

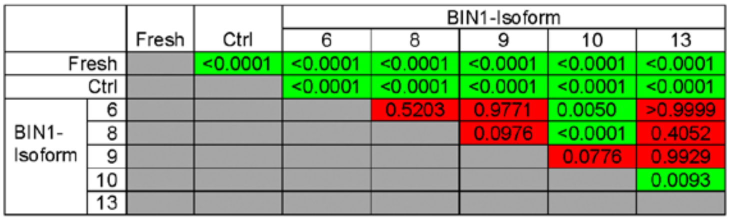

		Fresh	Ctrl	BIN1-Isoform				
				6	8	9	10	13
Fresh			<0.0001	<0.0001	<0.0001	<0.0001	<0.0001	<0.0001
Ctrl				<0.0001	<0.0001	<0.0001	<0.0001	<0.0001
BIN1-Isoform	6				0.5203	0.9771	0.0050	>0.9999
	8					0.0976	<0.0001	0.4052
	9						0.0776	0.9929
	10							0.0093
	13							

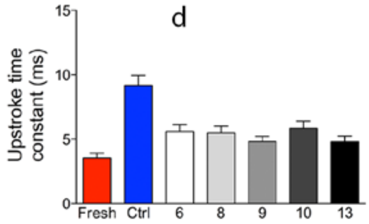

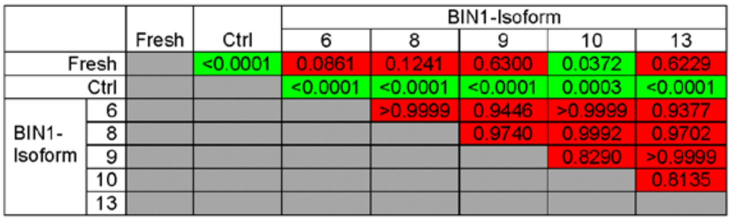

		Fresh	Ctrl	BIN1-Isoform				
				6	8	9	10	13
Fresh			<0.0001	0.0861	0.1241	0.6300	0.0372	0.6229
Ctrl				<0.0001	<0.0001	<0.0001	0.0003	<0.0001
BIN1-Isoform	6				>0.9999	0.9446	>0.9999	0.9377
	8					0.9740	0.9992	0.9702
	9						0.8290	>0.9999
	10							0.8135
	13							

E

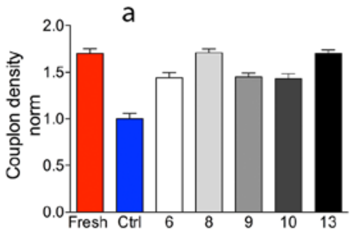

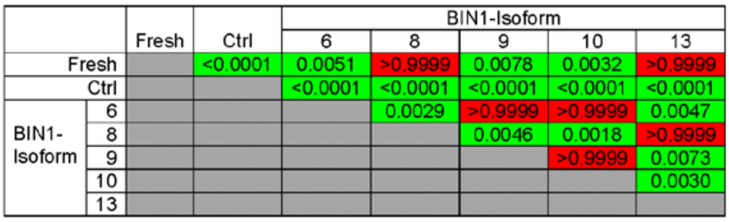

		Fresh	Ctrl	BIN1-Isoform				
				6	8	9	10	13
Fresh			<0.0001	0.0051	>0.9999	0.0078	0.0032	>0.9999
Ctrl				<0.0001	<0.0001	<0.0001	<0.0001	<0.0001
BIN1-Isoform	6				0.0029	>0.9999	>0.9999	0.0047
	8					0.0046	0.0018	>0.9999
	9						>0.9999	0.0073
	10							0.0030
	13							

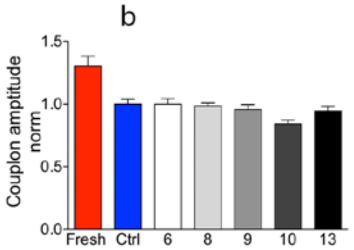

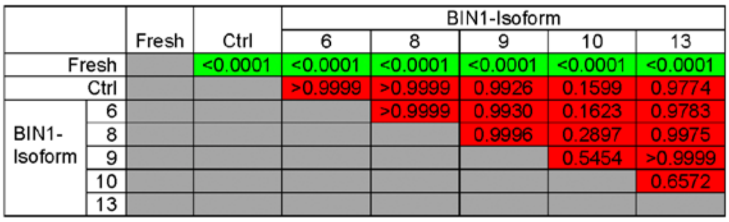

		Fresh	Ctrl	BIN1-Isoform				
				6	8	9	10	13
Fresh			<0.0001	<0.0001	<0.0001	<0.0001	<0.0001	<0.0001
Ctrl				>0.9999	>0.9999	0.9926	0.1599	0.9774
BIN1-Isoform	6				>0.9999	0.9930	0.1623	0.9783
	8					0.9996	0.2897	0.9975
	9						0.5454	>0.9999
	10							0.6572
	13							

Figure 5.12 Effects of human cardiac BIN1 isoforms on cultured rat cardiomyocytes measured by Fluo-4. A) Schematic diagram of experiment route**.** B) Representative confocal images of tubules and calcium release in cultured rat cardiomyocytes. The membrane was stained by CellMask DeepRed (red). Calcium release sites symbolizing functional RyR2/LTCC couplons were calculated by the CaCLEAN algorithm (green). Scale=10μm. C) Typical traces of calcium transients in each group. D) Statistics of tubule regularity (a), density (b), amplitude(c), and upstroke time of calcium transient (d). n= 72-82 cells from three independent experiments. E) Analysis of density (a) and amplitude (b) of EC couplons calculated by CaCLEAN algorithm. n = 60 cells from three independent experiments. Comparisons between groups were analyzed by one-way ANOVA and the P values were displayed in tables either as significant difference (green) or no significant difference (red). All data are presented as the mean ± s.e.m.

To quantify the results, four parameters - tubule regularity, tubule density, calcium transient amplitude, and upstroke time of calcium transient - were analyzed. The results showed that the tubule regularity was significantly increased in the BIN1 group when compared to the control (**Fig. 5.12D, a**). More obviously, after BIN1 overexpression the tubule density was much higher than that in control(**Fig. 5.12D, b**). As for calcium transients, indicating the functional state of EC-coupling, the amplitude was subsequently increased and the speed of the calcium upstroke was also faster than that in control cells (**Fig. 5.12D, c-d**). It is interesting to note that the isoform13 and isoform8 which contain exon11 appeared more potent than the other isoforms, both in alleviating T-tubule loss and in maintaining EC-coupling. To compare the changes in details, the properties of EC couplons were analyzed. The results showed that the density of EC couplons was significantly increased after BIN1 overexpression (**Fig. 5.12E, a**). Interestingly, the amplitude of their calcium release actually remained similar and no significant differences were found (**Fig. 5.12E, b**). Overall, these results suggested that BIN1 isoforms were effective in maintaining T-tubules as well as calcium handling in adult rat cardiomyocytes.

5.3.4 Effects of BIN1 isoforms on cardiac EC-coupling revealed by GCaMP6f-junctin

Fluo-4 is a small molecule dye that can diffuse freely in the cytosol. Therefore, it can be used as an indicator to precisely detect calcium in cardiomyocytes. In addition to Fluo-4, another type of calcium indicator, GCaMP6f-junctin (Shang et al. 2014), a genetically encoded calcium probe, was applied to measure the calcium signal changes locally in the present study. GCaMP6f is a genetically-encoded calcium indicator that reacts very fast to calcium change (T.-W. Chen et al. 2013). Junctin is a transmembrane protein located at the cardiac junctional sarcoplasmic reticulum and forms a quaternary complex with RyR2, triadin, and calsequestrin. The special spatial arrangement between junctin and RyR2 means that junctin can be used as a marker of junctional RyR2.

A

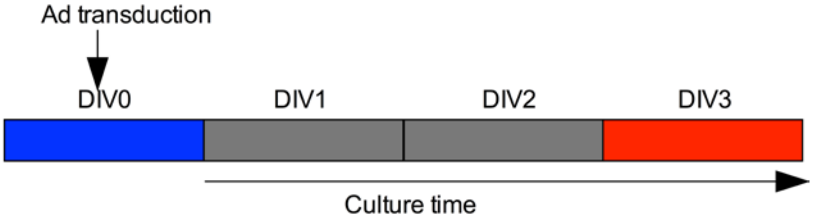

B

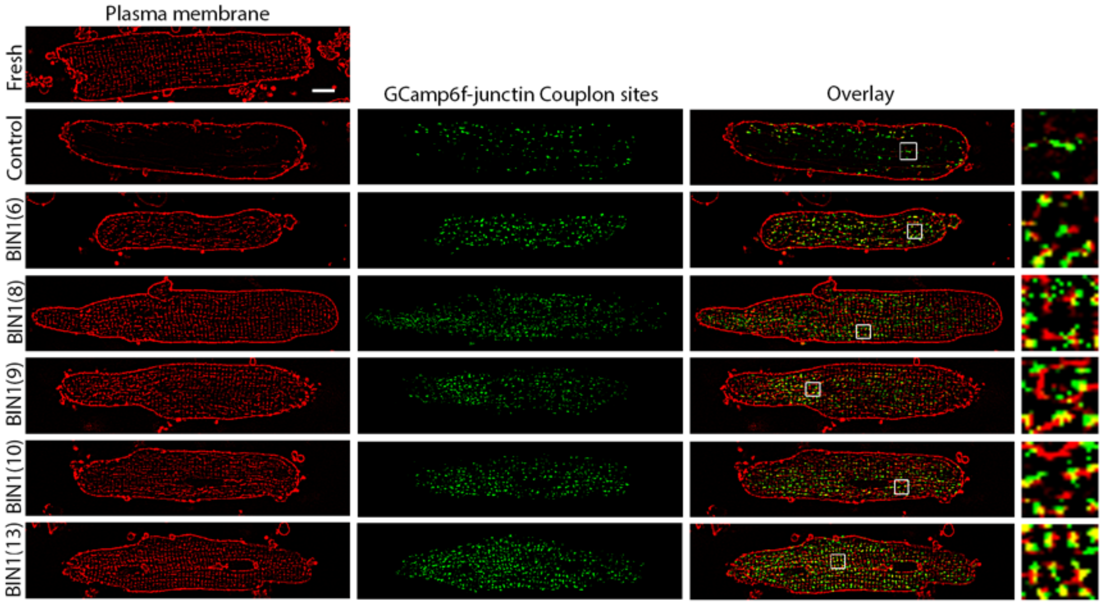
Plasma membrane
GCamp6f-junctin Couplon sites
Overlay
Fresh
Control
BIN1(6)
BIN1(8)
BIN1(9)
BIN1(10)
BIN1(13)

C

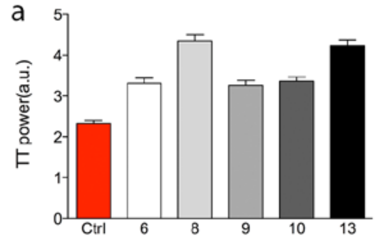

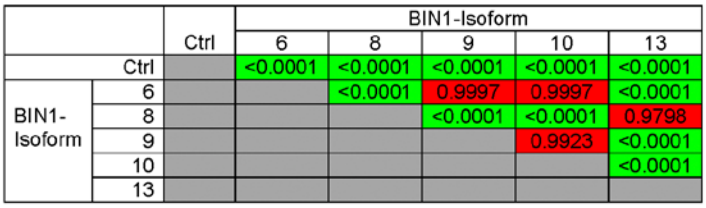

		Ctrl	BIN1-Isoform				
			6	8	9	10	13
	Ctrl		<0.0001	<0.0001	<0.0001	<0.0001	<0.0001
BIN1-Isoform	6			<0.0001	0.9997	0.9997	<0.0001
	8				<0.0001	<0.0001	0.9798
	9					0.9923	<0.0001
	10						<0.0001
	13						

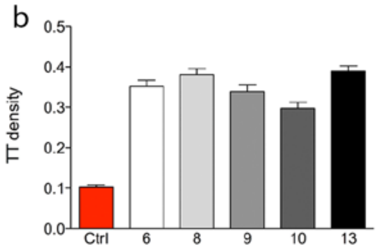

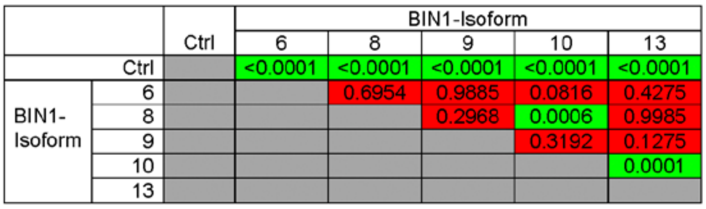

		Ctrl	BIN1-Isoform				
			6	8	9	10	13
	Ctrl		<0.0001	<0.0001	<0.0001	<0.0001	<0.0001
BIN1-Isoform	6			0.6954	0.9885	0.0816	0.4275
	8				0.2968	0.0006	0.9985
	9					0.3192	0.1275
	10						0.0001
	13						

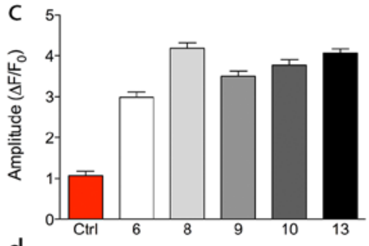

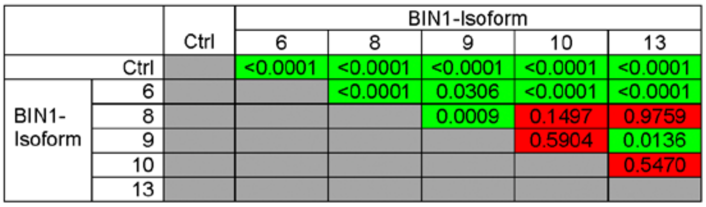

		Ctrl	BIN1-Isoform				
			6	8	9	10	13
	Ctrl		<0.0001	<0.0001	<0.0001	<0.0001	<0.0001
BIN1-Isoform	6			<0.0001	0.0306	<0.0001	<0.0001
	8				0.0009	0.1497	0.9759
	9					0.5904	0.0136
	10						0.5470
	13						

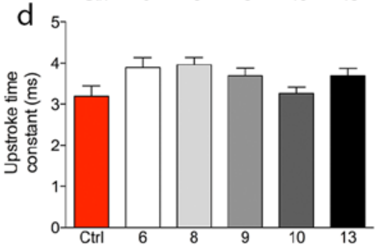

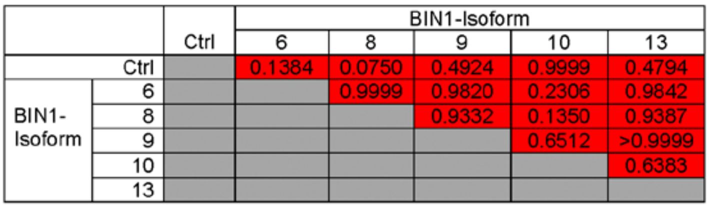

		Ctrl	BIN1-Isoform				
			6	8	9	10	13
	Ctrl		0.1384	0.0750	0.4924	0.9999	0.4794
BIN1-Isoform	6			0.9999	0.9820	0.2306	0.9842
	8				0.9332	0.1350	0.9387
	9					0.6512	>0.9999
	10						0.6383
	13						

Figure 5.13 Effects of human cardiac BIN1 isoforms on cultured rat cardiomyocytes studied with GCaMP6f-junctin. A) Schematic diagram of experiment route. B) Representative images of T-tubules and calcium release in cultured rat cardiomyocytes. Calcium release sites were highlighted by GCaMP6f-junctin (green). The membrane was stained by CellMask(red). Calcium release sites were calculated by the CaCLEAN algorithm indicating functional EC couplons. Scale = 10µm. C) Statistics of tubule regularity(a), tubule density(b), transient amplitude(c), and transient upstroke time(d). Comparisons between groups were analyzed by one-way ANOVA and the P values were displayed in tables either as significant difference (green) or no significant difference (red). n= 78-84 cells from three independent experiments. All data are presented as the mean ± s.e.m.

When GCaMP6f and junctin were combined together, the fusion protein can be used to detect focal calcium transients in EC couplons in situ, highly sensitively and specifically. Particularly, it is more direct in detecting functional EC couplons than Fluo-4 since it only expresses with functional EC couplons (Jones et al. 1995).

The experiment was carried out as previously described (**Fig. 5.12A**). Consistent with my Fluo-4 data, results with GCaMP6f revealed that cells expressing BIN1 showed an increased maintenance of both T-tubules and calcium transients compared to control cells (**Fig. 5.13B-C**). However, there was no difference in the transient upstroke time between the control and BIN1expressing cells. Loss of T-tubules was associated with a reduction in efficient EC-coupling. Similar to the Fluo-4 results, isoform13 and isoform8 appeared to display stronger effects than isoform 6, 9, and 10.

5.3.5 Effects of BIN1 isoforms on recovering cardiac T-tubules and EC-coupling

In order to examine the efficiency of BIN1 isoforms in restoring T-tubules and EC-coupling once T-tubule loss has occurred, a rescue experiment was designed and carried out (**Fig. 5.14A**). Rat cardiomyocytes were isolated and cultured for 48 hours before any other treatment, which led to a significant loss of T-tubules. Then cells were transduced with two different adenoviruses coding for different BIN1 isoforms and GCaMP6f-junctin, and cultured for an additional 72 hours. I used high-speed confocal imaging to investigate whether the structural and functional loss after 48h in culture could be rescued by overexpression of BIN1. As expected at the end of culture, there was only a very small amount of tubules left in control cells and the amplitude of the calcium transient following electrical stimulation was very small, far lower than those found in freshly isolated cardiomyocytes, which indicated a dramatic decline in efficient EC-coupling (**Fig. 5.14B**).

A

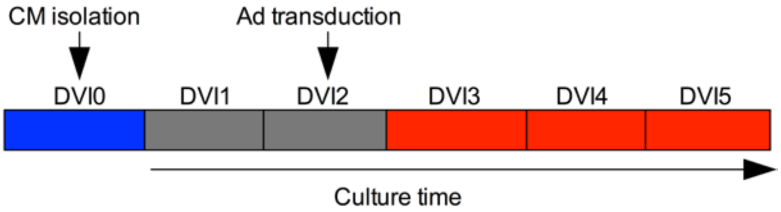

B

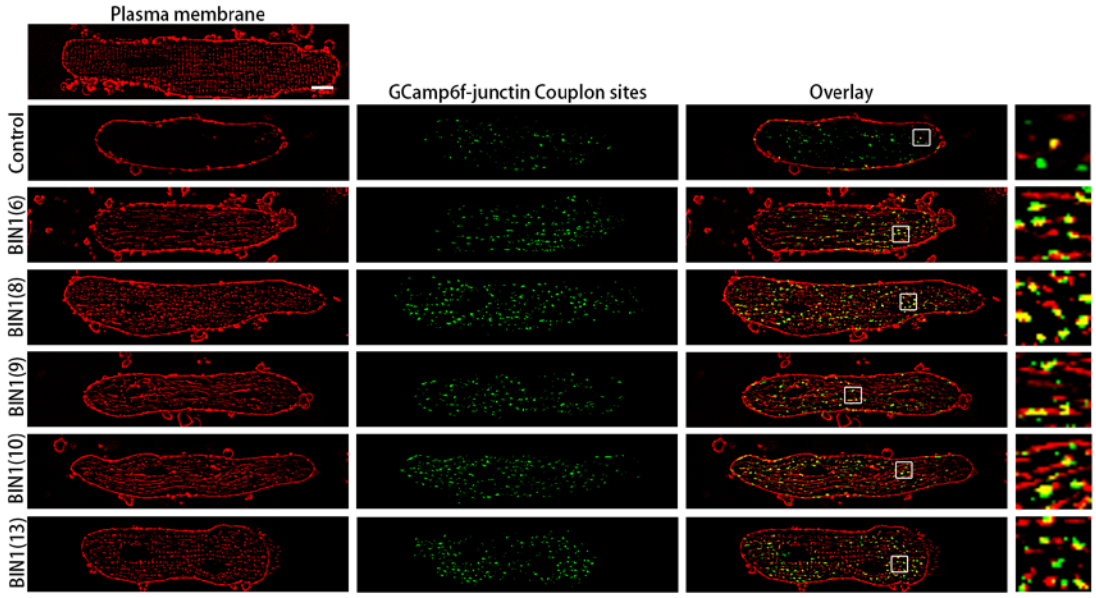
Plasma membrane
GCamp6f-junctin Couplon sites
Overlay
Control
BIN1(6)
BIN1(8)
BIN1(9)
BIN1(10)
BIN1(13)

C

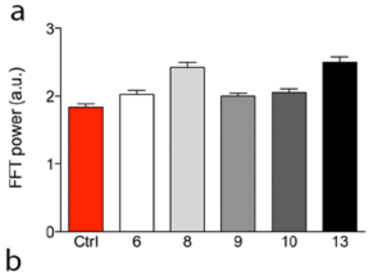

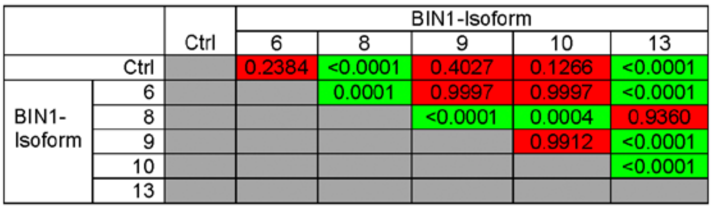

		Ctrl	BIN1-Isoform				
			6	8	9	10	13
	Ctrl		0.2384	<0.0001	0.4027	0.1266	<0.0001
BIN1-Isoform	6			0.0001	0.9997	0.9997	<0.0001
	8				<0.0001	0.0004	0.9360
	9					0.9912	<0.0001
	10						<0.0001
	13						

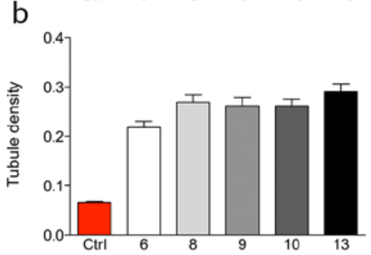

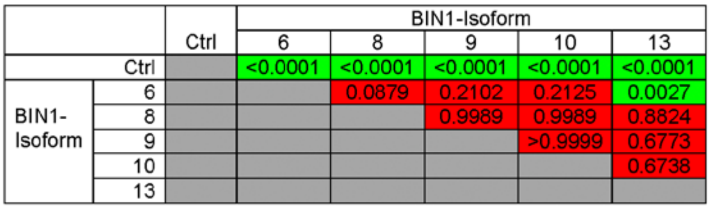

		Ctrl	BIN1-Isoform				
			6	8	9	10	13
	Ctrl		<0.0001	<0.0001	<0.0001	<0.0001	<0.0001
BIN1-Isoform	6			0.0879	0.2102	0.2125	0.0027
	8				0.9989	0.9989	0.8824
	9					>0.9999	0.6773
	10						0.6738
	13						

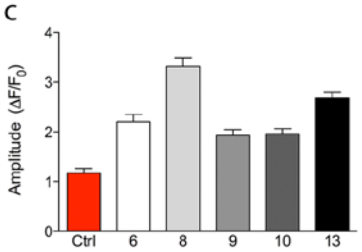

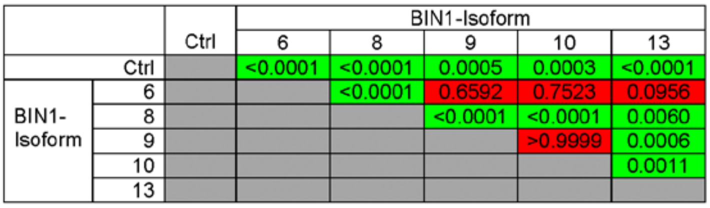

		Ctrl	BIN1-Isoform				
			6	8	9	10	13
	Ctrl		<0.0001	<0.0001	0.0005	0.0003	<0.0001
BIN1-Isoform	6			<0.0001	0.6592	0.7523	0.0956
	8				<0.0001	<0.0001	0.0060
	9					>0.9999	0.0006
	10						0.0011
	13						

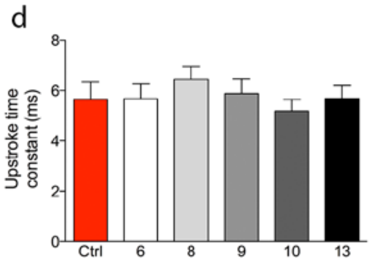

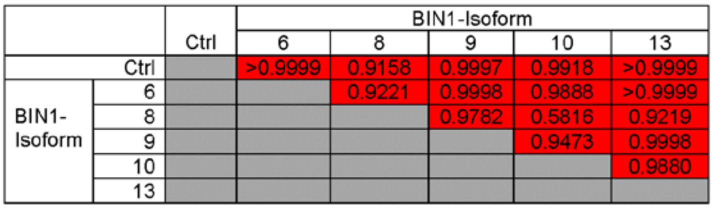

		Ctrl	BIN1-Isoform				
			6	8	9	10	13
	Ctrl		>0.9999	0.9158	0.9997	0.9918	>0.9999
BIN1-Isoform	6			0.9221	0.9998	0.9888	>0.9999
	8				0.9782	0.5816	0.9219
	9					0.9473	0.9998
	10						0.9880
	13						

Figure 5.14 Effects of human cardiac BIN1 isoforms on rescuing rat cardiomyocytes studied by GCaMP6f-junctin. A) Schematic diagram of experiment route**.** B) Representative images of T-tubules and calcium release in cultured rat cardiomyocytes. The membrane was stained by CellMask DeepRed. Calcium release sites were calculated by the CaCLEAN algorithm indicating functional EC-couplons. Scale = 10µm. C) Statistics of tubule regularity(a), tubule density(b), transient amplitude(c), and transient upstroke time(d). Comparisons between groups were analyzed by one-way ANOVA and the P values were displayed in tables either as significant difference (green) or no significant difference (red). n = 76-84 cells from three independent experiments. All data are presented as the mean ± s.e.m.

However, following the expression of BIN1 isoforms, the T- tubules were built and calcium transients were significantly restored compared to control (**Fig. 5.14B**). There were significant improvements in tubule regularity, tubule density, and amplitude of calcium transient in all cells expressing BIN1. Interestingly, I did not find any difference in the upstroke time of calcium transients (**Fig. 5.14C**).

5.4 Role of BIN1 in de-novo generation of T-tubules in hiPSC-derived cardiac myocytes

It is accepted that hiPSC-CMs are less mature than adult cardiomyocytes (Veerman et al. 2015; Lieu et al. 2009), which is partially attributed to the lack of T-tubules, limiting the efficiency of EC-coupling. There are very few reports of a successful generation of T-tubule-like structures in these cells (Parikh et al. 2017), posing a huge barrier for further maturation of hiPSC-CMs. As described above, I identified 5 BIN1 isoforms in human heart tissue, and found that all of them were capable of maintaining and restoring T-tubules and calcium handling in adult rat cardiomyocytes. Particularly, the effects of human BIN1 isoform8 and isoform13 appeared more pronounced than those of the other isoforms in both generating and restoring tubules and calcium cycling. Therefore, I thought of investigating their functions in hiPSC-CMs, inducing tubular structures and as a result of it, enhancing EC-coupling.

5.4.1 T-Tubule biogenesis induced by expression of BIN1 isoforms in hiPSC-CMs

To address this, hiPSC-CMs were isolated, cultured, and transduced with adenoviruses coding for the BIN1 isoform 8 and isoform 13 respectively. Cells were additionally probed with CellMask DeepRed to clarify membranes that are continuous with the extracellular space. The result indicated that both exon11-containing BIN1 isoforms were able to generate abundant tubules that were connected to the plasma membrane (**Fig. 5.15b-c,e-f**). In addition, these tubules were decorated with BIN1 as depicted by immunolabeling with anti-BIN1 antibodies suggesting that the biogenesis of these tubules was indeed linked to BIN1 expression (**Fig. 5.15h-i**). In contrast, hiPSC-CMs in the control without BIN1 expression had almost no tubule-like structures and BIN1 expression, confirming their deficiency in hiPSC-CMs (**Fig. 5.15a,d,g**).

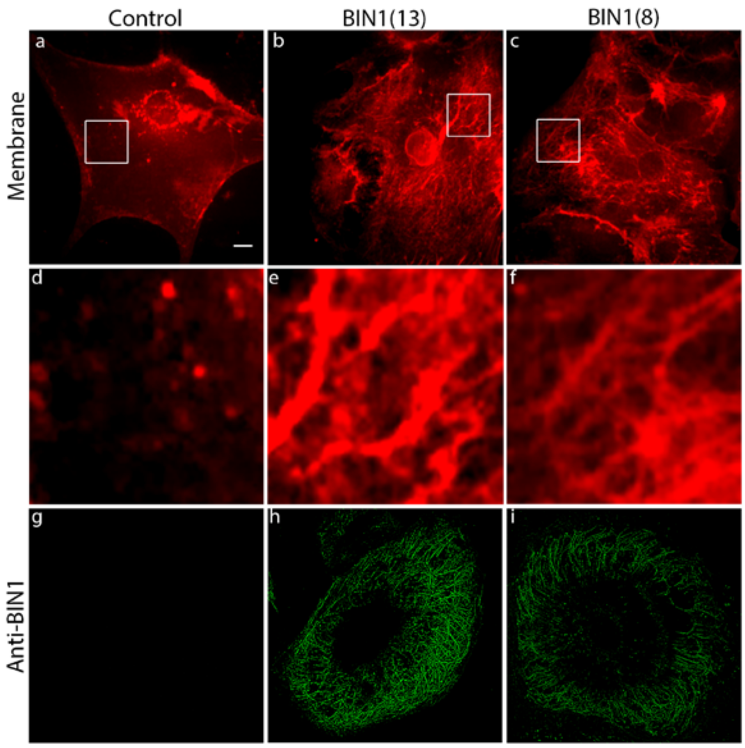

Figure 5.15 labeling of tubules induced by human BIN1 isoform 8 and 13 in iPSC-CMS. iPSC-CMs were transduced with adenoviruses coding for the BIN1 isoform13 and isoform8. The cell membrane was stained by CellMask DeepRed (red). Fixed cells were additionally probed with the anti-BIN1 antibody (green). Scale=10 µm.

5.4.2 Tafficking of LTCCs to BIN1-induced tubules

Just as the fact that T-tubules is necessary for the establishment of EC-coupling in adult cardiomyocytes, a newly built tubule system may similarly lay a structural foundation for further improvement of coupling between LTCCs and RyRs in hiPSC-CMs. It is well established that EC-coupling is mediated by Ca^{2+} entry through voltage-activated sarcolemmal LTCCs, which are mostly localized in T-tubules (T.-T. Hong et al. 2010). Proper trafficking and localization of LTCCs are critical for the development of EC couplons. Therefore, the expression pattern and relationship of

LTCCs with BIN1-induced tubules were analyzed in hiPSC-CMs by immunostaining.

A

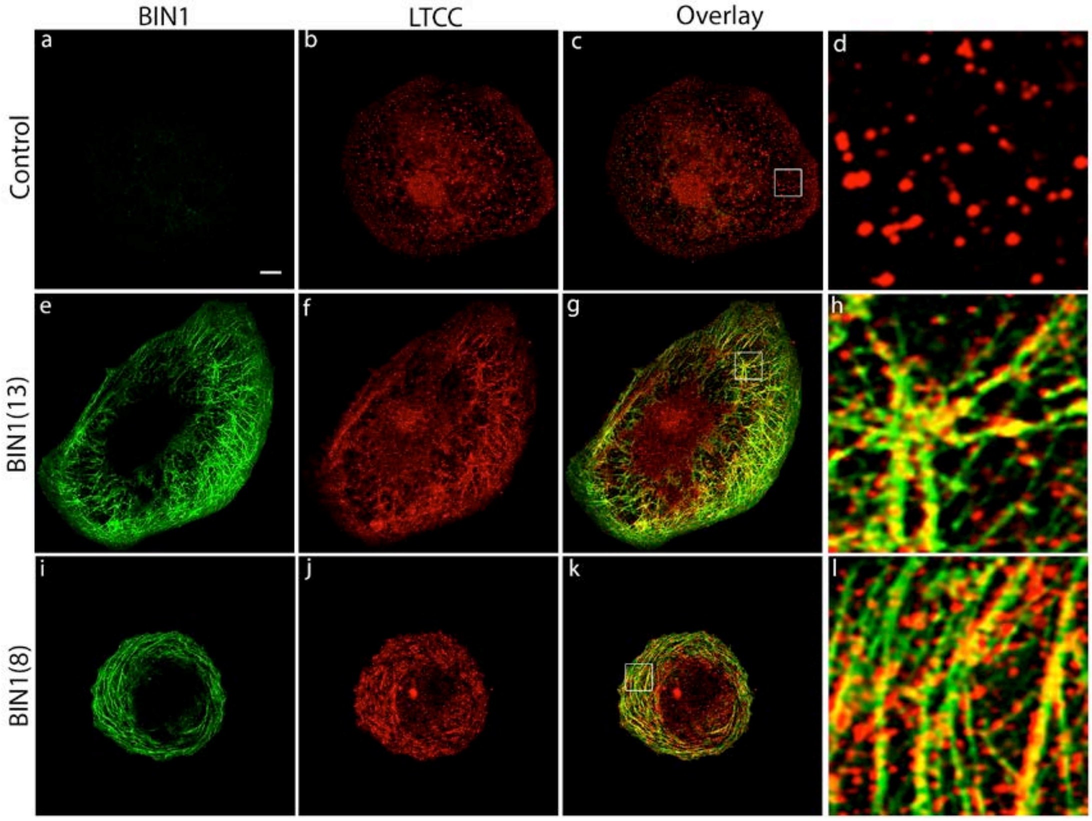
BIN1
LTCC
Overlay
a
b
c
d
Control
e
f
g
h
BIN1(13)
i
j
k
l
BIN1(8)

B

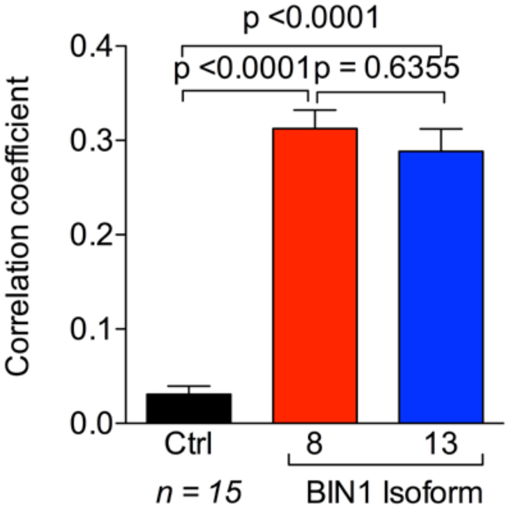

Figure 5.16 Immunostaining and correlation analysis of BIN1 and LTCC in hiPSC-CMs. A) Representative confocal images of hiPSC-CMs transduced with adenoviruses coding for BIN1 isoform13 and isoform8 immunolabeled

with anti-BIN1 (green) and anti-LTCC (red) antibodies. B) Pearson correlation coefficients for BIN1 and LTCC distribution. Comparisons between groups were analyzed by one-way ANOVA and the P values were displayed. n= 15 cells. Scale =10 μm.

hiPSC-CMs were isolated, cultured, and transduced with adenoviruses coding for BIN1 isoform 13 and isoform 8, and then fixed for double immunofluorescent labeling against BIN1 and LTCC. My data suggested that a significant proportion of LTCCs were indeed distributed along the newly formed tubules decorated by the anti-BIN1 antibody. I concluded that because of the newly formed tubules, the pattern of LTCC was apparently remodeled, now resembling the new tubular network (**Fig. 5.16A, e-l**). However, LTCCs in control cells lacking such a network appeared to distribute more randomly (**Fig. 5.16A, a-d**). The correlation was quantified by calculating the Pearson correlation coefficient, which was substantially increased in cells expressing BIN1, confirming the role of BIN1 in recruiting LTCCs to T-tubules (**Fig. 5.16B**). By contrast, when BIN1 was fused to TagRFPT at the C-terminus, the recruitment obviously decreased. When compared to the cells expressing TagRFPT-2A-BIN1, the colocalization was significantly lower, even though it was still able to produce tubules (**Fig. 5.17**).

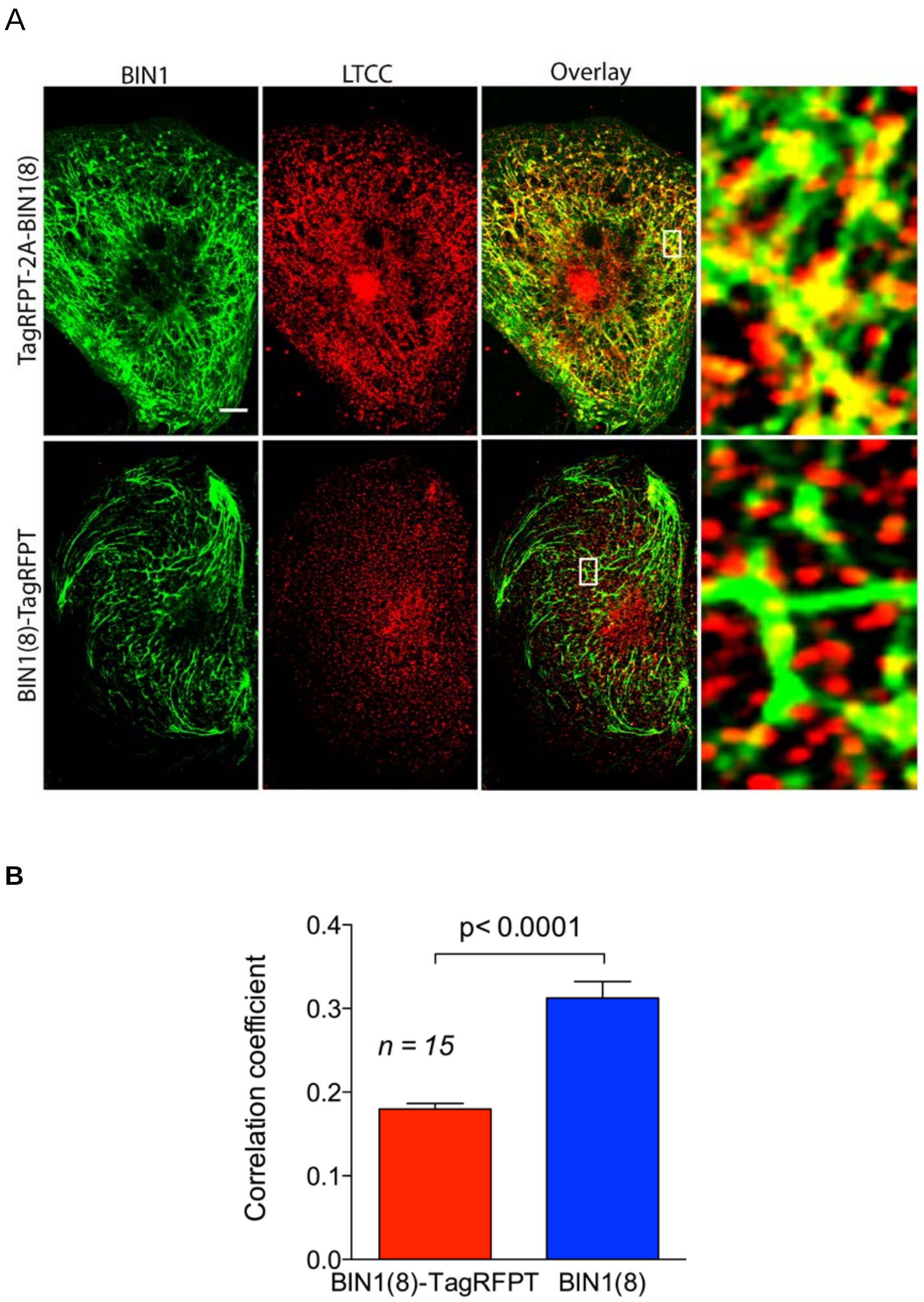
A
BIN1
LTCC
Overlay
TagRFPT-2A-BIN1(8)
BIN1(8)-TagRFPT
B
Correlation coefficient
0.4
0.3
0.2
0.1
0.0
p< 0.0001
n = 15
BIN1(8)-TagRFPT
BIN1(8)

Figure 5.17 Colocalization analysis of BIN1 and LTCC in hiPSC-CMs. Representative confocal images of hiPSC-CMs transduced with two types of adenoviruses coding for BIN1 isoform 8 probed by an anti-BIN1 (green) and anti-LTCC (red) antibodies. Upper panel, BIN1 with 2A fusion; low panel,

BIN1 with direct TagRFPT fusion in C-terminus domain. Statistic comparison was done by Student's t-test. n = 15 cells. Scale =10 μm.

5.4.3 Remodeling of the RyR2 distribution by BIN1-induced tubules

In addition to LTCC, another core ion channel involved in EC-coupling is the RyR2, which couples to LTCC in the dyadic space formed by the T-tubular and SR membrane. To investigate this, immunofluorescent analysis of BIN1 and RyR2 distribution was carried out in hiPSC-CMs transduced with adenoviruses coding for BIN1 isoforms 8 and 13. My results suggested following BIN1 overexpression, the distribution of RyR2 was significantly altered and readapted to those newly formed T-tubules, similarly to what I found for LTCCs (**Fig. 5.18A**). There was a significantly higher correlation between BIN1 and RyR2 in BIN1 expressing cells than in control cells. Interestingly, in control, RyR2 displayed a regular pattern with a periodic interval of around 2μm, which is similar to that in adult cardiomyocytes (**Fig. 5.8B**). Thus, following BIN1 expression, RyR2 was re-assembled in a pattern resembling the distribution of the BIN1-evoked T-tubules, suggesting a strong effect of BIN1 isoforms in RyR2 organization in the SR membrane.

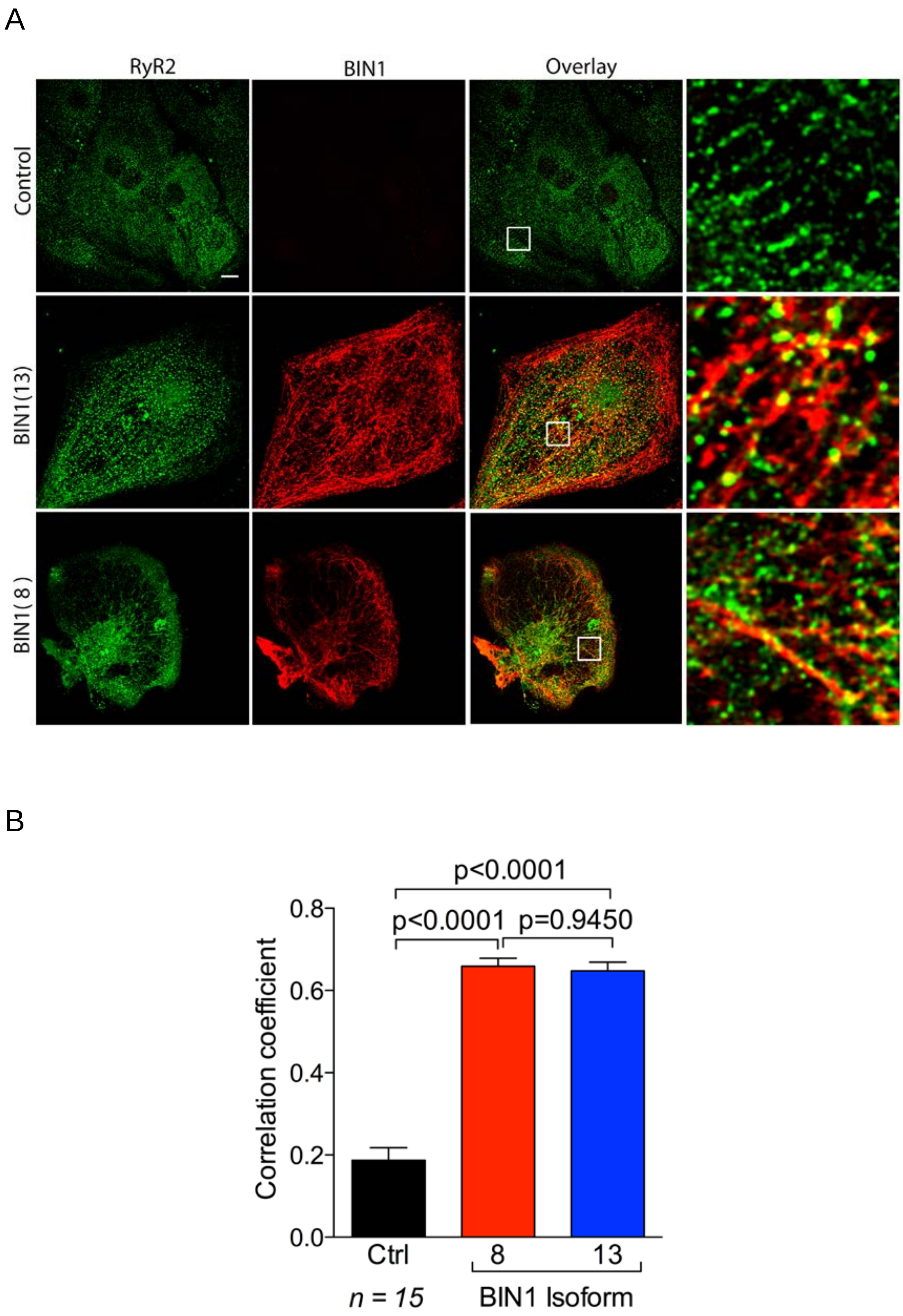
A
RyR2
BIN1
Overlay
Control
BIN1(13)
BIN1(8)
B
p<0.0001
p<0.0001
p=0.9450
Correlation coefficient
0.8
0.6
0.4
0.2
0.0
Ctrl
8
13
n = 15
BIN1 Isoform

Figure 5.18 Colocalization analysis of BIN1 and RyR2 in hiPSC-CMs. A) Representative confocal images of hiPSC-CMs transduced with adenovirus of BIN1 isoforms and stained by the anti-BIN1 (green) and anti-RyR2 (red)

antibodies. B) Pearson correlation coefficients between BIN1 and RyR2 distribution. Comparisons between groups were analyzed by one-way ANOVA and the P values were displayed. n = 15 cells. Scale =10 μm.

5.4.4 Effects of BIN1 expression on calcium handling in hiPSC-CMs analyzed by Fluo-4

Even though BIN1 isoforms induced T-tubule formation and the rearrangement of key compounds of EC-coupling, it still remains unclear whether these tubules are actually improving EC-coupling, or more specifically, can I identify functional EC couplons and calcium release around these tubules. For this, I examined calcium handling using Fluo-4. Briefly, hiPSC-CMs were transduced with adenoviruses coding for BIN1 and cultured for 72 hours. Cells were loaded with Fluo-4 and the plasma membrane was labeled by CellMask DeepRed and analyzed by confocal imaging. Imaging was employed to record calcium signals following electrical field stimulation of the cells. My data depicted that the amplitude of calcium transients was significantly higher in BIN1 expressing cells than that in control cells (**Fig. 5.19B, c-d**). The upstroke time constants were also smaller than control, suggesting faster calcium transient upstroke, hence more efficient EC-coupling (**Fig. 5.19B, e**).

To further analyze calcium release, the image series were processed by the CaCLEAN algorithm. Using the CaCLEAN data, the Pearson correlation coefficients between the identified EC-couplon sites and T-tubular membranes were calculated. My results showed that in BIN1 expressing cells the calcium release sites were closely associated with the T-tubules (**Fig. 5.19B, a**).

To further quantify calcium release sites and their relationship with BIN1-induced tubules, an additional approach was adopted by calculating the minimal distance between calcium release sites and their nearby tubular membrane. The results were assigned to three distances, 0μm, 0.5μm, and 1μm. The cumulative fraction of each distance was calculated. It became apparent that the fraction of active EC couplons in the proximity of cell membranes was increased in cells expressing BIN1 when compared to control cells (**Fig. 5.19B, b**).

A

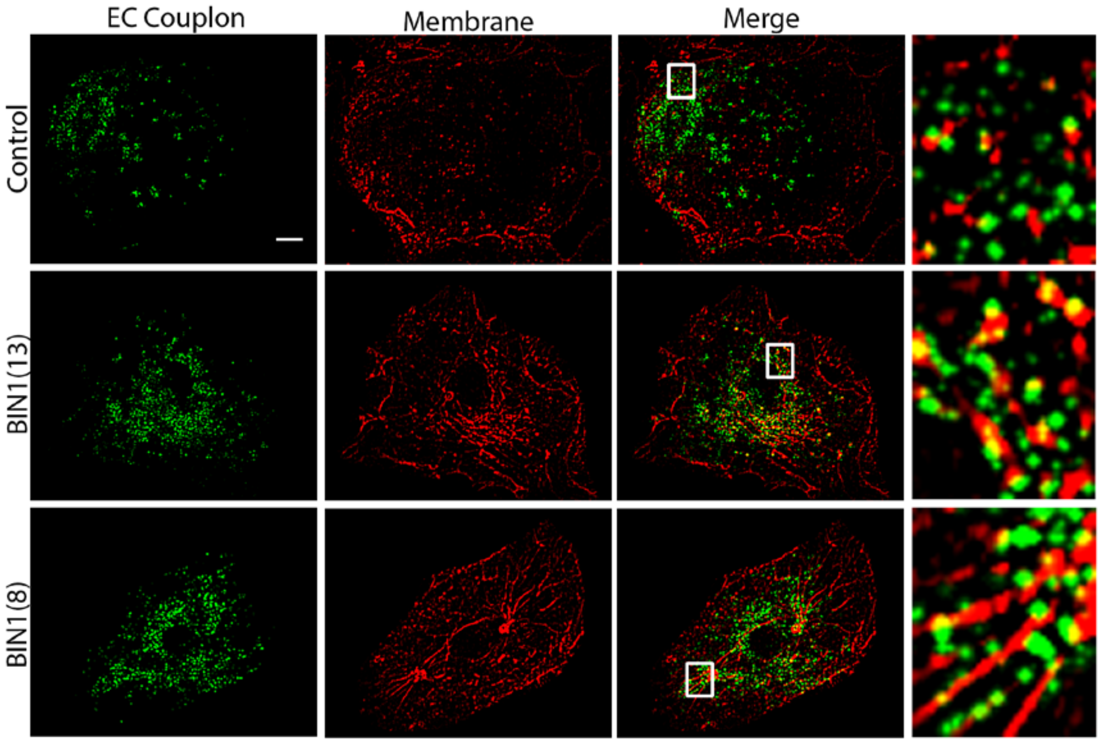

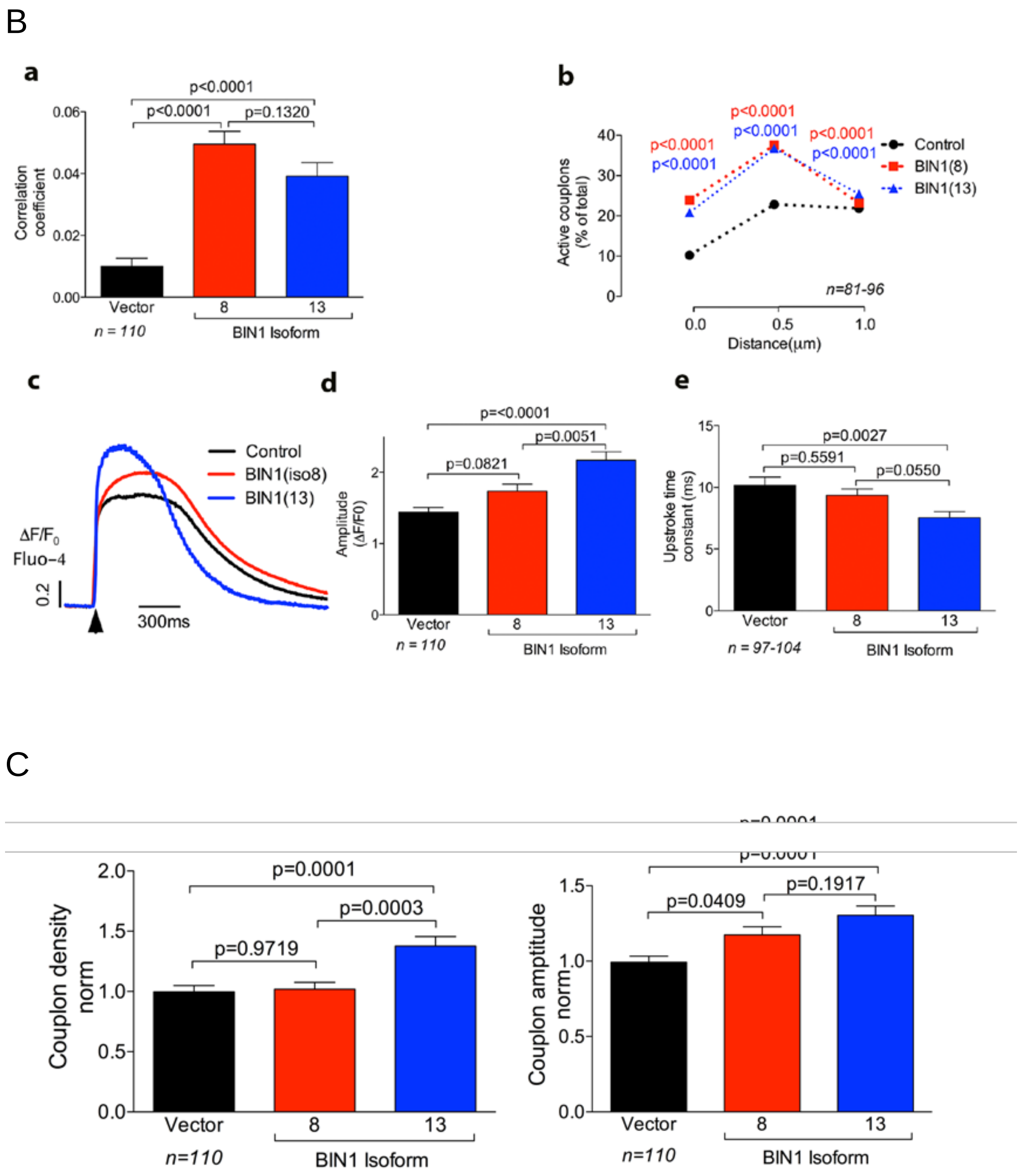

Figure 5.19 Analysis of calcium release measured by Fluo-4 in hiPSC-CMs with BIN1 overexpression. A) Representative images of calcium release and tubule formation in hiPSC-CMs of three groups (Control, BIN1(iso13), BIN1(iso8)). Calcium release sites were calculated by the CaCLEAN algorithm indicating EC couplons (green). The cell membrane was labeled by CellMask DeepRed (red). Scale =10μm B) Analysis of calcium release in hiPSC-CMs, quantified as a) correlation between EC couplons and tubular membrane; b) accumulative fraction of effective EC couplons; c) typical calcium transient trace; d) amplitude of calcium transient; e) upstroke

time constant of calcium transient. C). Analysis of EC couplons (density and amplitude) in hiPSC-CMs by CaCLEAN algorithm. Cells were from three independent experiments. Comparisons between groups were analyzed by one-way or two-way ANOVA and the P values were displayed. All data are presented as the mean ± s.e.m.

In addition, a more detailed analysis of the properties of EC couplons was carried out based on the CaCLEAN data. My data showed that cells expressing BIN1 isoform8 did not produce more EC couplons than control, while BIN1 isoform13 lead evoked a significant increase in the density of calcium release units (**Fig. 5.19C, a**). Moreover, overexpression of both isoforms resulted in an enhanced amplitude of functional calcium release from EC couplons (**Fig. 5.19C, b**). Combined together, these data indicated that BIN1-evoked T-tubules were functional in promoting EC-coupling by establishing more and stronger EC couplons around these newly formed tubules.

5.4.5 Effects of BIN1 isoforms on EC-couplons in hiPSC-CMs analyzed by expression of GCaMP6f-junctin

In addition to Fluo-4, the genetically-encoded calcium indicator GCaMP6f was also applied to study the effects of BIN1 isoforms on the calcium handling of hiPSC-CMs as previously described in cultured rat cardiomyocytes. Here GCaMP6f-junctin possesses particular advantages in this aspect because it is co-localized with RyR2. If the RyR2 forms functional couplon with LTCCs, the local calcium release during calcium transients will be revealed by

GCaMP6f. In other words, the signal of GCaMP6f-junctin can precisely localize the functional EC-couplons.

hiPSC-CMs were transduced with adenoviruses coding for BIN1 isoforms and GCaMPp6f-junctin, and cultured for three days before imaging. CellMask DeepRed was used to label the plasma membrane. Fast confocal imaging was employed to investigate calcium signals during electric field stimulation. To further analyze the localization and properties of EC-couplons, the algorithm CaCLEAN was applied as previously described. My results showed that following BIN1 expression, abundant T-tubules were formed, alongside apparent EC-couplons in close proximity to the newly generated T-tubules (**Fig. 5.20A, middle and right panel**). Control cells lacked tubular structures across the cytoplasm, and EC-couplons mostly appeared at the peripheral plasma membrane (**Fig. 5.20A, left panel**), indicating an inefficient EC-coupling in central regions and thus immature calcium handling.

To analyze the relationship between EC–couplons and tubules, two methods were employed as previously shown. Pearson correlation analysis of calcium release sites and tubules showed that there was an apparent increase in correlation for both BIN1 isoforms when compared to in the control situation (**Fig. 5.20B, b**). As before calcium release sites within distinct distances (0μm, 0.5μm, and 1μm) from membrane invaginations were considered effective EC-couplons instead of orphaned RyR clusters in the cytosol. Analysis of the spatial arrangement of the couplons indicated that there was a significant increase of active EC-couplons in close proximity to BIN1-evoked tubules (**Fig. 5.20B, a**).

Moreover, the “global’’ calcium transient amplitude in BIN1 expressing cells was enhanced when compared to that in control cells (**Fig. 5.20B, d**). The upstroke time constant of the calcium transients were also reduced (BIN1 isoform13), indicating improved efficiency of EC-coupling between LTCC and RyR2 (**Fig. 5.20B, e**).

In addition, I further studied the properties of EC couplons. My, results showed that the density of calcium release unit was increased in BIN1 expressing cells while the average release amplitudes of these units showed no significant difference between the control and BIN1 group (**Fig. 5.21C**).

In conclusion, all these data demonstrated that in particular the BIN1 isoform13 and also isoform8, when expressed in hiPSC-CMs, were capable of generating T-tubules, and substantially improved EC-coupling.

A

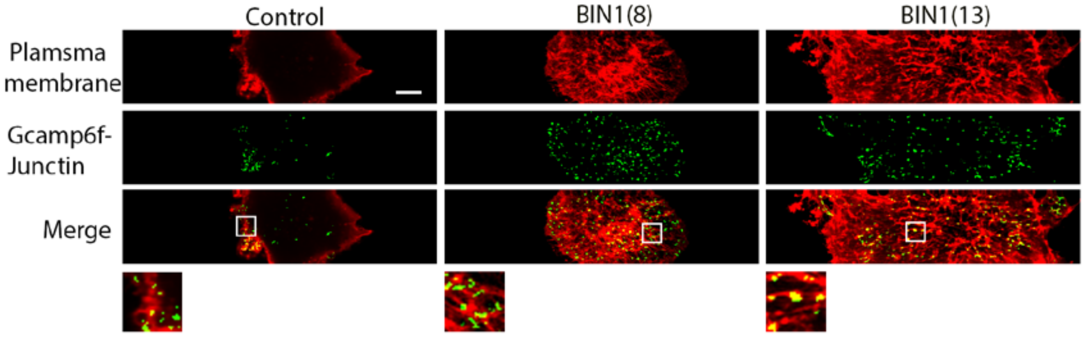

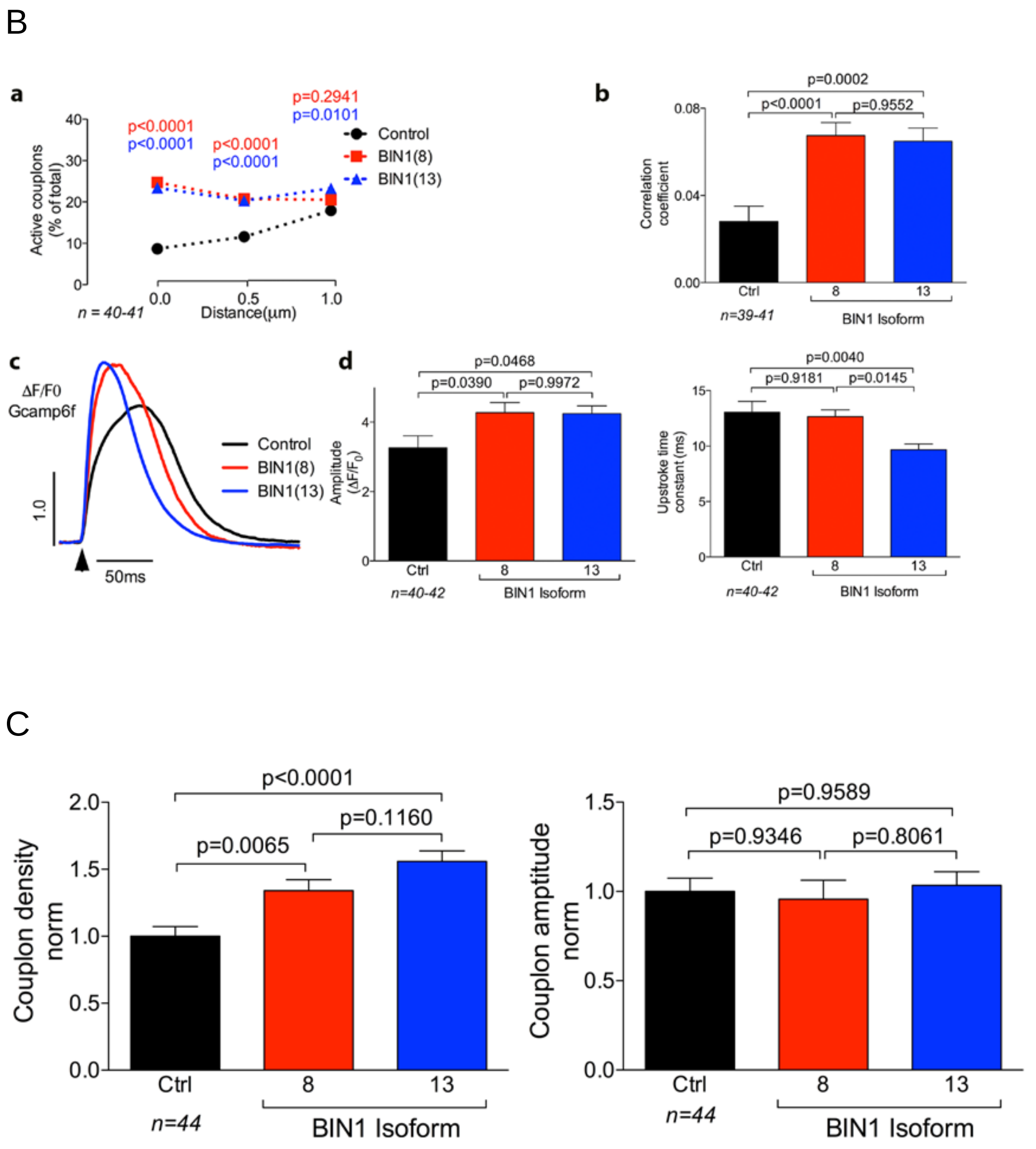

Figure 5.20 Analysis of calcium release measured by GCaMP6f-junctin in hiPSC-CMs with BIN1 overexpression. A) Representative images of calcium release and tubule formation in hiPSC-CMs in three groups (Control, BIN1(13), BIN1(8)). Calcium release sites were calculated by the CaCLEAN algorithm indicating EC couplons (green). The cell membrane was labeled by CellMask DeepRed membrane dye (red). Scale=10μm. B) Analysis of calcium release a) statistics of the cumulative fraction of EC-couplons within effective distances; b) Pearson correlation between active EC couplons and tubules; c) typical calcium transient traces of hiPSC-CMs in each group; d) statistics of

calcium transient amplitude in each group; e) statistics of the time constant of calcium transient upstroke in each group. C) Analysis of the density and amplitude of EC couplons Comparisons between groups were analyzed by one-way or two-way ANOVA and the P values were displayed. All data are presented as the mean ± s.e.m.

5.5 Supplemental Figure

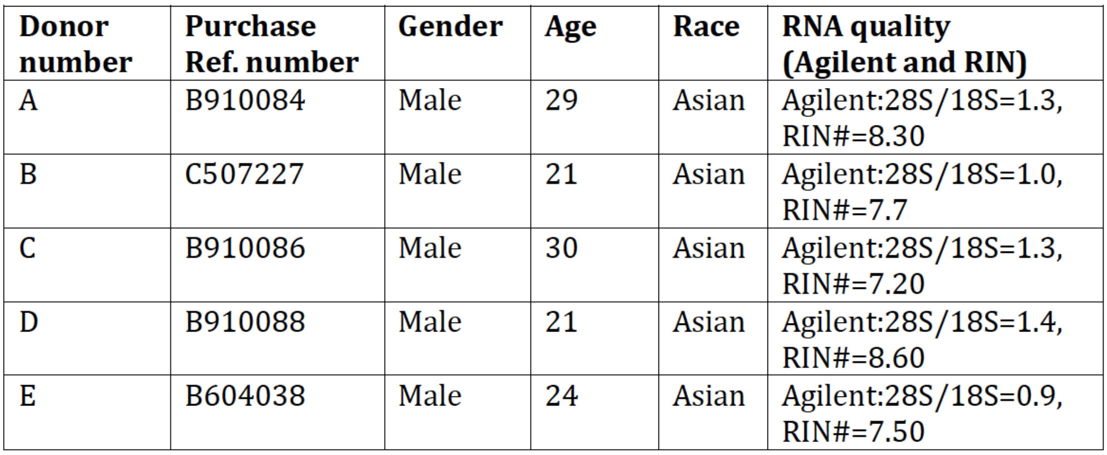

Donor number	Purchase Ref. number	Gender	Age	Race	RNA quality (Agilent and RIN)
A	B910084	Male	29	Asian	Agilent:28S/18S=1.3, RIN#=8.30
B	C507227	Male	21	Asian	Agilent:28S/18S=1.0, RIN#=7.7
C	B910086	Male	30	Asian	Agilent:28S/18S=1.3, RIN#=7.20
D	B910088	Male	21	Asian	Agilent:28S/18S=1.4, RIN#=8.60
E	B604038	Male	24	Asian	Agilent:28S/18S=0.9, RIN#=7.50

Supplemental Figure 1: Analysis of BIN1 splicing variants using RNA samples from healthy human heart tissue. The table summarized important data of the donors. The first column corresponds to the gel lanes of the PCR shown in Figure 5.1.

6. Discussions

6.1 Transcriptional splicing of BIN1 in human heart

EC-coupling is the cornerstone for the function of cardiomyocytes because it translates the electric signal into the mechanical activity of the cell and is eventually responsible for the heartbeat, which allows blood to be perfused throughout the entire body. EC-coupling is regulated by multiple factors, and one of the most important mechanisms is the interaction of two critical ion channels: LTCC in the sarcolemma membrane, which mediates calcium entry after depolarization of the membrane potential, and RyR2 in the sarcoplasmic reticulum membrane, which mediates calcium release from the calcium storing organelle the SR when activated by calcium entry. Both proteins are the principal building blocks of what is referred to as an EC-couplon (Bers 2002; Chopra & Knollmann 2013). Noteworthy, for EC couplons to operate efficiently, a highly specialized membrane structure—the T-tubule--is indispensable. Thus, understanding the regulatory mechanisms for the turnover of T-tubules is of utmost importance.

Several factors have been identified to play important roles in T-tubule biogenesis or maintenance, among which BIN1 is considered as the most important one (T. Hong & Shaw 2017). Disruption of the BIN1 gene during embryogenesis resulted in embryonic cardiomyopathy with disorganized myofibril formation, indicating its important role in cardiogenesis (Muller et al. 2003). A recent study found that T-tubule biogenesis was significantly impaired after BIN1 deletion in mouse cardiomyocytes even resulting in arrhythmia (T. Hong et al. 2014). All these studies indicate that BIN1 is highly associated with T-tubules and EC-coupling.

Previous studies have also shown that BIN1 is differentially spliced and that the splicing pattern may differ between cell types and species (Sakamuro et al. 1996; Butler et al. 1997; DuHadaway et al. 2003; T. Hong et al. 2014). However, neither the pattern of splicing nor the distinct roles of these splice variants in human cardiomyocytes has been studies as of now. Thus, it appears necessary to identify BIN1 splice variants in human hearts and characterize their effects in cardiomyocytes.

In my study, for the first time the transcriptional profile of BIN1 was investigated in RNA samples of healthy human hearts. Through the combination of PCR, cDNA cloning and sequencing, I could identify five different BIN1 splice variants, whose pattern was distinct from that found in the mouse heart (**Figure 6.1**). The BIN1 gene contains 20 exons that are differently spliced into different isoforms, including the brain-specific isoforms 1-7, the muscle-specific isoform 8 as well as the ubiquitously distributed isoforms 9 and 10 (Ellis et al. 2012; Mao et al. 1999; Wechsler-Reya et al. 1997; Toussaint et al. 2011; Butler et al. 1997; Tsutsui et al. 1997). A previous study on the mouse heart revealed four BIN1 isoforms: isoform6 (BIN1+e13+e17)**,** isoform9 (BIN1+e17), isoform10 (BIN1), and isoformX (BIN1+e13) (T. Hong et al. 2014). Here BIN1 refers to the most conserved and smallest BIN1 isoform, or isoform10, which is only composed of the N-BAR domain and SH3 domain. Since the isoform(BIN1+e13) is not included in the NCBI database, the name isoformX was given. The pattern of isoforms identified in the human heart was distinctly didferent and comprised isoform6 (BIN1+e13+e17), isoform8 (BIN1+e11+e17), isoform9 (BIN1+e17), isoform10 (BIN1), and isoform13 (BIN1+e11). Interestingly, a recent study on rat hearts revealed an additional pattern of BIN1 splice variants: isoform6 (BIN1+e13+ex17), isoformX (BIN1+e13), isoform8 (BIN1+e11+e17), isoform9 (BIN1+e17), isoform10 (BIN1+exon17), isoform13 (BIN1+e11) (L.-L. Li et al. 2020). These data indicated that all BIN1 isoforms found in mouse and human hearts occured in rat heart. From this it becomes obvious that the transcriptional profiles of BIN1 in the heart are distinctly different across species though with some overlap. The reason for such differences is still elusive. Moreover, it is unclear why several BIN1 isoforms are expressed simultaneously and what roles they play respectively in cardiomyocytes. Nevertheless, one feels tempted to speculate about functional differences between the splice variants (see below).

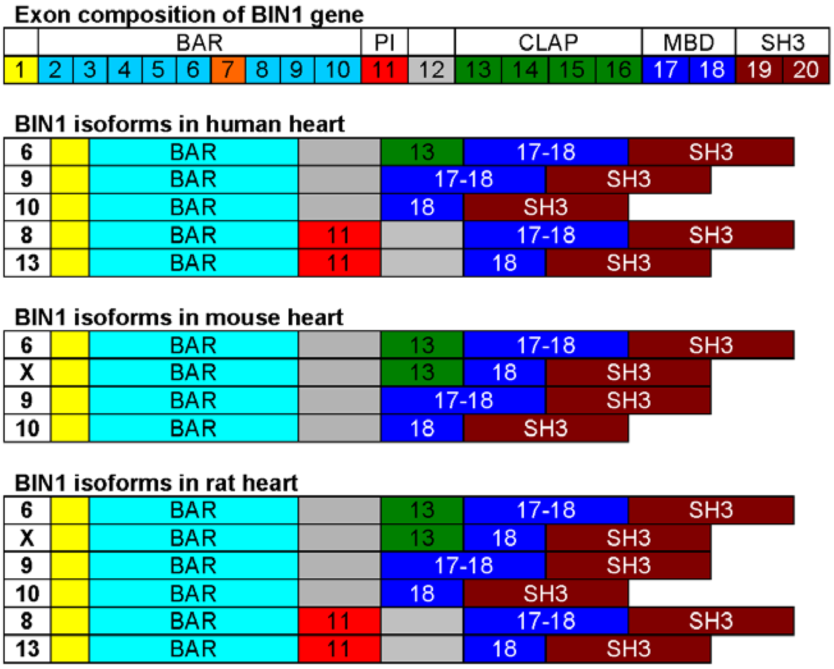
Exon composition of BIN1 gene
BAR
PI
CLAP
MBD
SH3
1
2
3
4
5
6
7
8
9
10
11
12
13
14
15
16
17
18
19
20
BIN1 isoforms in human heart
6
9
10
8
13
BAR
11
13
17-18
18
SH3
BIN1 isoforms in mouse heart
6
X
9
10
BIN1 isoforms in rat heart

Figure 6.1 Schematic illustration of BIN1 splice variants in human, mouse and rat cardiomyocytes. The data of human cardiac BIN1 isoforms are based on my results while those of mouse and rat are from previous reports (T. Hong et al. 2014; L.-L. Li et al. 2020).

Another interesting detail of my analysis is that two of the isoforms contain exon11. Exon11 is a 45-base pair sequence that encodes the so-called polybasic phosphoinositide (PI) binding motif, which enhances BIN1's affinity towards certain negatively charged membrane lipids (PtdIns (4,5)P2 and/or PtdIns3P and Ptdins5P) (Lee et al. 2002; Kojima et al. 2004). It has been speculated that BIN1 potentially targets to T-tubules through such a mechanism. Although previous studies reported that these isoforms are skeletal muscle-specific, my results demonstrated their expression in the human heart. This finding is also consistent with data from rat hearts (L.-L. Li et al. 2020). As for BIN1 isoform9 and isoform10 they are expressed ubiquitously in a multitude of cell types. In rat heart, data suggest these isoforms may coordinate the accumulation of exon11-containg BIN1 splice variants to the Z-lines (L.-L. Li et al. 2020). In this way, they may help to organize BIN1-induced T-tubules. With respect to isoform6, which includes exon13 that encodes the CLAP (Clathrin/AP2) binding region, the study in mouse hypothesized that it was mainly responsible for folding the T-tubule membrane and building the so-called ‘‘fuzzy space’’ in the subplasmalemmal space that is very important for cardiac EC-coupling (Lederer et al. 1990; T. Hong et al. 2014).

6.2 Properties of human BIN1 isoforms

As described above, BIN1’s most important function appears to be the generation of T-tubules, a process that is indispensable for efficient EC-coupling. I hypothesize that the particular exon composition found for the identified isoforms might indeed determine their functional role. In order to investigate such properties, I designed different types of plasmids and initially expressed them in HEK cells. As expected, when TagRFPT was fused to the N-terminus, all isoforms failed to form any tubules. Instead, they displayed a diffused cytoplasm distribution without signs of membrane invaginations. This result confirmed that the N-terminal BAR domain is essential for membrane curvature and tubule formation (Mayor & Pagano 2007;J.Q. Wu et al. 2006; Ochoa et al. 2000). Thus, the N-terminus has to remain untouched.

Compared to other BAR domain proteins (e.g.endophilin) that are mostly associated with dynamic membrane processes such as endocytosis (Simunovic et al. 2015), BIN1 can stabilize deep membrane invaginations. The folding capability of BIN1 is highly associated with its protein domains. As previously reported, N-BAR domains can assemble themselves cooperatively on the membrane interface (Adam et al. 2015). The N-terminal amphipathic helix H0 plays a crucial role in triggering the assembly of tubules and mediating the polymerization of BIN1 proteins through locking the neighboring N-BAR domain (Adam et al. 2015; Z. Chen et al. 2016). The BAR domain is an all-α helical homodimer with a banana-shaped curvature that can deform membranes (Adam et al. 2015). With clusters of positively charged amino acids, the concave surface of the dimer can specifically bind to negatively charged membrane lipids (Adam et al. 2015). Therefore, any alteration in the N-terminus, such as protein fusion, will probably alter the conformation of the N-BAR domain and consequently reduce its affinity toward membrane lipids. This eventually leads to the dissociation of the protein from the plasma membrane and the failure to initiate membrane curvature and invagination.

The fusion of TagRFPT to the C-terminus of BIN1 yielded a protein that was competent in evoking T-tubules, confirming the necessity of a functional N-BAR domain for membrane deformation. These results suggested that the SH3 domain is less relevant for tubule formation. Instead, the SH3 domain is considered as the regulatory region of BIN1 and has multiple roles in protein-protein interaction (Nicot et al. 2007; Picas et al. 2014). For example, SH3 domains interact with several proline-rich domains (PRDs) such as dynamin2, recruiting it to participate in T-tubule formation in the muscular cells (Grabs D et al.1997; Picas L et al. 2014). SH3 domains have also been found to bind to the PI motif of BIN1 itself interpreted as an intramolecular autoinhibition (Kojima et al. 2004) (Wu & Baumgart 2014). So far, several mutations (Q573X, K575X, X593HfsX54, and X594DfsX53) have been reported in the SH3 domain, which can result in neuromuscular disorders referred to as centronuclear myopathy (CNM), which manifests muscle weakness in different degrees (Böhm et al. 2010; Böhm et al. 2014; Nicot et al. 2007). These mutations cause either a truncation or a frameshift and result in a protein with abnormal functions. Particularly, owing to a premature stop codon, the K575X mutation results in a 20%-truncation of the SH3 domain adversely affecting its dynamin interactions (Böhm et al. 2014; Nicot et al. 2007). Interestingly, even though the BIN1-dynamin interaction is reduced due to that mutation, *in vitro* BIN1-evoked membrane tubulation remains similar or even higher (Wu & Baumgart 2014). A possible explanation may be that this mutation also reduces the autoinhibition mentioned above (Kojima et al. 2004; Wu & Baumgart 2014).

Although the C-terminal fusion protein had no apparent effect on the tubule formation, it is necessary for other important functions in cardiomyocytes such as recruiting LTCCs to the T-tubules (T.-T. Hong et al. 2010). When the membrane is scaffolded by BIN1, microtubules are dynamically tethered to those membrane niches resulting in a specific LTTS delivery to such membrane patches (T.-T. Hong et al. 2010). When BIN1’s C-terminus is altered, it can still induce membrane tubules but its ability to recruit LTCCs to such membrane invaginations is abrogated (T.-T. Hong et al. 2010). Actually, my results also indicated that when TagRFPT was fused to the C-terminus of BIN1 the LTCC was much less colocalized with BIN1 in hiPSC-CMs (**Fig. 5.17**). Based on these findings, I refrained from altering BIN1's C- and N-terminus by e.g. protein fusion.

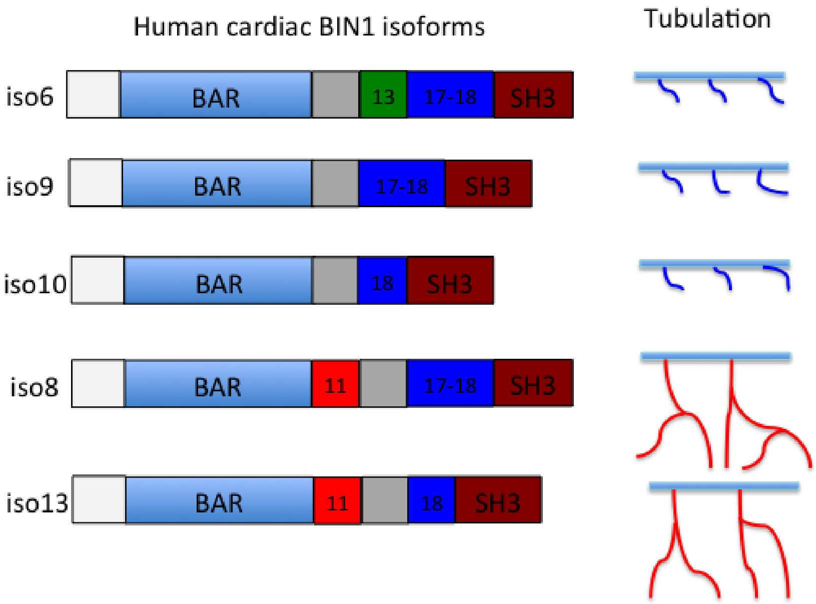
Human cardiac BIN1 isoforms
Tubulation
iso6
BAR
13
17-18
SH3
iso9
BAR
17-18
SH3
iso10
BAR
18
SH3
iso8
BAR
11
17-18
SH3
iso13
BAR
11
18
SH3

Figure 6.2 Schematic comparison of tubule biogenesis of human cardiac BIN1 splicing variants. While isoform6, 9, 10 mostly produce short membrane invaginations; the exon11-containing isoforms (8 and 13) can produce long and branching tubules connecting to the cell membrane.

In order to tag BIN1 isoforms while maintaining their properties, another strategy was adopted in my study. By linking membrane-localized TagRFPT and BIN1 through a very short 2A peptide, I successfully expressed two independent proteins simultaneously, and TagRFPT can be used as a reporter for BIN1 expression. Since the discovery of the "self-cleaving" 2A peptides, they have been exploited successfully to express multiple proteins under the control of a single promoter (de Felipe 2004; Osborn et al. 2005). Present in several viruses, the 2A-like sequence can mediate protein translation from a single open reading frame (Donnelly et al. 2001). Particularly, it is assumed to prevent the formation of a usual peptide bond on the ribosome between the last glycine and proline without hindering the translation of both proteins (Luke et al. 2008). As a result, after translation the 2A peptide cleaves at that site and there is only one proline amino acid left on the N-terminus of BIN1 protein (e.g. TagRFPT-2A-BIN1). Therefore, the effect on BIN1's N-BAR domain can be probably neglected. My results also demonstrated that BIN1 isoforms expressed in this way successfully produced tubules without obvious cytosolic localization. Hence, it can be assumed that results originating from experiments using these constructs are more likely to resemble BIN1's normal befaviour than those with C- or N-terminally fused proteins.

A central finding in my study was that the abilities to evoke tubulation are actually not identical among the BIN1 isoforms identified in the human heart samples. Isoform8 and isoform13, the two isoforms containing the exon11-encoded PI domain, were more potent than others (**Figure 6.2**). They were able to induce long tubules with a minimum of residual cytoplasmic distribution. In contrast, the other isoforms were only able to induce shorter tubules with noticeable protein retention in the cytoplasm. This may be due to their different structures. The major difference between isoform8/13 and isoform 6/9/10, is that the former two possess the PI motif encoded by exon11. As previously mentioned, the PI binding motif is a short polybasic amino acid sequence (RKKSKLFSRLTTKKN) (Wechsler-Reya et al. 1997; Nicot et al. 2007; Butler et al. 1997) with a high affinity towards certain negatively charged lipids, especially the phosphatidylinositol-4-phosphate and phosphatidylinositol-4,5-bisphosphate(PI(4,5)P2) (Lee et al. 2002). Because of that, the PI binding motif can significantly enhance tubulation by targeting BIN1 to the membrane domain enriched in those lipids. Additionally, it is also important for autoinhibition mentioned above (Wu & Baumgart 2014; Kojima et al. 2004). My results appear to be consistent with such findings, highlighting the importance of exon11 in membrane folding induced by BIN1.

It should be noted that although isoform 8 contains one more exon, the exon17, than isoform13, I did not find significant differences in terms of their ability to evoke tubulation. As for isoform6, the only human cardiac BIN1 isoform containing exon13, a previous study showed that in the mouse heart it was the major isoform responsible for T-tubule generation (T. Hong et al. 2014). However, my study failed to confirm that for the human BIN1 splice variant regardless of the expression in HEK cells, rat ventricular myocytes, or hiPSC-CMs.

6.3 Behaviour of BIN1 isoforms in adult rat cardiomyocytes

To directly investigate the role of the identified human BIN1 isoforms in cardiac myocytes, I adopted the model of cultured rat adult ventricular myocytes (Mitcheson et al. 1998; Ibarra et al. 2004; Viero et al. 2008; Xu & Colecraft 2009). It has the advantage of offering a tightly controlled experimental system and spontaneous development of detubulation (loss of T-tubules) mimicking the loss of T-tubular structure occurring during pathological conditions such as heart failure.

To measure calcium signals, two different labeling approaches were employed, namely, a small molecular dye, Fluo-4, and a genetically encoded calcium sensor that detects calcium locally at the dyadic cleft, junction-GCaMP6f (Shang et al. 2014). Combined together, they ought to provide a comprehensive picture of calcium handling and EC coupling following the expression of various BIN1 splice variants.

To investigate the effects of BIN1 isoforms in more details, I designed two types of experiments: maintenance and rescue. In the maintenance experiment, BIN1 was expressed alongside the culture of rat adult cardiomyocytes to see if it could relieve the decrease of T-tubules and EC-coupling. In the rescue experiment, however, BIN1 was expressed after the cells were cultured for some time when the T-tubules have lost to some extent. In this way, it is possible to see if BIN1 could restore the T-tubules as well as calcium handling.

In my study, I found when the adult rat ventricular myocytes were cultured for a three-day period, the expression of BIN1 decreased significantly compared to the expression directly after isolation. Concomitant to that the extent of T-tubules and amplitude of global calcium transients significantly declined. I utilized such a model to study the effect of BIN1 on maintaining T-tubules. When rat cardiomyocytes were transduced with adenoviruses coding for BIN1 at the day of isolation, the level of BIN1 proteins was increased, and T-tubules, as well as calcium transients, were maintained after three days when compared to control myocytes without transduction or with transduction of TagRFPT alone. These results were both confirmed in the experiments using either Fluo-4 or GCaMP6f-junctin. In the maintenance experiment in which Fluo-4 was applied, I even analyzed the changes of couplon properties. Although the amplitude remained unchanged, there was a significant increase of couplon density in cells expressing BIN1 isoforms. In the rescue experiment using GcaMP6f-junctin to label calcium, similar positive effects of BIN1 were also observed. BIN1 overexpression restored the T-tubules and EC-coupling of rat cardiomyocytes to a large extent even when these cells were cultured for two days prior to it. These data indicated that BIN1 expression was efficient in sustaining a functional T-tubule system and EC-coupling.

It was reported that the level of BIN1 expression is highly associated with T-tubules as well as calcium handling in cardiomyocytes. In one study heart failure was induced by ventricular tachypacing in sheep and through ascending aortic banding in ferrets (Caldwell et al. 2014). In these two models, the levels of BIN1 declined significantly in ventricular cardiomyocytes along with a reduced T-tubular system. In addition, the BIN1 expression and extent of the T-tubular system in atrial myocytes of failing sheep hearts also declined (Caldwell et al. 2014). When BIN1 was knockdown by small interfering RNA, the density of T-tubules was also reduced (Caldwell et al. 2014). In another study using freshly isolated cardiac myocytes from non-failing and advanced-stage failing human hearts, during a three-day culture, they noticed a substantial decrease of BIN1, and the level of LTCC and the fraction of its distribution in T-tubules were also profoundly reduced, which is consistent with my observations (T.-T. Hong et al. 2012). When BIN1 was knocked down in mouse and zebrafish hearts, calcium handling was impaired, resulting in cardiac dysfunction (T.-T. Hong et al. 2012; L. L. Smith et al. 2014). When overexpressed in BIN1-deleted mouse cardiomyocytes, either the T-tubules or the EC-coupling was restored(T. Hong et al. 2014). All these results, combined with my data, suggest that BIN1 plays an important role in maintaining T-tubules and calcium handling in cardiomyocytes.

It is noteworthy that all human cardiac BIN1 isoforms were able to alleviate the loss of T-tubule but to different degrees, while only the isoforms containing exon13 and exon17 regenerated tubules in the study of mouse heart (T. Hong et al. 2014). Since BIN1 isoforms have capabilities for membrane invaginating, it is reasonable to assume that they all have some positive effects on T-tubules instead of being useless. For example, a study in rat hearts indicated that the ubiquitous BIN1 isoforms 9 and 10 also participated in the organization of T-tubules and their overexpression reduced the remodeling of T-tubule complexity in a rat model of myocardial infarction (L.-L. Li et al. 2020).

Another interesting finding is that the two BIN1 isoforms 8 and 13 with exon11-encoded PI motif performed significantly better than others in maintaining both T-tubules and EC-coupling (**Fig. 5.12**). As described before, the PI motif is a short polybasic amino-acid sequence encoded by exon11 and displays a high affinity towards certain lipids such as PI (4,5) P2, which is enriched in T-tubules (Lee et al. 2002; Nicot et al. 2007). Because of that, they exhibit stronger abilities in inducing tubules. As for other isoforms, they were only able to generate shorter tubules. It is also noteworthy that exon11-containing BIN1 isoforms were reported to be necessary for LTCC trafficking (T.-T. Hong et al. 2010). Combined together, BIN1 isoforms with exon11 appear more capable of maintaining T-tubules and EC-coupling.

To further characterize BIN1 in cardiomyocytes, I designed a second approach in adult rat ventricular myocytes to investigate BIN1's ability to regenerate T-tubules after loss using GCaMP6f-junctin to label calcium release. My data showed that all BIN1 isoforms, in particular those with exon11, significantly restored the T-tubule system of cardiomyocytes after an almost complete loss of T-tubules. With respect to calcium transient, cells transduced with adenoviruses coding for BIN1 displayed increased amplitudes when compared to control cells with no transduction or transduction with the fluorescent protein alone. These results were consistent with what was observed in the maintenance experiments discussed above. Similarly, isoforms with exon11 displayed greater effects than others, which may also be attributed to the special properties of the PI domain.

LTCC and RyR2 are the two major components of EC-couplons that mediate calcium-induced calcium release. My study found that when cells were cultured for three days, the densities of both RyR2 and LTCC were significantly decreased. Particularly, LTCCs were distributed in a more random and irregular pattern, contributing to the decreased colocalization with RyR2. In contrast, BIN1 overexpression obviously maintained the expression of RyR2 and LTCC and most important of all, the coupling, resulting in a much higher correlation compared to the control. The data implies that the improvement of EC-coupling in BIN1-expressing myocytes was attributed – at least to a great extent - to its effects on RyR2 and LTCC. Previous studies have reported that BIN1 was able to recruit LTCC to the T-tubular membrane via microtubules (T.-T. Hong et al. 2010). They further described that trafficking of and targeted delivery of LTCC were both mediated by the SH3 domain of BIN1 (T.-T. Hong et al. 2010). As for RyR2, previous research has suggested that BIN1-induced microdomains were able to recruit RyR to the dyadic cleft, especially upon the activation of β-AR, which contributed to the maintenance of EC-couplons as well as calcium handling (Y. Fu et al. 2016).

Another interesting finding in my study is that during *in vitro* culture, the expression of junctophilin-2 was reduced and disorganized with the loss of T-tubules (**Fig. 5.9**). When cells were transduced with adenoviruses coding for BIN1, the expression and arrangement of junctophilin-2 appeared significantly maintained after the loss. Because the expression of both RyR2 and junctophilin-2 were maintained, they displayed a higher colocalization with each other than the control, which was crucial to the stability of dyads and EC couplons (**Fig. 5.10**). Several previous studies have reported that junctophilin-2 plays a crucial role in the maturation of T-tubules and stabilization of EC-couplons (Hill & Diwan 2013; B. Chen et al. 2013). Furthermore, the reduction of junctophilin-2 is significantly linked to the impairment of calcium handling and cardiac dysfunction (Landstrom et al. 2007; Reynolds et al. 2013; Quick et al. 2017). It was reported in skeletal muscle that there is even a physical interaction between junctophilin and the C-terminus of Cav1.1, through which calcium channels are recruited to the junctional membrane and couple to RyR1 (Nakada et al. 2018). Although there is currently no confirmation of such a mechanism in cardiomyocytes, junctophilin-2 may still act in a similar manner and contribute to orchestration of the EC-coupling machinery. Therefore, the maintenance of junctophilin-2 in rat cardiomyocytes may add to the attenuation of EC-coupling decline. As for the positive effects of BIN1 on junctophilin-2, the mechanism is still unclear. Since junctophilin-2 is a plasma membrane binding protein, the maintenance of T-tubules by BIN1 may have a positive effect on the anchoring of junctophilin-2 to the dyadic space.

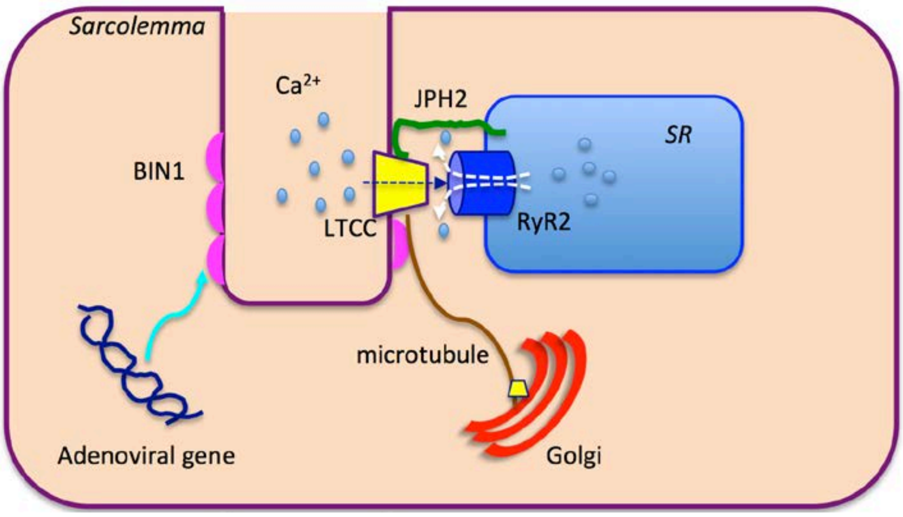

Figure 6.3 Schematic illustration of the effect and mechanism of BIN1 on adult rat cardiomyocytes. BIN1 contributes to the T-tubule maintenance by its membrane folding ability. At the same time, LTCC is also maintained

coupling with RyR2. The preservation of Junctophilin-2 helps keep the dyads and stabilize EC-coupling.

There are some limitations in the present study. Although an easily accessible model, cultured adult rat cardiomyocyte are not an ideal model to study the effects of BIN1 since it is an *in vitro* model, which cannot completely mimic the *in vivo* situation. To better appereciate and study the roles of BIN1 isoforms, animal models of heart failure are expected be used in the future. As for the rescue experiment, BIN1 could be knockdown or knockout before overexpression, which can exclude the effects of remaining endogenous BIN1 proteins. However, currently I have no access to appropriate knockdown or knockout animal models. In addition, it is unrealistic to knock out genes in cultured adult cardiomycytes *in vitro* since they can only last 3-5 days during culture. Despite such shortcomings, the culturing of isolated adult rat cardiomyocytes still stands as a reliable platform, not only because of its easy accessibility and assessment, but also due to the detubulation and decrease of calcium handling during the culturing process, which highlights the physiopathological changes occurring in heart failure. Therefore, it provides a relatively suitable context to examine the effects of BIN1 isoforms.

What I did not resolve is how BIN1 helps building and maintaining T-tubules mechanistically. Based on what has been known, there may be two possible mechanisms governing these processes. The first one involves the direct membrane folding effects of BIN1 isoforms. Supplementing BIN1 protein by viral transduction can compensate the loss of endogenous BIN1 protein and T-tubules following pathological insults, and eventually helps stabilizing the T-tubule system. Actually, a previous report has indicated that when cardiomyocytes were detubulated by formamide exposure, a large part of the tubule system still remain inside the cell but just lost their connection to the sarcolemma (Brette F et al. 2002). When tubules are discontinued from cell membrane, action potentials are unable to travel through T-tubules and activate LTCCs to initiate calcium entry followed by CICR in the interior of the myocyte. Therefore, BIN1 may contribute to the continuity of tubules with sarcolemma. The other possible mechanism is that BIN1 may recruite other proteins such as LTCC to T-tubules and maintain LTCC-RyR2 coupling (T.-T. Hong et al. 2010). Based on my observations, both of these mechanisms may contribute.

In summary, my study, for the first time, identified the pattern of BIN1 isoforms in healthy human cardiomyocytes and revealed their protective effects on adult cardiac myocytes, both structurally and functionally. Based on the encouragingly positive effects of BIN1, especially isoforms with exon11, they may be valuable for therapeutic applications in the future.

6.4 Effects of BIN1 isoforms on EC-coupling in hiPSC-CMs

Although hiPSC-CMs exhibit some of the properties of adult cardiomyocytes such as automatic beating, it is undeniable that these cells remain quite immature compared to their adult counterparts. Specifically, hiPSC-CMs do not display any membrane invaginations such as T-tubules, which restrains the effeciency of EC-coupling (Veerman et al. 2015). In addition, current protocols for differentiating cardiac myocytes from hiPSCs are only able to produce a mixture of different subtypes, including nodal-, atrial-, and ventricular-like cells, identified by their distinctive electrophysiological (Karakikes et al. 2015; Z. Chen et al. 2017). For these reasons, it appears imperative to promote further differentiation of hiPSC-CMs. In particular, it is crucial to resolve one of the core obstacles, the absence of T-tubules. With the help of T-tubules, hiPSC-CMs may develop more mature calcium handling. Unfortunately, so far there are very few reports of successfully inducing T-tubule generation in hiPSC-CMs.

Based on my previous results in adult rat ventricular myocytes, it was quite tempting to explore these isoforms, particularly those with exon11, in hiPSC-CMs to verify whether they could similarly evoke functional T-tubules. Firstly, I indeed found that hiPSC-CMs expressed low levels of BIN1 protein. Following viral transduction of BIN1 isoform8/13 expression, robust tubule-like structures could be identified that were continuous with the outer plasma membrane indicated by the positive staining by CellMask DeepRed. Although these tubules were organized irregularly, they laid at least a structural foundation for future development. Without such a structure, it is almost impossible to build effective coupling between the sarcolemmal LTCC and junctional RyR2, two of which that are separated a long distance outside of the dyadic space. Interestongly, the expressed BIN1 isoforms in hiPSC-CMs displayed a similar capability of inducing membrane tubulation to that found in HEK cells and adult rat cardiomyocytes.

While membrane invaginations enable the conduction of action potentials into deeper layers of the cardiac myocyte, only EC-couplon decorating such T-tubules could restore their role in EC-coupling. It thus appeared necessary to investigate the underlying transformations imposed by such new tubules. My data from the immunolabeling experiments clearly demonstrated that LTCCs were enriched along those tubules (**Fig. 5.16**). This finding was of substantial significance because it demonstrated that these tubules were not simply hollow membrane structures without functions, but were decorated with key ion channels, which may be functional in EC-coupling. These results are consistent with previous reports that exon11-containing BIN1 isoforms are responsible for LTCC recruitment in cardiomyocytes (T.-T. Hong et al. 2010).

In addition, the distribution of RyR2 was also altered by BIN1-expression and T-tubule formation. In control hiPSC-CMs RyR2-immunolabeling displayed a regular, striated or onion-like concentric pattern with an interval of around 2μm, similar to that in adult cardiomyocytes. However, following the expression of BIN1 this pattern was remodeled and attracted to the new branching pattern of the newly generated tubules. This remodeling was accompanied by a significant increase in the colocalization between LTCCs and RyR2s (**Fig. 5.18**). It was reported that in addition to LTCC recruitment, BIN1-induced microdomains also affected the localization of RyR2, particularly in β-AR regulated CICR as well as LTCC-RyR coupling at the dyads (Y. Fu et al. 2016). When BIN1 expression is reduced in acquired heart failure, the reorganization of BIN1-related microdomains may decrease, causing a weaker recruitment of phosphorylated-RyR to dyads and resulting in impaired EC-coupling (Y. Fu et al. 2016). Therefore, BIN1 may have a direct effect on the distribution of RyR2. In summary, my results demonstrated that BIN1-induced tubules were not functionally futile; instead they modified the arrangement of the key ion channels of EC-couplons.

Based on the above findings, it appears that BIN1 expression promotes formation of EC couplons in hiPSC-CMs. To verify this hypothesis, I measured calcium in hiPSC-CMs using both Fluo-4 and GCaMP6f-junctin as previously described. With either approach, my results demonstrated that both exon11-containing BIN1 isoforms significantly improved calcium transients when compared to the control group (**Fig. 5.19-20**). Isoform13 appeared more effective than isoform8. When analyzing the distribution of EC couplons, I found that most couplons were positioned close to the cellular circumfence in BIN1-negative cells while a significant proportion of the new EC couplons were arranged in the proximity of newly generated T-tubules in BIN1-expressing cells. I also found a significant correlation between EC couplons and BIN1-induced tubules. The analysis of EC couplons also revealed a higher density of couplons in BIN1-expressing hiPSC-CMs. Therefore, all these findings demonstrated that EC-coupling was significantly enhanced in hiPSC-CMs through BIN1 overexpression both, structurally by restoring a T-tubule like network and functionally by enhancing EC-coupling efficiency.

This appears to be a rather important finding because there is currently very little advance in this area. Actually, ever since the emerging of hiPSC-CMs, T-tubule biogenesis has been a hard nut to crack. Even though multiple strategies have been developed and there are some improvement in the maturity of the cells, few of them ever succeeded in inducing T-tubule formation (Lundy et al. 2013; Lieu et al. 2013; Kensah et al. 2013; Cao et al. 2012; Nunes et al. 2013; Thavandiran et al. 2013; Salick et al. 2014). Only a latest study reported that T-tubule like structures were generated by applying two hormones (thyroid and glucocorticoid hormones) to hiPSC-CMs cultured on a specially prepared Matrigel mattress (Parikh et al. 2017). Nevertheless, the mechanistic background of this is still elusive and such excessive hormone treatments most likely trigger a plethora of signalling pathways resulting in gross remodeling of the hiPSC-CM. Most important of all, it is controversial whether these tubules are functional or not. For example, there is no evidence in the study demonstrating that LTCC and RyR2 are recruited to these tubules. Moreover, there is no direct evidence that there are calcium release sites or EC-couplons along the tubules. A recent seminal study on hESC-CMs by De La Mata and co-workers employed expression of BIN1 isoform 8 and showed generation of membrane invaginations, enhanced calcium cycling, increased membrane expression of LTCC and an enhanced proximity of LTCCs and RyRs on the hundreds of nanometer scale (La Mata et al. 2019). Despite that, it neither offered a reason why they use BIN1 isoform8 nor provided any direct evidence of functional couplons established in the proximity of the BIN1-evoked T-tubules. In contrast, my study demonstrated that expression of human BIN1 isoforms induced tubule formation and clear functional improvement of EC-coupling. Particularly, I employed the novel developed CaCLEAN algorithm published recently for a direct identification and characterization of EC-couplons in beating cardiomyocytes (Tian et al. 2017), which provides much more direct insights into EC-coupling than previous reports. These data were supplementd by the application of the genetically encoded calcium sensor junction-GCaMP6f that measured calcium directly at the EC-couplon. Data from these experiments strongly supported my previous findings with Fluo-4.

Although my study has demonstrated that BIN1 splice variants with exon11 greatly promoted the development of a T-tubule like membrane system and EC-coupling in hiPSC-CMs, there are still several limitations. One of them is that these tubules were randomly organized without a clear striped arrangement, which is very different from those in adult cardiomyocytes. This may be at least partially due to the fact that hiPSC-CMs themselves are not mature, not only in calcium handling, but also in cytoskeletons, resembling early neonatal cardiomyocytes. Adding to that, these cells are mostly of a round or polygonal shape, chaotically aligned with each other, strikingly in contrast to rod, cylinder-shaped adult cardiomyocytes (Zwi et al. 2009). Accordingly, inner skeleton elements such as α-actinin are not correctly arrayed, which may contribute to the irregularity of BIN1-evoked T-tubules. Another explanation is that although exon11-containing BIN1 isoforms are robust in generating tubules, they are unable to correctly arrange these tubules to the Z-lines of the contractile filaments. A recent study in rat heart verified such a hypothesis. The results demonstrated that although BIN1 isoform10 were very weak in giving rise to the tubules, it coordinated the exon11-related isoforms to accumulate at the Z-lines, therefore contribute to the correct arrangement of T-tubules (L.-L. Li et al. 2020). Since only exon11-containing BIN1 isoforms were expressed in my study, they alone may be insufficient to organize tubules to the correct intracellular structure.

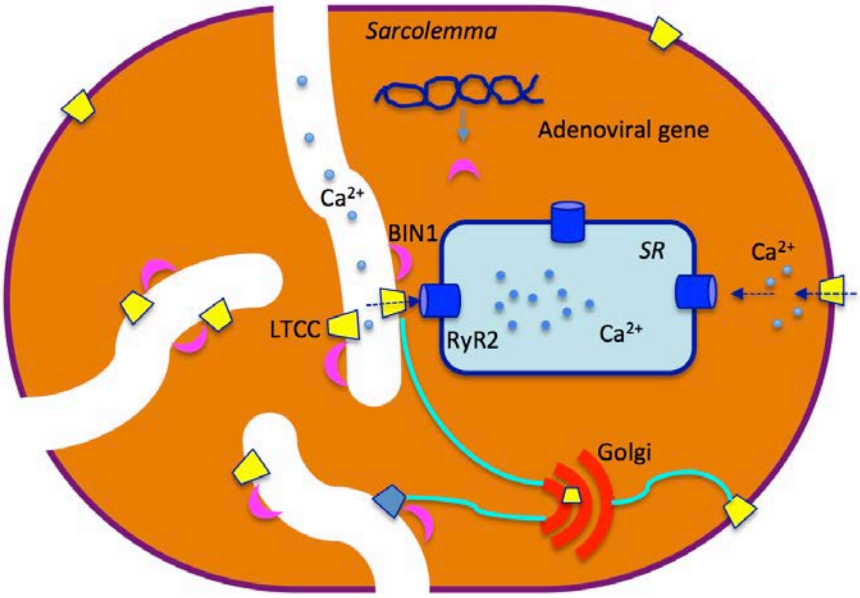

Figure 6.4 Schematic illustration of the effect and mechanism of BIN1 on hiPSC-CMs. BIN1 initiates tubule biogenesis and deliver LTCCs to the tubular compartments. Upon the tubule formation, LTCCs and RyR2 get proximate to each other and even establish the coupling with each other. In this way the EC-coupling of hiPSC-CMs is promoted.

In line with that, additional factors may affect T-tubule generation and placement in cardiomyocytes and BIN1 alone may not be sufficient to generate a fully functional T-tubular system. Other factors such as junctophilin-2 (JPH2) may also be required to coordinate components of EC-coupling and their spatial arrangement. JPH2 is a structural protein spanning the dyadic space to bridge and define the distance between the sarcolemma and SR membrane (Takeshima et al. 2000). Multiple reports have shown that JPH2 is necessary for the maturation and maintenance of T-tubules as well as EC-coupling (Reynolds et al. 2013; B. Chen et al. 2013). When mutated or dysregulated, it can lead to dis-organization of EC-coupling, calcium mishandling as well as cardiac dysfunction (Beavers et al. 2013; W. Wang et al. 2014; Prins et al. 2016; Quick et al. 2017; Landstrom et al. 2007) (Landstrom et al. 2007). When overexpressed, JPH2 can normalize RyR2-mediated calcium handling and attenuate heart function (Reynolds et al. 2013; Guo et al. 2014). Since JPH2 expression is relatively low in hiPSC-CMs, it may be advantageous for enhancing and/or supplementing the effects of BIN1.

Another important factor that should be considered is the culture environment of hiPSC-CMs. hiPSC-CMs are generally cultured *in vitro*, which are significantly different from the *in vivo* context in which adult cardiomyocytes grow and are supported. For example, there is a certain degree of tissue pressure and strain under physiological conditions, which are heavily absent *in vitro*. Such degrees of stress are considered necessary for the growing and organization of T-tubules. Either high-pressure in cardiomyopathy or low-pressure *in vitro* culture may lead to a loss or remodeling of T-tubules (Tulloch et al. 2011; Mihic et al. 2014). Therefore, imposing mechanical load indeed promote the maturation of hiPSC-CMs.

Moreover, the culturing base and supporting environment may also be extremely important in shaping the maturation of hiPSC-CMs. The physiological context of cardiomyocytes is much more complicated than a simple plastic dish. Under that condition, hiPSC-CMs normally grow into flat, polygonal, and irregular shapes with very small thickness, which is far from the adult arrangement. It has been reported that using 3D fibrin-based cardiac patch cultures combined with passive tension, hESC-CMs were aligned more uniformly and exhibited much higher conduction velocities, longer sarcomeres and an increased expression of cardiac contractile related genes such as cTnT, αMHC, CASQ2 and SERCA2 (Zhang et al. 2013). Another study using 3D cultivation with electrical stimulation (biowires) demonstrated their ability to generate 3D, aligned cardiac tissue with regular striation, increased myofibril ultrastructural organization and elevated electrophysiological and improved calcium handling (Nunes et al. 2013). Therefore, when combined with advanced culturing strategies, BIN1-induced tubules may become more mature and better incorporated in hiPSC-CMs.

6.5 Overall conclusion

In conclusion, in the present study, the transcriptional profile of BIN1 in human heart tissue was studied and five different isoforms were identified for the first time, demonstrating a set of BIN1 isoforms that is distinctly different from those of mouse. In particular, two isoforms were found to contain exon11, which was considered to be specific to skeletal muscle up to now. All these isoforms have different degrees of capabilities to form tubules and contribute to the maintenance of T-tubules and EC-coupling in adult rat cardiomyocytes. Here, BIN1 isoform8 and isoform13, the exon11-containing isoforms, proved to be the most potent variants. Moreover, my results also depicted that T-tubules were induced by

BIN1 overexpression in hiPSC-CMs. More importantly, my results demonstrated that these new T-tubules were decorated with functional EC couplons. Therefore, my work revealed the role of human BIN1 isoforms either in adult cardiomyocytes or in hiPSC-CMs, providing a new strategy by targeting T-tubule biogenesis for both, potentially improving cardiac function in pathological conditions and promoting the structural and functional development of hiPS-CMs.

7. Reference

Adam, J., Basnet, N. & Mizuno, N., 2015. Structural insights into the cooperative remodeling of membranes by amphiphysin/BIN1. *Scientific reports*, 5(1), p.15452.

Aherrahrou, Z. et al., 2015. Knock-out of nexilin in mice leads to dilated cardiomyopathy and endomyocardial fibroelastosis. *Basic Research in Cardiology*, 111(1), pp.1–10.

Alexandre Fabiato, 1983. Calcium-induced release of calcium from the cardiac sarcoplasmic reticulum. *American journal of physiology. Cell physiology*, 254(1), pp.C1–C14.

Asghari, P. et al., 2014. Nonuniform and variable arrangements of ryanodine receptors within mammalian ventricular couplons. *Circulation research*, 115(2), pp.252–262.

Ayettey, A.S. & Navaratnam, V., 1978. The T-tubule system in the specialized and general myocardium of the rat. *Journal of anatomy*, 127(Pt 1), pp.125–140.

Baddeley, D. et al., 2009. Optical single-channel resolution imaging of the ryanodine receptor distribution in rat cardiac myocytes. *Proceedings of the National Academy of Sciences of the United States of America*, 106(52), pp.22275–22280.

Baker, A. et al., 1997. Polyethylenimine (PEI) is a simple, inexpensive and effective reagent for condensing and linking plasmid DNA to adenovirus for gene delivery. *Gene therapy*, (4), pp.773–782. Available at: https://www.nature.com/articles/3300471.

Balijepalli, R.C. & Kamp, T.J., 2008. Caveolae, ion channels and cardiac arrhythmias. *Progress in biophysics and molecular biology*, 98(2-3), pp.149–160.

Bansal, D. et al., 2003. Defective membrane repair in dysferlin-deficient muscular dystrophy. *Nature*, 423(6936), pp.168–172.

Bassani, R.A., Bassani, J.W. & Bers, D.M., 1995. Relaxation in ferret ventricular myocytes: role of the sarcolemmal Ca ATPase., 430(4), pp.573–578.

Bauerfeind, R., Takei, K. & De Camilli, P., 1997. Amphiphysin I is associated with coated endocytic intermediates and undergoes stimulation-dependent dephosphorylation in nerve terminals. *The Journal of biological chemistry*, 272(49), pp.30984–30992.

Beavers, D.L. et al., 2013. Mutation E169K in junctophilin-2 causes atrial fibrillation due to impaired RyR2 stabilization. *Journal of the American College of Cardiology*, 62(21), pp.2010–2019.

Bers, D.M., 2002. Cardiac excitation–contraction coupling. *Nature*, 415, pp.198–205.

Bers, D.M. & Perez-Reyes, E., 1999. Ca channels in cardiac myocytes: structure and function in Ca influx and intracellular Ca release. *Cardiovascular research*, 42(2), pp.339–360.

Bodi, I. et al., 2005. The L-type calcium channel in the heart: the beat goes on. *The Journal of clinical investigation*, 115(12), pp.3306–3317.

Böhm, J. et al., 2014. Adult-onset autosomal dominant centronuclear myopathy due to BIN1 mutations. *Brain : a journal of neurology*, 137(Pt 12), pp.3160–3170.

Böhm, J. et al., 2013. Altered splicing of the BIN1 muscle-specific exon in humans and dogs with highly progressive centronuclear myopathy. G. A. Cox, ed. *PLoS genetics*, 9(6), p.e1003430.

Böhm, J. et al., 2010. Case report of intrafamilial variability in autosomal recessive centronuclear myopathy associated to a novel BIN1 stop mutation. *Orphanet journal of rare diseases*, 5(1), p.35.

Brette, F., Sallé, L. & Orchard, C.H., 2006. Quantification of calcium entry at the T-tubules and surface membrane in rat ventricular myocytes. *Biophysical journal*, 90(1), pp.381–389.

Burridge, P.W. et al., 2014. Chemically defined generation of human cardiomyocytes. *Nature methods*, 11(8), pp.855–860.

Butler, M.H. et al., 1997. Amphiphysin II (SH3P9; BIN1), a member of the amphiphysin/Rvs family, is concentrated in the cortical cytomatrix of axon initial segments and nodes of ranvier in brain and around T tubules in skeletal muscle. *The Journal of cell biology*, 137(6), pp.1355–1367.

Cabra, V., Murayama, T. & Samsó, M., 2016. Ultrastructural Analysis of Self-Associated RyR2s. *Biophysical journal*, 110(12), pp.2651–2662.

Caldwell, J.L. et al., 2014. Dependence of cardiac transverse tubules on the BAR domain protein amphiphysin II (BIN-1). *Circulation research*, 115(12), pp.986–996.

Cannell, M.B., Cheng, H. & Lederer, W.J., 1995. The Control of Calcium Release in Heart Muscle. *Science (New York, N.Y.)*, 268(5213), pp.1045–1049.

Cannell, M.B., Crossman, D.J. & Soeller, C., 2006. Effect of changes in action potential spike configuration, junctional sarcoplasmic reticulum micro-architecture and altered t-tubule structure in human heart failure. *Journal of muscle research and cell motility*, 27(5-7), pp.297–306.

Cao, N. et al., 2012. Ascorbic acid enhances the cardiac differentiation of induced pluripotent stem cells through promoting the proliferation of cardiac progenitor cells. *Cell research*, 22(1), pp.219–236.

Catterall, W.A., 2011. Voltage-gated calcium channels. *Cold Spring Harbor perspectives in biology*, 3(8), pp.a003947–a003947.

Catterall, W.A. et al., 2005. International Union of Pharmacology. XLVIII. Nomenclature and structure-function relationships of voltage-gated calcium channels. *Pharmacological reviews*, 57(4), pp.411–425.

Chal, J. et al., 2015. Differentiation of pluripotent stem cells to muscle fiber to model Duchenne muscular dystrophy. *Nature biotechnology*, 33(9), pp.962–969.

Chambers, S.M. et al., 2009. Highly efficient neural conversion of human ES and iPS cells by dual inhibition of SMAD signaling. *Nature biotechnology*, 27(3), pp.275–280.

Chan, Y.-C. et al., 2013. Electrical stimulation promotes maturation of cardiomyocytes derived from human embryonic stem cells. *Journal of cardiovascular translational research*, 6(6), pp.989–999.

Chen, B. et al., 2013. Critical roles of junctophilin-2 in T-tubule and excitation-contraction coupling maturation during postnatal development. *Cardiovascular research*, 100(1), pp.54–62.

Chen, T.-W. et al., 2013. Ultrasensitive fluorescent proteins for imaging neuronal activity. *Nature*, 499(7458), pp.295–300.

Chen, Z. et al., 2017. Subtype-specific promoter-driven action potential imaging for precise disease modelling and drug testing in hiPSC-derived cardiomyocytes. *European heart journal*, 38(4), pp.292–301.

Chen, Z. et al., 2016. The N-Terminal Amphipathic Helix of Endophilin Does Not Contribute to Its Molecular Curvature Generation Capacity. *Journal of the American Chemical Society*, 138(44), pp.14616–14622.

Chen-Izu, Y. et al., 2006. Three-dimensional distribution of ryanodine receptor clusters in cardiac myocytes. *Biophysical journal*, 91(1), pp.1–13.

Cheng, H. & Lederer, W.J., 2008. Calcium sparks. *Physiological reviews*, 88(4), pp.1491–1545.

Cheng, H., Lederer, W.J. & Cannell, M.B., 1993. Calcium sparks: elementary events underlying excitation-contraction coupling in heart muscle. *Science (New York, N.Y.)*, 262(5134), pp.740–744.

Ching, L.L., Williams, A.J. & Sitsapesan, R., 2000. Evidence for Ca(2+) activation and inactivation sites on the luminal side of the cardiac ryanodine receptor complex. *Circulation research*, 87(3), pp.201–206.

Chopra, N. & Knollmann, B.C., 2013. Triadin regulates cardiac muscle couplon structure and microdomain Ca2+ signalling: a path towards ventricular arrhythmias. *Cardiovascular research*, 98(2), pp.187–191.

Chu, A. et al., 1990. Ryanodine as a probe for the functional state of the skeletal muscle sarcoplasmic reticulum calcium release channel. *Molecular pharmacology*, 37(5), pp.735–741.

Cleemann, L. & Morad, M., 1991. Role of Ca2+ channel in cardiac excitation-contraction coupling in the rat: evidence from Ca2+ transients and contraction. *The Journal of physiology*, 432, pp.283–312.

Copello, J.A. et al., 1997. Heterogeneity of Ca2+ gating of skeletal muscle and cardiac ryanodine receptors. *Biophysical journal*, 73(1), pp.141–156.

Coupé, P. et al., 2012. A CANDLE for a deeper in vivo insight. *Medical Image Analysis*, 16(4), pp.849–864.

Cowling, B.S. et al., 2017. Amphiphysin (BIN1) negatively regulates dynamin 2 for normal muscle maturation. *Journal of Clinical Investigation*, 127(12), pp.4477–4487.

de Felipe, P., 2004. Skipping the co-expression problem: the new 2A “CHYSEL” technology. *Genetic vaccines and therapy*, 2(1), p.13.

Di Maio, A. et al., 2007. T-tubule formation in cardiacmyocytes: two possible mechanisms? *Journal of muscle research and cell motility*, 28(4-5), pp.231–241.

Dolphin, A.C., 2012. Calcium channel auxiliary α2δ and β subunits: trafficking and one step beyond. *Nature reviews. Neuroscience*, 13(8), pp.542–555.

Domínguez, J.N. et al., 2008. Tissue distribution and subcellular localization of the cardiac sodium channel during mouse heart development. *Cardiovascular research*, 78(1), pp.45–52.

Donnelly, M.L. et al., 2001. Analysis of the aphthovirus 2A/2B polyprotein 'cleavage' mechanism indicates not a proteolytic reaction, but a novel translational effect: a putative ribosomal 'skip'. *The Journal of general virology*, 82(Pt 5), pp.1013–1025.

Drago, I. et al., 2012. Mitochondrial Ca2+ uptake contributes to buffering cytoplasmic Ca2+ peaks in cardiomyocytes. *Proceedings of the National Academy of Sciences of the United States of America*, 109(32), pp.12986–12991.

DuHadaway, J.B. et al., 2003. Immunohistochemical analysis of Bin1/Amphiphysin II in human tissues: diverse sites of nuclear expression and losses in prostate cancer. *Journal of cellular biochemistry*, 88(3), pp.635–642.

Egawa, N. et al., 2012. Drug screening for ALS using patient-specific induced pluripotent stem cells. *Science translational medicine*, 4(145), pp.145ra104–145ra104.

Ellis, J.D. et al., 2012. Tissue-specific alternative splicing remodels protein-protein interaction networks. *Molecular cell*, 46(6), pp.884–892.

Ezerman, E.B. & Ishikawa, H., 1967. Differentiation of the sarcoplasmic reticulum and T system in developing chick skeletal muscle in vitro. *The Journal of cell biology*, 35(2), pp.405–420.

Fearnley, C.J., Roderick, H.L. & Bootman, M.D., 2011. Calcium signaling in cardiac myocytes. *Cold Spring Harbor perspectives in biology*, 3(11), pp.a004242–a004242.

Ferguson, D.G. & Leeson, T.S., 1983. Postnatal development of sarcolemmal invaginations in right atrial myocardium of the rat. *Acta anatomica*, 117(4), pp.289–302.

Fill, M. & Copello, J.A., 2002. Ryanodine receptor calcium release channels. *Physiological reviews*, 82(4), pp.893–922.

Flucher, B.E., Takekura, H. & Franzini-Armstrong, C., 1993. Development of the excitation-contraction coupling apparatus in skeletal muscle: association of sarcoplasmic reticulum and transverse tubules with myofibrils. *Developmental biology*, 160(1), pp.135–147.

Forbes, M.S. & Sperelakis, N., 1976. The presence of transverse and axial tubules in the ventricular myocardium of embryonic and neonatal guinea pigs. *Cell and tissue research*, 166(1), pp.83–90.

Forbes, M.S. & van Neil, E.E., 1988. Membrane systems of guinea pig myocardium: ultrastructure and morphometric studies. *The Anatomical record*, 222(4), pp.362–379.

Forbes, M.S., Hawkey, L.A. & Sperelakis, N., 1984. The transverse-axial tubular system (TATS) of mouse myocardium: its morphology in the developing and adult animal. *The American journal of anatomy*, 170(2), pp.143–162.

FOWLER, M., 2004. Functional consequences of detubulation of isolated rat ventricular myocytes. *Cardiovascular research*, 62(3), pp.529–537.

Franzini-Armstrong, C., 1991. Simultaneous maturation of transverse tubules and sarcoplasmic reticulum during muscle differentiation in the mouse. *Developmental biology*, 146(2), pp.353–363.

Franzini-Armstrong, C., Landmesser, L. & Pilar, G., 1975. Size and shape of transverse tubule openings in frog twitch muscle fibers. *The Journal of cell biology*, 64(2), pp.493–497.

Franzini-Armstrong, C., Protasi, F. & Ramesh, V., 1999. Shape, size, and distribution of Ca(2+) release units and couplons in skeletal and cardiac muscles. *Biophysical journal*, 77(3), pp.1528–1539.

Frisk, M. et al., 2016. Elevated ventricular wall stress disrupts cardiomyocyte t-tubule structure and calcium homeostasis. *Cardiovascular research*, 112(1), pp.443–451.

Frost, A., Unger, V.M. & De Camilli, P., 2009. The BAR domain superfamily: membrane-molding macromolecules. *Cell*, 137(2), pp.191–196.

Fu, J.-D. et al., 2011. Distinct roles of microRNA-1 and -499 in ventricular specification and functional maturation of human embryonic stem cell-derived cardiomyocytes. M. Rota, ed. *PloS one*, 6(11), p.e27417.

Fu, Y. et al., 2016. Isoproterenol Promotes Rapid Ryanodine Receptor Movement to Bridging Integrator 1 (BIN1)-Organized Dyads. *Circulation*, 133(4), pp.388–397.

Fugier, C. et al., 2011. Misregulated alternative splicing of BIN1 is associated with T tubule alterations and muscle weakness in myotonic dystrophy. *Nature medicine*, 17(6), pp.720–725.

Funakoshi, S. et al., 2016. Enhanced engraftment, proliferation, and therapeutic potential in heart using optimized human iPSC-derived cardiomyocytes. *Scientific reports*, 6(1), p.19111.

Furuichi, T. et al., 1994. Multiple types of ryanodine receptor/Ca2+ release channels are differentially expressed in rabbit brain. *The Journal of neuroscience : the official journal of the Society for Neuroscience*, 14(8), pp.4794–4805.

GA, L. & A, P., 1996. Calcium Concentration and Movement in the Diadic Cleft Space of the Cardiac Ventricular Cell. *Biophysical journal*, 70(3), pp.1169–1182.

Gabella, G., 1978. Inpocketings of the cell membrane (caveolae) in the rat myocardium. *Journal of ultrastructure research*, 65(2), pp.135–147.

Gaburjakova, J. & Gaburjakova, M., 2014. Coupled gating modifies the regulation of cardiac ryanodine receptors by luminal Ca(2+). *Biochimica et biophysica acta*, 1838(3), pp.867–873.

Gao, T. et al., 1997. Identification and subcellular localization of the subunits of L-type calcium channels and adenylyl cyclase in cardiac myocytes. *The Journal of biological chemistry*, 272(31), pp.19401–19407.

Giannini, G. et al., 1992. Expression of a ryanodine receptor-Ca2+ channel that is regulated by TGF-beta. *Science (New York, N.Y.)*, 257(5066), pp.91–94.

Grant, A.O., 2009. Cardiac ion channels. *Circulation. Arrhythmia and electrophysiology*, 2(2), pp.185–194.

Guo, A. et al., 2013. Emerging mechanisms of T-tubule remodelling in heart failure. *Cardiovascular research*, 98(2), pp.204–215.

Guo, A. et al., 2014. Overexpression of junctophilin-2 does not enhance baseline function but attenuates heart failure development after cardiac stress. *Proceedings of the National Academy of Sciences of the United States of America*, 111(33), pp.12240–12245.

Haddock, P.S. et al., 1999. Subcellular [Ca2+]i gradients during excitation-contraction coupling in newborn rabbit ventricular myocytes. *Circulation research*, 85(5), pp.415–427.

Hassel, D. et al., 2009. Nexilin mutations destabilize cardiac Z-disks and lead to dilated cardiomyopathy. *Nature medicine*, 15(11), pp.1281–1288.

Hayashi, T. et al., 2009. Three-dimensional electron microscopy reveals new details of membrane systems for Ca2+ signaling in the heart. *Journal of cell science*, 122(Pt 7), pp.1005–1013.

Hazeltine, L.B. et al., 2012. Effects of substrate mechanics on contractility of cardiomyocytes generated from human pluripotent stem cells. *International journal of cell biology*, 2012(7), pp.508294–13.

He, J. et al., 2001. Reduction in density of transverse tubules and L-type Ca(2+) channels in canine tachycardia-induced heart failure. *Cardiovascular research*, 49(2), pp.298–307.

Heinzel, F.R. et al., 2008. Remodeling of T-tubules and reduced synchrony of Ca2+ release in myocytes from chronically ischemic myocardium. *Circulation research*, 102(3), pp.338–346.

Heinzel, F.R. et al., 2002. Spatial and temporal inhomogeneities during Ca2+ release from the sarcoplasmic reticulum in pig ventricular myocytes. *Circulation research*, 91(11), pp.1023–1030.

Hill, J.A. & Diwan, A., 2013. Ca(2+) leak in atrial fibrillation: junctophilin-2 stabilizes ryanodine receptor. *Journal of the American College of Cardiology*, 62(21), pp.2020–2022.

Hofhuis, J. et al., 2017. Dysferlin mediates membrane tubulation and links T-tubule biogenesis to muscular dystrophy. *Journal of cell science*, 130(5), pp.841–852.

Hong, T. & Shaw, R.M., 2017. Cardiac T-Tubule Microanatomy and Function. *Physiological reviews*, 97(1), pp.227–252.

Hong, T. et al., 2014. Cardiac BIN1 folds T-tubule membrane, controlling ion flux and limiting arrhythmia. *Nature medicine*, 20(6), pp.624–632.

Hong, T.-T. et al., 2012. BIN1 is reduced and Cav1.2 trafficking is impaired in human failing cardiomyocytes. *Heart rhythm*, 9(5), pp.812–820.

Hong, T.-T. et al., 2010. BIN1 localizes the L-type calcium channel to cardiac T-tubules. K. R. Chien, ed. *PLoS biology*, 8(2), p.e1000312.

Hüser, J., Lipsius, S.L. & Blatter, L.A., 1996. Calcium gradients during excitation-contraction coupling in cat atrial myocytes. *The Journal of physiology*, 494 (Pt 3)(Pt 3), pp.641–651.

Ibarra, C. et al., 2004. Insulin-like growth factor-1 induces an inositol 1,4,5-trisphosphate-dependent increase in nuclear and cytosolic calcium in cultured rat cardiac myocytes. *The Journal of biological chemistry*, 279(9), pp.7554–7565.

Inoue, M. & Bridge, J.H.B., 2003. Ca2+ sparks in rabbit ventricular myocytes evoked by action potentials: involvement of clusters of L-type Ca2+ channels. *Circulation research*, 92(5), pp.532–538.

Inui, M., Saito, A. & Fleischer, S., 1987. Purification of the ryanodine receptor and identity with feet structures of junctional terminal cisternae of sarcoplasmic reticulum from fast skeletal muscle. *The Journal of biological chemistry*, 262(4), pp.1740–1747.

Ishikawa, H., 1968. Formation of elaborate networks of T-system tubules in cultured skeletal muscle with special reference to the T-system formation. *The Journal of cell biology*, 38(1), pp.51–66.

Itzhaki, I. et al., 2011. Calcium handling in human induced pluripotent stem cell derived cardiomyocytes. M. Pera, ed. *PloS one*, 6(4), p.e18037.

Ivashchenko, C.Y. et al., 2013. Human-induced pluripotent stem cell-derived cardiomyocytes exhibit temporal changes in phenotype. *American journal of physiology. Heart and circulatory physiology*, 305(6), pp.H913–22.

Jones, L.R. et al., 1995. Purification, Primary Structure, and Immunological Characterization of the 26-kDa Calsequestrin Binding Protein (Junctin) from Cardiac Junctional Sarcoplasmic Reticulum*. *The Journal of biological chemistry*, 270(51), pp.30787–30796.

Kamakura, T. et al., 2013. Ultrastructural maturation of human-induced pluripotent stem cell-derived cardiomyocytes in a long-term culture. *Circulation journal : official journal of the Japanese Circulation Society*, 77(5), pp.1307–1314.

Kanemura, H. et al., 2013. Pigment epithelium-derived factor secreted from retinal pigment epithelium facilitates apoptotic cell death of iPSC. *Scientific reports*, 3(1), p.2334.

Kang, T.M. & Hilgemann, D.W., 2004. Multiple transport modes of the cardiac Na+/Ca2+ exchanger. *Nature*, 427(6974), pp.544–548.

Karakikes, I. et al., 2015. Human induced pluripotent stem cell-derived cardiomyocytes: insights into molecular, cellular, and functional phenotypes.

Circulation research, 117(1), pp.80–88.

Kawai, M., Hussain, M. & Orchard, C.H., 1999. Excitation-contraction coupling in rat ventricular myocytes after formamide-induced detubulation. *The American journal of physiology*, 277(2), pp.H603–9.

Keith, A. & Flack, M., 1907. The Form and Nature of the Muscular Connections between the Primary Divisions of the Vertebrate Heart. *Journal of anatomy and physiology*, 41(Pt 3), pp.172–189.

Kennah, E. et al., 2009. Identification of tyrosine kinase, HCK, and tumor suppressor, BIN1, as potential mediators of AHI-1 oncogene in primary and transformed CTCL cells. *Blood*, 113(19), pp.4646–4655.

Kensah, G. et al., 2013. Murine and human pluripotent stem cell-derived cardiac bodies form contractile myocardial tissue in vitro. *European heart journal*, 34(15), pp.1134–1146.

Kim, C. et al., 2010. Non-cardiomyocytes influence the electrophysiological maturation of human embryonic stem cell-derived cardiomyocytes during differentiation. *Stem cells and development*, 19(6), pp.783–795.

Kirk, M.M. et al., 2003. Role of the transverse-axial tubule system in generating calcium sparks and calcium transients in rat atrial myocytes. *The Journal of physiology*, 547(Pt 2), pp.441–451.

Klinge, L. et al., 2010. Dysferlin associates with the developing T-tubule system in rodent and human skeletal muscle. *Muscle & nerve*, 41(2), pp.166–173.

Klinge, L. et al., 2007. From T-tubule to sarcolemma: damage-induced dysferlin translocation in early myogenesis. *FASEB journal : official publication of the Federation of American Societies for Experimental Biology*, 21(8), pp.1768–1776.

Kojima, C. et al., 2004. Regulation of Bin1 SH3 domain binding by phosphoinositides. *The EMBO journal*, 23(22), pp.4413–4422.

La Mata, De, A. et al., 2019. BIN1 Induces the Formation of T-Tubules and Adult-Like Ca2+ Release Units in Developing Cardiomyocytes. *Stem cells (Dayton, Ohio)*, 37(1), pp.54–64.

Lai, F.A. et al., 1988. Purification and reconstitution of the calcium release channel from skeletal muscle. *Nature*, 331(6154), pp.315–319.

Landstrom, A.P. et al., 2007. Mutations in JPH2-encoded junctophilin-2 associated with hypertrophic cardiomyopathy in humans. *Journal of molecular and cellular cardiology*, 42(6), pp.1026–1035.

Laury-Kleintop, L.D. et al., 2015. Cardiac-specific disruption of Bin1 in mice enables a model of stress- and age-associated dilated cardiomyopathy. *Journal of cellular biochemistry*, 116(11), pp.2541–2551.

Laver, D.R. et al., 1995. Cytoplasmic Ca2+ inhibits the ryanodine receptor from cardiac muscle. *The Journal of membrane biology*, 147(1), pp.7–22.

Lederer, W.J., Niggli, E. & Hadley, R.W., 1990. Sodium-calcium exchange in excitable cells: fuzzy space. *Science (New York, N.Y.)*, 248(4953), p.283.

Lee, E. et al., 2002. Amphiphysin 2 (Bin1) and T-tubule biogenesis in muscle. *Science (New York, N.Y.)*, 297(5584), pp.1193–1196.

Lenaerts, I. et al., 2009. Ultrastructural and functional remodeling of the coupling between Ca2+ influx and sarcoplasmic reticulum Ca2+ release in right atrial myocytes from experimental persistent atrial fibrillation. *Circulation research*, 105(9), pp.876–885.

Leprince, C. et al., 1997. A new member of the amphiphysin family connecting endocytosis and signal transduction pathways. *The Journal of biological chemistry*, 272(24), pp.15101–15105.

Li, L.-L. et al., 2020. Nanobar Array Assay Revealed Complementary Roles of BIN1 Splice Isoforms in Cardiac TTubule Morphogenesis. *Nano Letters*, 20(9), pp.6387–6395.

Li, S., Chen, G. & Li, R.A., 2013. Calcium signalling of human pluripotent stem cell-derived cardiomyocytes. *The Journal of physiology*, 591(21), pp.5279–5290.

Liang, P. et al., 2013. Drug screening using a library of human induced pluripotent stem cell-derived cardiomyocytes reveals disease-specific patterns of cardiotoxicity. *Circulation*, 127(16), pp.1677–1691.

Lieu, D.K. et al., 2009. Absence of transverse tubules contributes to non-uniform Ca(2+) wavefronts in mouse and human embryonic stem cell-derived cardiomyocytes. *Stem cells and development*, 18(10), pp.1493–1500.

Lieu, D.K. et al., 2013. Mechanism-based facilitated maturation of human pluripotent stem cell-derived cardiomyocytes. *Circulation. Arrhythmia and electrophysiology*, 6(1), pp.191–201.

Lin-Lin Li, Q.-J.G.H.-Y.L.J.-H.L.Y.Y.X.X.H.-T.L.J.H.S.S.H.L.H.Y.H.D.W.B.C.A.S.-Q.W., 2020. Nanobar Array Assay Revealed Complementary Roles of BIN1 Splice Isoforms in Cardiac T-Tubule Morphogenesis. pp.1–9.

Linkert, M. et al., 2010. Metadata matters: access to image data in the real world. *The Journal of cell biology*, 189(5), pp.777–782.

Liu, C. et al., 2019. Nexilin Is a New Component of Junctional Membrane Complexes Required for Cardiac T-Tubule Formation. *Circulation*, 140(1), pp.55–66.

Liu, J. et al., 2009. Facilitated maturation of Ca2+ handling properties of human embryonic stem cell-derived cardiomyocytes by calsequestrin expression. *American journal of physiology. Cell physiology*, 297(1), pp.C152–9.

Luisier, F. et al., 2010. Fast interscale wavelet denoising of Poisson-corrupted images. 90(2), pp.415–427.

Luke, G.A. et al., 2008. Occurrence, function and evolutionary origins of "2A-like" sequences in virus genomes. *The Journal of general virology*, 89(4), pp.1036–1042.

Lundy, S.D. et al., 2013. Structural and functional maturation of cardiomyocytes derived from human pluripotent stem cells. *Stem cells and development*, 22(14), pp.1991–2002.

Lyon, A.R. et al., 2009. Loss of T-tubules and other changes to surfacetopography in ventricular myocytes from failinghuman and rat heart. pp.1–6.

Macquaide, N. et al., 2015. Ryanodine receptor cluster fragmentation and redistribution in persistent atrial fibrillation enhance calcium release. *Cardiovascular research*, 108(3), pp.387–398.

Maherali, N. et al., 2007. Directly reprogrammed fibroblasts show global epigenetic remodeling and widespread tissue contribution. *Cell stem cell*, 1(1), pp.55–70.

Mao, N.C. et al., 1999. The murine Bin1 gene functions early in myogenesis and defines a new region of synteny between mouse chromosome 18 and human chromosome 2. *Genomics*, 56(1), pp.51–58.

Marx, S.O. et al., 2001. Coupled gating between cardiac calcium release channels (ryanodine receptors). *Circulation research*, 88(11), pp.1151–1158.

Matousek, M. & Posner, E., 1969. Purkyne"s(Purkinje"s)Muscle. *British heart journal*, 31(6), pp.718–721.

McMahon, H.T., Wigge, P. & Smith, C., 1997. Clathrin interacts specifically with amphiphysin and is displaced by dynamin. *FEBS letters*, 413(2), pp.319–322.

Mihic, A. et al., 2014. The effect of cyclic stretch on maturation and 3D tissue formation of human embryonic stem cell-derived cardiomyocytes. *Biomaterials*, 35(9), pp.2798–2808.

Mitcheson, J.S., Hancox, J.C. & Levi, A.J., 1996. Action potentials, ion channel currents and transverse tubule density in adult rabbit ventricular myocytes maintained for 6 days in cell culture., 431(6), pp.814–827.

Mitcheson, J.S., Hancox, J.C. & Levi, A.J., 1998. Cultured adult cardiac myocytes: future applications, culture methods, morphological and electrophysiological properties. *Cardiovascular research*, 39(2), pp.280–300.

Mohler, P.J., Davis, J.Q. & Bennett, V., 2005. Ankyrin-B Coordinates the Na/K ATPase, Na/Ca Exchanger, and InsP3 Receptor in a Cardiac T-Tubule/SR Microdomain I. Benjamin, ed. *PLoS biology*, 3(12), pp.e423–10.

Moretti, A. et al., 2010. Patient-specific induced pluripotent stem-cell models for long-QT syndrome. *The New England journal of medicine*, 363(15), pp.1397–1409.

Muller, A.J. et al., 2003. Targeted disruption of the murine Bin1/Amphiphysin II gene does not disable endocytosis but results in embryonic cardiomyopathy with aberrant myofibril formation. *Molecular and cellular biology*, 23(12), pp.4295–4306.

Nakada, T. et al., 2018. Physical interaction of junctophilin and the CaV1.1 C terminus is crucial for skeletal muscle contraction. *Proceedings of the National Academy of Sciences of the United States of America*, 115(17), pp.4507–4512.

Nakai, J. et al., 1990. Primary structure and functional expression from cDNA of the cardiac ryanodine receptor/calcium release channel. *FEBS letters*, 271(1-2), pp.169–177.

Nakanishi, S., Kuwajima, G. & Mikoshiba, K., 1992. Immunohistochemical localization of ryanodine receptors in mouse central nervous system. *Neuroscience research*, 15(1-2), pp.130–142.

Nerbonne, J.M. & Kass, R.S., 2005. Molecular physiology of cardiac repolarization. *Physiological reviews*, 85(4), pp.1205–1253.

New, W. & Trautwein, W., 1972. The ionic nature of slow inward current and its relation to contraction., 334(1), pp.24–38.

Neylon, C.B. et al., 1995. Multiple types of ryanodine receptor/Ca2+ release channels are expressed in vascular smooth muscle. *Biochemical and biophysical research communications*, 215(3), pp.814–821.

Nicot, A.-S. et al., 2007. Mutations in amphiphysin 2 (BIN1) disrupt interaction with dynamin 2 and cause autosomal recessive centronuclear myopathy. *Nature genetics*, 39(9), pp.1134–1139.

Nissan, X. et al., 2011. Functional melanocytes derived from human pluripotent stem cells engraft into pluristratified epidermis. *Proceedings of the National Academy of Sciences of the United States of America*, 108(36), pp.14861–14866.

Nunes, S.S. et al., 2013. Biowire: a platform for maturation of human pluripotent stem cell-derived cardiomyocytes. *Nature methods*, 10(8), pp.781–787.

Ohtsuka, T. et al., 1998. Nexilin: A Novel Actin Filament-binding Protein Localized at Cell–Matrix Adherens Junction. *The Journal of cell biology*, 143(5), pp.1227–1238.

Okita, K., Ichisaka, T. & Yamanaka, S., 2007. Generation of germline-competent induced pluripotent stem cells. *Nature*, 448(7151), pp.313–317.

Osborn, M.J. et al., 2005. A picornaviral 2A-like sequence-based tricistronic vector allowing for high-level therapeutic gene expression coupled to a dual-reporter system. *Molecular therapy : the journal of the American Society of Gene Therapy*, 12(3), pp.569–574.

Otsuji, T.G. et al., 2010. Progressive maturation in contracting cardiomyocytes derived from human embryonic stem cells: Qualitative effects on electrophysiological responses to drugs. *Stem cell research*, 4(3), pp.201–213.

Owen, D.J. et al., 1998. Crystal structure of the amphiphysin-2 SH3 domain and its role in the prevention of dynamin ring formation. *The EMBO journal*, 17(18), pp.5273–5285.

Page, E., 1978. Quantitative ultrastructural analysis in cardiac membrane physiology. *American journal of physiology. Cell physiology*, 235(5), pp.C147–C158.

Page, E. & Surdyk-Droske, M., 1979. Distribution, surface density, and membrane area of diadic junctional contacts between plasma membrane and terminal cisterns in mammalian ventricle. *Circulation research*, 45(2), pp.260–267.

Parikh, S.S. et al., 2017. Thyroid and Glucocorticoid Hormones Promote Functional T-Tubule Development in Human-Induced Pluripotent Stem Cell-Derived Cardiomyocytes. *Circulation research*, 121(12), pp.1323–1330.

Park, I.-H. et al., 2008. Reprogramming of human somatic cells to pluripotency with defined factors. *Nature*, 451(7175), pp.141–146.

Parton, R.G. et al., 1997. Caveolin-3 associates with developing T-tubules during muscle differentiation. *The Journal of cell biology*, 136(1), pp.137–154.

Periasamy, M. & Huke, S., 2001. SERCA pump level is a critical determinant of Ca(2+)homeostasis and cardiac contractility. *Journal of molecular and cellular cardiology*, 33(6), pp.1053–1063.

Peter, B.J. et al., 2004. BAR domains as sensors of membrane curvature: the amphiphysin BAR structure. *Science (New York, N.Y.)*, 303(5657), pp.495–499.

Picas, L. et al., 2014. BIN1/M-Amphiphysin2 induces clustering of phosphoinositides to recruit its downstream partner dynamin. *Nature Communications*, 5(5647), pp.1–12.

Prins, K.W. et al., 2016. Microtubule-Mediated Misregulation of Junctophilin-2 Underlies T-Tubule Disruptions and Calcium Mishandling in mdx Mice. *JACC. Basic to translational science*, 1(3), pp.122–130.

Quick, A.P. et al., 2017. Novel junctophilin-2 mutation A405S is associated with basal septal hypertrophy and diastolic dysfunction. *JACC. Basic to translational science*, 2(1), pp.56–67.

Radisic, M. et al., 2004. Functional assembly of engineered myocardium by electrical stimulation of cardiac myocytes cultured on scaffolds. *Proceedings of the National Academy of Sciences of the United States of America*, 101(52), pp.18129–18134.

Rao, C. et al., 2013. The effect of microgrooved culture substrates on calcium cycling of cardiac myocytes derived from human induced pluripotent stem cells. *Biomaterials*, 34(10), pp.2399–2411.

Razzaq, A. et al., 2001. Amphiphysin is necessary for organization of the excitation-contraction coupling machinery of muscles, but not for synaptic vesicle endocytosis in Drosophila. *Genes & development*, 15(22), pp.2967–2979.

Ren, Y. et al., 2011. Small molecule Wnt inhibitors enhance the efficiency of BMP-4-directed cardiac differentiation of human pluripotent stem cells. *Journal of molecular and cellular cardiology*, 51(3), pp.280–287.

Reynolds, J.O. et al., 2013. Junctophilin-2 is necessary for T-tubule maturation during mouse heart development. *Cardiovascular research*, 100(1), pp.44–53.

Richards, M.A. et al., 2011. Transverse tubules are a common feature in large mammalian atrial myocytes including human. *American journal of physiology. Heart and circulatory physiology*, 301(5), pp.H1996–2005.

Roguin, A., 2006. Wilhelm His Jr. (1863–1934)—The man behind the bundle. *Heart rhythm*, 3(4), pp.480–483.

Royer, B. et al., 2013. The myotubularin-amphiphysin 2 complex in membrane tubulation and centronuclear myopathies. *EMBO reports*, 14(10), pp.907–915.

Saha, K. & Jaenisch, R., 2009. Technical challenges in using human induced pluripotent stem cells to model disease. *Cell stem cell*, 5(6), pp.584–595.

Sakamuro, D. et al., 1996. BIN1 is a novel MYC-interacting protein with features of a tumour suppressor. *Nature genetics*, 14(1), pp.69–77.

Salick, M.R. et al., 2014. Micropattern width dependent sarcomere development in human ESC-derived cardiomyocytes. *Biomaterials*, 35(15), pp.4454–4464.

Sato, D., Shannon, T.R. & Bers, D.M., 2016. Sarcoplasmic Reticulum Structure and Functional Properties that Promote Long-Lasting Calcium Sparks. *Biophysical journal*, 110(2), pp.382–390.

Savio-Galimberti, E. et al., 2008. Novel features of the rabbit transverse tubular system revealed by quantitative analysis of three-dimensional reconstructions from confocal images. *Biophysical journal*, 95(4), pp.2053–2062.

Schmitt, N., Grunnet, M. & Olesen, S.-P., 2014. Cardiac potassium channel subtypes: new roles in repolarization and arrhythmia. *Physiological reviews*, 94(2), pp.609–653.

Scriven, D.R., Dan, P. & Moore, E.D., 2000. Distribution of proteins implicated in excitation-contraction coupling in rat ventricular myocytes. *Biophysical journal*, 79(5), pp.2682–2691.

Scriven, D.R.L. et al., 2002. The molecular architecture of calcium microdomains in rat cardiomyocytes. *Annals of the New York Academy of Sciences*, 976, pp.488–499.

Sedarat, F. et al., 2000. Colocalization of dihydropyridine and ryanodine receptors in neonate rabbit heart using confocal microscopy. *American journal of physiology. Heart and circulatory physiology*, 279(1), pp.H202–9.

Seki, S. et al., 2003. Fetal and postnatal development of Ca2+ transients and Ca2+ sparks in rat cardiomyocytes. *Cardiovascular research*, 58(3), pp.535–548.

Severs, N.J. et al., 1985. Morphometric analysis of the isolated calcium-tolerant cardiac myocyte. Organelle volumes, sarcomere length, plasma membrane surface folds, and intramembrane particle density and distribution. *Cell and tissue research*, 240(1), pp.159–168.

Shalom-Feuerstein, R. et al., 2013. Impaired epithelial differentiation of induced pluripotent stem cells from ectodermal dysplasia-related patients is rescued by the small compound APR-246/PRIMA-1MET. *Proceedings of the National Academy of Sciences of the United States of America*, 110(6), pp.2152–2156.

Shang, W. et al., 2014. Imaging Ca2+ nanosparks in heart with a new targeted biosensor. *Circulation research*, 114(3), pp.412–420.

Sharp, A.H. et al., 1993. Differential immunohistochemical localization of inositol 1,4,5-trisphosphate- and ryanodine-sensitive Ca2+ release channels in rat brain. *The Journal of neuroscience : the official journal of the Society for Neuroscience*, 13(7), pp.3051–3063.

Simunovic, M. et al., 2015. When Physics Takes Over: BAR Proteins and Membrane Curvature. *Trends in Cell Biology*, 25(12), pp.780–792.

Smith, L.L., Gupta, V.A. & Beggs, A.H., 2014. Bridging integrator 1 (Bin1) deficiency in zebrafish results in centronuclear myopathy. *Human molecular genetics*, 23(13), pp.3566–3578.

Smith, M.J. et al., 2015. In Vitro T-Cell Generation From Adult, Embryonic, and Induced Pluripotent Stem Cells: Many Roads to One Destination. *Stem cells (Dayton, Ohio)*, 33(11), pp.3174–3180.

Sobie, E.A. et al., 2006. The Ca 2+ leak paradox and rogue ryanodine receptors: SR Ca 2+ efflux theory and practice. *Progress in biophysics and molecular biology*, 90(1-3), pp.172–185.

Soeller, C. & Baddeley, D., 2013. Super-resolution imaging of EC coupling protein distribution in the heart. *Journal of molecular and cellular cardiology*, 58, pp.32–40.

Soeller, C. & Cannell, M.B., 1999. Examination of the transverse tubular system in living cardiac rat myocytes by 2-photon microscopy and digital image-processing techniques. *Circulation research*, 84(3), pp.266–275.

Sommer, J.R., 1995. Comparative anatomy: in praise of a powerful approach to elucidate mechanisms translating cardiac excitation into purposeful contraction. *Journal of molecular and cellular cardiology*, 27(1), pp.19–35.

Sparks, A.B. et al., 1996. Cloning of ligand targets: systematic isolation of SH3 domain-containing proteins. *Nature biotechnology*, 14(6), pp.741–744.

Spinozzi, S. et al., 2020. Nexilin Is Necessary for Maintaining the Transverse-Axial Tubular System in Adult Cardiomyocytes. *Circulation: Heart Failure*, 13(7), pp.e51823–10.

Stern, M.D., 1992. Theory of excitation-contraction coupling in cardiac muscle. *Biophysical journal*, 63(2), pp.497–517.

Stern, M.D., Pizarro, G. & Ríos, E., 1997. Local control model of excitation-contraction coupling in skeletal muscle. *The Journal of general physiology*, 110(4), pp.415–440.

SUMA, K., 2003. Sunao Tawara: A Father of Modern Cardiology. *Pacing Clin Electrophysiol*, 24(1), pp.88–96. Available at: https://onlinelibrary.wiley.com/doi/abs/10.1046/j.1460-9592.2001.00088.x.

Swift, F. et al., 2006. Slow diffusion of K+ in the T tubules of rat cardiomyocytes. *Journal of applied physiology (Bethesda, Md. : 1985)*, 101(4), pp.1170–1176.

Synnergren, J. et al., 2012. Global transcriptional profiling reveals similarities and differences between human stem cell-derived cardiomyocyte clusters and heart tissue. *Physiological genomics*, 44(4), pp.245–258.

Takahashi, K. & Yamanaka, S., 2006. Induction of pluripotent stem cells from mouse embryonic and adult fibroblast cultures by defined factors. *Cell*, 126(4), pp.663–676.

Takasato, M. et al., 2015. Kidney organoids from human iPS cells contain multiple lineages and model human nephrogenesis. *Nature*, 526(7574), pp.564–568.

Takei, K., Slepnev, V.I. & Pietro De Camilli, V.H., 1999. Functional partnership between amphiphysin and dynamin in clathrin- mediated endocytosis. 1(1), pp.33–39.

Takekura, H., Shuman, H. & Franzini-Armstrong, C., 1993. Differentiation of membrane systems during development of slow and fast skeletal muscle fibres in chicken. *Journal of muscle research and cell motility*, 14(6), pp.633–645.

Takeshima, H. et al., 2000. Junctophilins: a novel family of junctional membrane complex proteins. *Molecular cell*, 6(1), pp.11–22.

Takeshima, H. et al., 1989. Primary structure and expression from complementary DNA of skeletal muscle ryanodine receptor. *Nature*, 339(6224), pp.439–445.

Tan, M.-S., Yu, J.-T. & Tan, L., 2013. Bridging integrator 1 (BIN1): form, function, and Alzheimer's disease. *Trends in molecular medicine*, 19(10), pp.594–603.

Thavandiran, N. et al., 2013. Design and formulation of functional pluripotent stem cell-derived cardiac microtissues. *Proceedings of the National Academy of Sciences of the United States of America*, 110(49), pp.E4698–707.

Tian, Q. et al., 2017. An adaptation of astronomical image processing enables characterization and functional 3D mapping of individual sites of excitation-contraction coupling in rat cardiac muscle. *eLife*, 6, p.665.

Tian, Q. et al., 2012. Functional and morphological preservation of adult ventricular myocytes in culture by sub-micromolar cytochalasin D supplement. *Journal of molecular and cellular cardiology*, 52(1), pp.113–124.

Tidball, J.G., Cederdahl, J.E. & Bers, D.M., 1991. Quantitative analysis of regional variability in the distribution of transverse tubules in rabbit myocardium. *Cell and tissue research*, 264(2), pp.293–298.

Toussaint, A. et al., 2011. Defects in amphiphysin 2 (BIN1) and triads in several forms of centronuclear myopathies. *Acta neuropathologica*, 121(2), pp.253–266.

Tsutsui, K. et al., 1997. cDNA cloning of a novel amphiphysin isoform and tissue-specific expression of its multiple splice variants. *Biochemical and biophysical research communications*, 236(1), pp.178–183.

Tulloch, N.L. et al., 2011. Growth of engineered human myocardium with mechanical loading and vascular coculture. *Circulation research*, 109(1), pp.47–59.

Umeda, K. et al., 2015. Long-term expandable SOX9+ chondrogenic ectomesenchymal cells from human pluripotent stem cells. *Stem cell reports*, 4(4), pp.712–726.

Veerman, C.C. et al., 2015. Immaturity of human stem-cell-derived cardiomyocytes in culture: fatal flaw or soluble problem? *Stem cells and development*, 24(9), pp.1035–1052.

Viero, C. et al., 2008. A primary culture system for sustained expression of a calcium sensor in preserved adult rat ventricular myocytes. *Cell calcium*, 43(1), pp.59–71.

Voldstedlund, M., Vinten, J. & Tranum-Jensen, J., 2001. cav-p60 expression in rat muscle tissues. Distribution of caveolar proteins. *Cell and tissue research*, 306(2), pp.265–276.

Wagner, E. et al., 2012. Stimulated emission depletion live-cell super-resolution imaging shows proliferative remodeling of T-tubule membrane structures after myocardial infarction. *Circulation research*, 111(4), pp.402–414.

Walker, M.A. et al., 2014. Superresolution modeling of calcium release in the heart. *Biophysical journal*, 107(12), pp.3018–3029.

Wang, H. et al., 2010. Mutations in NEXN, a Z-Disc Gene, Are Associated with Hypertrophic Cardiomyopathy. *The American Journal of Human Genetics*, 87(5), pp.687–693.

Wang, W. et al., 2014. Reduced junctional Na+/Ca2+-exchanger activity contributes to sarcoplasmic reticulum Ca2+ leak in junctophilin-2-deficient mice. *American journal of physiology. Heart and circulatory physiology*, 307(9), pp.H1317–26.

Way, M. & Parton, R.G., 1995. M-caveolin, a muscle-specific caveolin-related protein. *FEBS letters*, 376(1-2), pp.108–112.

Wechsler-Reya, R. et al., 1997. Structural analysis of the human BIN1 gene. Evidence for tissue-specific transcriptional regulation and alternate RNA splicing. *The Journal of biological chemistry*, 272(50), pp.31453–31458.

Wechsler-Reya, R.J., Elliott, K.J. & Prendergast, G.C., 1998. A role for the putative tumor suppressor Bin1 in muscle cell differentiation. *Molecular and cellular biology*, 18(1), pp.566–575.

Wei, S. et al., 2010. T-tubule remodeling during transition from hypertrophy to heart failure. *Circulation research*, 107(4), pp.520–531.

Wernig, M. et al., 2007. In vitro reprogramming of fibroblasts into a pluripotent ES-cell-like state. *Nature*, 448(7151), pp.318–324.

Wigge, P. et al., 1997. Amphiphysin heterodimers: potential role in clathrin-mediated endocytosis. *Molecular biology of the cell*, 8(10), pp.2003–2015.

Wright, P.T. et al., 2014. Caveolin-3 regulates compartmentation of cardiomyocyte beta2-adrenergic receptor-mediated cAMP signaling. *Journal of molecular and cellular cardiology*, 67, pp.38–48.

Wu, T. & Baumgart, T., 2014. BIN1 membrane curvature sensing and generation show autoinhibition regulated by downstream ligands and PI(4,5)P2. *Biochemistry*, 53(46), pp.7297–7309.

Xu, X. & Colecraft, H.M., 2009. Primary culture of adult rat heart myocytes.

Journal of visualized experiments : JoVE, (28), p.e1308.

Yang, X. et al., 2014. Tri-iodo-l-thyronine promotes the maturation of human cardiomyocytes-derived from induced pluripotent stem cells. *Journal of molecular and cellular cardiology*, 72, pp.296–304.

Yin, C.C. & Lai, F.A., 2000. Intrinsic lattice formation by the ryanodine receptor calcium-release channel. *Nature cell biology*, 2(9), pp.669–671.

Yu, J. et al., 2007. Induced pluripotent stem cell lines derived from human somatic cells. *Science (New York, N.Y.)*, 318(5858), pp.1917–1920.

Zhang, D. et al., 2013. Tissue-engineered cardiac patch for advanced functional maturation of human ESC-derived cardiomyocytes. *Biomaterials*, 34(23), pp.5813–5820.

Zorzato, F. et al., 1990. Molecular cloning of cDNA encoding human and rabbit forms of the Ca2+ release channel (ryanodine receptor) of skeletal muscle sarcoplasmic reticulum. *The Journal of biological chemistry*, 265(4), pp.2244–2256.

Zwi, L. et al., 2009. Cardiomyocyte differentiation of human induced pluripotent stem cells. *Circulation*, 120(15), pp.1513–1523.

8. Acknowledgement

It is surprising that six years have ticked away since I came here from China. Homburg is such a lovely city, small, peaceful, and very beautiful, which has bestowed me numerous unforgettable memories. Universitätsklinikum des Saarlandes is such a great medical center, active, multidisciplinary, and fully resourced, which has provided me with a perfect platform for researches. As for the department of Molecular Cell Biology, where I have spent most of the time, it is a remarkable laboratory and has entitled me to almost everything I need to complete my researches. Thanks to the well-equipped conditions and all the kind people here, I am eventually able to reach the finishing line of the journey, which is full of challenges, disappointments, and of course, surprises.

First of all, I would like to give my full gratefulness to my supervisor, Prof. Dr. Peter Lipp. He is a great scientist with profound perceptions and a huge amount of experience in biomedical research and has done many great works in the field of cardiology. Thanks for Peter's kind offer, I am able to come here and extend my research into the field of the heart. During the whole process, Peter has given me enormous support and many good pieces of advice. Every time when I come across a difficult problem, he is always there to encourage and inspire me, and help me out of the tough times. Particularly, he always gives us quite a lot of space and flexibility to think and try by ourselves, which has really promoted me to develop an independent and critical way of thinking. I feel very fortunate to carry out my Ph.D. program here under the promotion of Prof. Dr. Peter Lipp.

In addition, I would like to give my thankfulness to Dr. Qinghai Tian, who is also my supervisor. Similarly from China, Qinghai completely understands my situation due to the same mother language and educational background. From the very beginning, he has given me lots of help in almost every aspect ranging from daily life to academic researches. As the supervisor, he has guided me patiently to this area even although I knew very little about it. Dr. Qinghai has established profound expertise from molecular cell biology to microscopic imaging with huge amounts of experience in computer programming and data analysis. Whenever I run into a complex problem, he can always offer me constructive suggestions and very practical tools. Moreover, Dr. Qinghai has also shared with me various kinds of information and ideas, and has always given me a hand whenever needed. I really appreciate what he has done for me in the past years.

I would also like to thank Dr. Xinhui and Dr. Sandra, both of whom have given me much help in the experiments. Before I came here, I had hardly any experience in molecular biology, which is very important in my program. Dr. Xin and Dr. Sandra are both experts in this field and have shown me patiently how to do it from the scratch. With their assistance and sharing, I am able to conquer many obstacles and move my steps forward.

Besides, I would like to give my sincere gratitude to Tanja and Sabrina, who are the technicians of the lab. Tanja manages a great many of the daily affairs, from ordering reagents to fulfilling ordinary experiments. She has done a lot to maintain the smooth operation of the lab, which enables us a well-organized and orderly-regulated environment to work in. As for Sabrina, she is a very professional technician and is especially good at cell isolation. A major part of my program is based on the culture of rat cardiomyocytes, which is quite a tricky skill that requires enormous time and energy. Due to Sabrina's contribution, I can always readily get the cells I need and complete my experiments. I really appreciate their devotions to the lab and great help to me.

I would like to appreciate Prof. Dr. Alessandra Moretti and Dr. Zhifen for kindly preparing hiPSC-CMs for me to carry out my research. One of the major focuses of my research is hiPSC-CM. They have continuously supplied me with lots of baths of hiPSC-CMs, which is really important to my program. Without their donations, all my ideas could be nothing but hypotheses.

Moreover, I would like to appreciate Dr. Wenying's work for me. Since a large part of my work is based on hiPSC-CM, Dr. Wenying has spent lots of time and energy on isolating and culturing these cells, which is really a time-consuming process. Without her support, I would not be able to finish my research program.

I would like to give my particular gratitude to Cony and Karin. As the secretaries of the lab, they are very professional, responsible, and considerate, and have managed countless daily lab affairs for us. Whenever I encounter a problem or an issue that I am not familiar with, they will always kindly do whatever they can to help me out. Due to their dedication, I am able to focus most of my attention on the research.

In addition, I also appreciate what the other colleagues have done for me. In the past years they have helped me in many ways. Eli, Laura S. and Ramona have done a lot in animal management. Moli, Laura.H, and Julia have shared with me lots of experience and helped me establish good research habits. Polia, on the other hand, has always encouraged me, especially when I feel frustrated. I really appreciate everything they have done for me.

Besides, I am very thankful to my Chinese friends here in Homburg. Most of them are also doing researches in different labs. Since I came here, they have offered me much help from life to work. They have shared with me many great ideas about life and work. Most important of all, we have spent many happy moments together, which is a great supplement to my life here.

Finally, I would like to give my full gratitude from the bottom of my heart to my parents and relatives, who have been continuously supportive of me. It is not easy to be separated from my beloved family, particularly when they also need me. However, they have given me so much support and sustained me to complete my program. Whenever I feel down, they always comfort me and boost my confidence. They are my firmest wall that I can rely on and the coziest harbor that I can rest in. Without their great and selfless devotion, it is unbelievable and unimaginable for me to run this far. I can never be grateful enough to them for everything they have done for me.

9. Curriculum Vitae

The curriculum vitae was removed from the electronic version of the doctoral thesis for reasons of data protection.

Aus datenschutzrechtlichen Gründen wird der Lebenslauf in der elektronischen Fassung der Dissertation nicht veröffentlicht.

Tag der Promotion:	25.11.2021
Dekan:	Prof. Dr. M. D. Menger
Berichterstatter:	Prof. P. Lipp
	Prof. M. Boehm